NASA-CR-16782
19820025618

DOE/NASA/0109-1

Solar SR82-4-4792-28

Advanced Ceramic Coating Development for Industrial/Utility Gas Turbines

James W. Vogan and Alvin R. Stetson
Solar Turbines Incorporated

January 1982

Prepared for
NATIONAL AERONAUTICS AND SPACE ADMINISTRATION
Lewis-Research Center

for
U.S. DEPARTMENT OF ENERGY
Office of Fossil Energy Programs
Heat Engines and Heat Recovery Division

DOE/NASA/0109-1
NASA CR 167852
Solar SR82-4-4792-28

Advanced Ceramic Coating Development for Industrial/Utility Gas Turbines

James W. Vogan and Alvin R. Stetson
Solar Turbines Incorporated
San Diego, California 92138

January 1982

Prepared for
NATIONAL AERONAUTICS AND SPACE ADMINISTRATION
Lewis-Research Center
Cleveland, Ohio
Under Contract DEN3-109

for
U.S. DEPARTMENT OF ENERGY
Office of Fossil Energy Programs
Heat Engines and Heat Recovery Division
Washington, DC 20545
Under Interagency Agreement DE-A101-7ET-13111

This Page Intentionally Left Blank

TABLE OF CONTENTS

TABLE OF CONTENTS (CONT)

LIST OF TABLES

This Page Intentionally Left Blank

LIST OF FIGURES

LIST OF FIGURES (CONT)

LIST OF FIGURES (CONT)

LIST OF FIGURES (CONT)

LIST OF FIGURES (CONT)

LIST OF FIGURES (CONT)

LIST OF FIGURES (CONT)

EXECUTIVE SUMMARY

Thermal barrier coatings are a cost-effective means of increasing gas turbine engine efficiency. They need to be modified to reduce their susceptibility to attack by corrosive elements, such as vanadium and sulfur, in dirty fuel.

The objective of the program was to develop thermal barrier coatings (TBC's) for use in industrial/utility gas turbines that would operate on dirty fuel.

Twenty-one different coating systems, based on four ceramic coatings, were screened. Initial tests were performed by cyclic furnace exposure to select the most promising coating structures and compositions for further study. The four ceramic coatings, applied over NiCrAlY and CoCrAlY bond coats, were furnace tested as duplex, triplex and graded TBC structures using a MAR-M421 substrate. The ceramic starting materials were:

- $ZrO_2.8Y_2O_3$
- $MgO.Al_2O_3$
- $ZrO.TiO_2$
- $ZrO_2.MgO$

Based on their resistance to spallation and phase stability during furnace exposure, duplex $ZrO_2.8Y_2O_3$ and $CaO.TiO_2$ coating systems were selected for further development and test.

Three 500-hour and two 1000-hour burner rig tests were conducted with $CaO.TiO_2$ and $ZrO_2.8Y_2O_3$ TBC's. The fuels used in these tests varied from clean Diesel No. 2 to contamination levels of 50 ppm of vanadium and 150 ppm of magnesium through the use of fuel additives. The zirconia coatings were found to be sensitive to vanadium and were destabilized from their cubic structure after prolonged exposure to combustion products generated by fuels containing high levels of vanadium. When magnesium was added to the fuel it displaced calcium from the calcium titanate lattice; no coating loss was associated with this reaction.

The presence of high levels of contamination in the fuel interferred with normal combustor operation during the test program. In the tests using a level of 50 ppm vanadium and 150 ppm magnesium heavy deposits were developed. These occurred both on the test specimens and on the fuel injector. To maintain proper combustor operation it was necessary to shut down and remove the deposits mechanically every 50 to 100 hours of operation. The test specimens also developed heavy deposits. These deposits made visual examiantion for coating loss during test impractical since they could not be readily distinguished from the TBC's. In actual engine operation they would be expected to reduce aerodynamic efficiency and restrict the flow of hot gases. Routine

cleaning and maintenance operations are not sufficient to control this build-up and specialized cleaning techniques would be required in normal engine operation.

Calcium silicate, calcium titanate and zirconia-8% yttria TBC's were also applied to first-stage Mars gas turbine blades. These blades were installed for a 550-hour engine accelerated endurance run. During the test foreign object damage occurred. No major coating failure due to foreign object damage was observed. Heavy spallation developed on the pressure face of the calcium silicate coated blades. Variations in coating loss between blades was partially attributed to coating thickness variations.

Engineering analyses were performed to determine the effect of TBC's on the Mars 10,800 hp gas turbine engine. These analyses assumed that the first- and second-stage nozzles and first-stage blades would be coated. The following results were predicted:

- Cooling air requirements reduced 50 percent
- Shaft horsepower output increased 2.76 percent
- Specific fuel consumption reduced 4.7 percent

In addition, thermal transients and the resultant thermal fatigue in the coated components would be reduced, resulting in increased component life.

The program results indicate that yttria-stabilized zirconia and calcium titanate TBC's can be used on static components in production engines. The calcium titanate TBC's are more stable when using dirty fuels. Both coatings are process-sensitive. Coating integrity is affected not only by coating composition and process parameters, but also by substrate temperature during application, substrate composition, and part geometry. These effects must be established for each component prior to release for production.

1

INTRODUCTION

The development of ceramic coatings to lower metal temperatures and to improve its resistance to the combustion products of low-grade fuels is a logical approach to reducing gas turbine cooling losses and improving component resistance to hot corrosion when using dirty fuels. Coating systems now in use have shown severe problems when exposed to these low-grade fuels. Contaminants, such as vanadium and phosphorus, tend to attack these coatings and eventually lead to coating failure.

This program was initiated to study the attack mechanism and develop improved coatings with enhanced service life. Plasma spray was selected as the primary means of application. Reference to the literature indicated that two approaches had the highest probability of success. These were reduction of the yttrium content in the MCrAlY bond coat and modification of the ceramic system. Both approaches were studied in this program.

To ensure the production of meaningful data, it is essential that evaluation of materials be based on engineering requirements of an operating gas turbine of known characteristics. The program testing was based on the operating conditions of Solar's 10,800 hp Mars industrial gas turbine. It has a turbine rotor inlet temperature (TRIT) of 982 to 1057°C. The first- and second-stage vanes and the first-stage blades are air cooled. The metal temperatures of the first-stage blades lie in the 650°-816°C range during operation. This engine will show immediate benefit from application of a ceramic coating to the first- and second-stage vanes. External vane film cooling holes can be eliminated and internal cooling will be adequate with all cooling air exiting from the trailing edge of the vane. Not only will component costs be significantly reduced and reliability increased, but more efficient cooling air management will yield a significant fuel savings. Application of a ceramic coating to the first-stage blades will provide further benefits through the reduction of cooling air requirements. Numerous other areas also exist where resistance to corrosion and the allowance for higher surface temperatures are also of benefit.

The program was subdivided into three experimental and analytical tasks, as follows:

Task I - Coating Development and Test

Task II - Preliminary Coating Design Criteria

Task III - Endurance Testing

In Task I, 21 plasma-deposited compositions of four generic types and a baseline coating were screened. These were:

Type I - Outgrowth coatings from a NASA-Lewis NiCrAlY/yttria-stabilized zirconia concept

Type II - Spinel structure coatings ($MgAl_2O_4$)

Type III - Perovskite structure coatings ($CaTiO_3$)

Type IV - Two-phase coatings ($MgO-ZrO_2$) (Solar baseline).

In the Type I coatings, CoCrAlY bond coats were included based on recent results obtained at NASA-Lewis by Zaplatynsky (Ref. 1). This could increase stability of the cubic ZrO_2. The basis for selection of the Type II and Type III coatings was thermodynamic stability of the structure. Both are inherently stable cubic compounds, unlike Type I coatings which rely on a solid-solution additive (Y_2O_3) to stabilize the cubic structure. Loss of Y_2O_3 by reaction with impurities decreases the crystallographic stability, producing disruptive allotropic transformation to monoclinic and tetragonal phases. In each class of coatings, approaches were included for strain accommodation in the coatings by grading from metal to pure ceramic.

The Type IV coating was included as a second baseline. This coating is used commercially on combustion liners and other components requiring thermal insulation. Solar has used it effectively in turbine test activities.

Several methods were used to evaluate the coatings. Initial screening of the coating system was by furnace exposure to provide a metal temperature of 982°C with periodic cooling to 260°C to provide thermal shock. Visual examination at each cooling cycle, combined with metallurgical evaluation at completion of the test, was used to evaluate the coating system.

Subsequent to the initial screening tests, additional tests were preformed using hollow bar specimens in a burner rig. These specimens were exposed to combustion flames generated by clean and dirty fuels to evaluate the corrosion effects of combustion products. This test included thermal cycling to create periodic thermal stresses in the coating system.

Laboratory measurements were also made to determine specific coating characteristics such as bond strength and strain tolerance.

Concurrent with the Task I experimental effort, Task II, a design and analytical study, was carried out to further refine coating selection for the vanes, blades and combustor. Properties of the coating systems selected in Task I were fed into Task II to provide the data necessary for quantitative cycle analysis. From the Task I (experimental) and Task II (analytical) efforts, the best systems were selected and tested in Task III (1000-hour rig tests). These tests were long enough to demonstrate the coating reliability. In addition to these laboratory endurance tests, an engine endurance test was performed. This test encompassed the coating of first-stage cooled turbine blades. These blades were installed in a test engine and subjected to a 550-hour cyclic accelerated engine endurance test.

At the conclusion of this program, sufficient data was generated to establish the value of TBC's and to prepare recommendations regarding their incorporation into gas turbines operating on low-grade fuels as well as uprated production engines.

Analytical studies showed that, with the Mars engine, immediate benefits could be realized by applying a TBC to the first- and second-stage vanes and to the first-stage blades. This coating would allow a 50 to 55 percent reduction in cooling air requirements for these components. As a result, specific fuel consumption would be reduced by 1.40 percent and a gain in shaft horsepower of 2.76 percent could be realized for this engine.

Engine testing demonstrated that, except for leading edge areas, TBC's could be applied to first-stage turbine blades that would last for the normal life of the component. The severe erosive conditions and high heat fluxes encountered by the leading edges of the first-stage turbine blades caused loss of coating in this area.

Yttria-stabilized zirconia and calcium titanate coatings remained intact on the pressure and suction faces of the blades.

The laboratory tests showed that advanced TBC's could be applied to engine components that would reduce or prevent attack by contaminants in low-grade fuels.

This Page Intentionally Left Blank

2

MATERIALS AND LABORATORY TEST PROCEDURES

Furnace cyclic oxidation tests, furnace corrosion tests, and burner rig testing with and without fuel contaminants were used to select coatings for engine and endurance testing.

2.1 MATERIALS

Five bond coat compositions and four ceramic coating compositions were used in initial screening tests. The compositions of the bond and zirconia coatings are reported in Table 1.

Table 1

Composition of Bond and Zirconia Coatings

Bond Coat					
	Received				
Specified	Al(%)	Cr(%)	Ni(%)	Co(%)	Y(%)
NiCrAl/0.5Y	6.26	18.8	Bal.	-	0.49
NiCrAl/0.2Y	6.31	18.72	Bal.	-	0.18
NiCrAl/0.8Y	6.46	18.68	Bal.	-	0.72
CoCrAlY	6.30	18.63	-	Bal.	0.71
NiCrAl	5.60	19.2	72.2	-	-
Zirconia Coat					
Type	MgO(%)	ZrO_2(%)	Y_2O_3(%)		
MgO-ZrO_2 (19202)	22.38	74.62	-		
MgO-ZrO_2 (19122)	21.11	77.16	-		
MgO-ZrO_2 (19288)	21.61	76.22	-		
ZrO_2-Y_2O_3 (8226-A-1)	-	92.0	7.0		

Calcium titanate ($CaO.TiO_2$) and spinel ($MgO.Al_2O_3$) were obtained as compounds to provide two additional ceramic starting materials.

The bond coat compositions were selected on the basis of data obtained from the literature. The MCrAlY coatings have been found stable under turbine operating conditions and it was believed that reducing yttrium content would enhance performance.

The magnesium zirconate coating is widely used and was selected to provide a baseline coating system. The yttria-stabilized zirconia system has also been widely tested. Laboratory data indicates that its performance is superior to magnesium zirconate. It was selected as the best coating available at the program's initiation.

One problem reported with zirconia compositions is destabilization of the zirconia structure when exposed to vanadium and other elements. The two additional materials were selected to provide inherently stable cubic structures. Both are compounds and were expected to be less sensitive to attack by fuel contaminants than stablized zirconia.

During the program MAR-M421, a turbine blade alloy, was the principal substrate. Two additional alloys, X-45M and Hastelloy X, were used as representative vane and combustion alloys and were included in the endurance tests at the end of the program. The alloy compositions are given in Table 2.

2.2 THERMAL BARRIER COATING (TBC) DEPOSITION

At the initiation of the program, $ZrO_2.8Y_2O_3$ was selected as the baseline coating. A specimen with this coating is shown in Figure 1. It was produced from a commercial powder that was reportedly produced by sintering. The coating is characterized by large pores near the bondline and a denser surface layer. The powder used in producing this coating was also supplied to a vendor with instructions to produce a similar coating. The result of this experiment is shown in Figure 2. The resulting coating is considerably more porous than the baseline coating with individual pores considerably larger, reflecting the effect of minor process vaiables on coating structure.

Subsequent coatings were developed using a fused $ZrO_2.8Y_2O_3$ powder. The manufacturing processes used to produce each powder are proprietary. The primary difference observed between the two materials was the degree of lattice transformation in the starting powder. The material identified as sintered was less than 40 percent cubic. The material identified as fused approached 90 percent cubic. Both deposited as 90 to 95 percent cubic. Initial coatings applied using fused material had structures similar to the initial baseline coating. These were applied at 50 volts and 350 amps using an argon/ hydrogen plasma gas. Substrate temperature was held to a maximum of 177°C by air cooling. However, the coatings were extremely sensitive to thermal shock. Gun current was increased to 450 amps and the voltage raised to 55 volts by increasing the hydrogen content of the gas. The substrate temperature was also raised to approximately 260°F by reducing the cooling air. The resulting structure is shown in Figure 3. The coating has finely distributed pores and a uniform overall appearance.

Table 2

Alloys for Ceramic Coating Evaluation

Composition	MAR-M421 (Blades)	X-45M (Alloy)	Hastelloy X (Combustor)
Nickel	Balance	9.5-11.5	Balance
Cobalt	9.5	Balance	0.5- 2.5
Chromium	15.8	28.5-30.5	20.5-23.0
Aluminum	4.3	-	-
Titanium	1.8	-	-
Molybdenum	2.0	-	8.0-10.0
Tungsten	3.8	6.5- 7.5	0.2- 2.0
Columbium	2.0	-	-
Carbon	0.15	-	0.05-0.15
Manganese	0.20 max.	-	1.0 max.
Silicon	0.20 max.	0.75- 1.0	1.0 max.
Iron	-	0.0- 2.0	17.0-20.0
Boron	-	-	-
Zirconium	-	-	-

Similar variations were encountered in the calcium titanate coating. As power levels and deposition temperatures were increased coating structure varied from high porosity to that shown in Figure 4. The ceramic phase of the calcium titanate structure appeared fused or glassy when compared with the zirconia coatings. Excessive power levels tended to create coating stress levels that led to internal cracking, both parallel to and normal to the surface. The most successful coatings were produced at an arc current of 425 amperes and 55 volts.

The plasma spray conditions selected for coating the standard test specimens were: current - 425 amps; voltage - 55 volts; distance - 75 mm; surface speed - 15 m/min.; and substrate temperature - 321°-368°C. These parameters were developed for the 6.4 mm diameter hollow test specimens. Some evidence was obtained indicating the alloys, other than MAR-M421, would require modification of the spray test parameters for optimum coatings. The time available did not permit further development of the plasma spray process.

2.3 FURNACE CYCIC OXIDATION TESTS

The specimens used in the furnace tests were MAR-M421 discs 12 mm in diameter by 5 mm thick. The discs were coated on one side with the thermal barrier coating (TBC) to be tested. A chromel-alumel thermocouple was attached to the opposite face. A typical cross section is shown in Figure 5.

Twenty-two of these specimens were installed in the specimen holders. In addition, three uncoated specimens were installed with thermocouples welded to front and back faces to provide baseline data for comparing with the response of coated specimens to the test environment. An illustration of a test panel with 25 specimens installed is shown in Figure 6. To perform the cyclic oxidation test, the panel is installed in a furnace opening as shown in Figure 7. Immediately behind the panel is an insulating block mounted on the shaft of an air-operated cylinder controlled by a cyclic sequence timer. During test the block is used in conjunction with cooling air to control the coldface temperature of the test specimens. With the block installed and the cooling air off, the specimen uniformly approaches furnace temperature. With the block removed the back-face temperature approaches the reduced metal temperature experienced in an air-cooled turbine component. The standard cycle was 50 mintes hot and 10 minutes cooled. This cycle was repeated continuously throughout the test period. In addition the test panel was removed from the furace, once in each 24-hour period, to visually examine the specimens for spallation or other evidence of coating failure. After the test was completed the specimens were sectioned, mounted and polished for metallurgical examination. Tests were conducted at 1150°, 1032° and 871°C.

The 50-hour furnace cyclic test at 1150°C was conducted at a constant furnace temperature. During test the following temperatures were measured:

- Furnace temperature - 1150°C
- Uncooled specimens

  Hot face - 1110°C
  Cold face - 1100°C

- Cooled coated specimens (avg)

  Hot face - 1075°C
  Cold face - 933°C

Under these conditions the front face was cycled between 1075° and 1110°C every hour and the back face cycled between 933° and 1100°C during the same period.

The 50-hour furnace cyclic test at 1032°C was similar to the first test. It differed in that the furance temperature was decreased to 1032°C and the specimens were cycled once every 24 hours to ambient temperature to increase the thermal stress experienced in the coating.

In the 100-hour furnace cyclic test at 871°C the furnace temperature was again reduced. Test duration was increased and the specimens were cooled by convection to ambient temperature twice each 24-hour period.

During coating deposition, coating thicknesses were determined from the increase in specimen thickness. The measurements were made with a micrometer. Metallographic sections showed that the true thickness varied. This was attributed to coating surface irregularities inherent in the plasma spray

process. An empirical scale was established relating micrometer measurements during application to true coating thickness. Using this scale, coating thickness was then controlled to $\pm$0.05 mm.

2.4 FURNACE CORROSION TESTS

Prior to conducting burner rig tests on the TBC's, two additional furnace tests were conducted to determine the effect of fuel impurities on coating structures. Four compositions were tested: (1) $ZrO_2.8Y_2O_3$; (2) $CaO.TiO_2$; (3) $MgO.Al_2O_3$; and (4) $ZrO_2.24MgO$. The test method used is a Solar standard procedure for determining hot corrosion of turbine components. For this series of tests the specimens were cut from MAR-M421 turbine blades and coated. The specimens, 1.27 cm by 1.9 cm, were pre-heated to 162° $\pm$13°C and then dipped in a salt solution of the following composition: Na_2SO_4 - 95 gm; NaCl - 5 gm; and H_2O - 400 ml. This produced a salt deposit of 1.5 to 2.0 mg/cm^2 on the surface under test. The specimens were then furnace heated in air to 760°C for 16 hours, cooled, rinsed and lightly brushed to remove loose surface deposits. The entire test cycle was repeated three additional times. After testing the specimens were sectioned and examined metallurgically for evidence of corrosive attack. A second test was conducted using the same procedure except that the furnace temperature was increased to 870°C to increase the severity of attack.

In the second corrosion test series, sodium, vanadium and sulfur were used in the form of $NaVO_3$ and Na_2SO_4. The salt proportions in the test solution were adjusted to give a sodium-to-vanadium ratio of 2.24. The average salt deposit was 1.5 mg/cm^2 and furnace temperature was maintained at 870°C. Cycling and salt replenishment followed that of the previous test. A third test was then performed in a similar manner using Na_3PO_4 salt in addition to give equal concentratios of sulfur and phosphorus while maintaining a constant sodium-to-vanadium ratio of 2.24.

2.5 BURNER RIG TESTING

Three burner rig tests were used to determine the effect of fuel composition and combustion products on the coatings. A schematic of the test rig is given in Figure 8. This facility will test up to ten specimens at a time. The specimens were machined from hollow test bars, as shown in the insert, and thermocouples were installed at the burner centerline to monitor metal temperature. The specimen holder provides cooling air to the specimens for control of substrate temperature during test. In operation the holder is rotated at 1725 rpm. Thermocouple leads are connected through slip rings to a multipoint recorder which provides a record of temperature during the test. Figure 9 is a photograph of specimens undergoing testing. The burner rig shroud has been removed for illustrative purposes. The burners used in these tests operate on Diesel No. 2 and air. When required for test purposes, additives are used in the fuel, either as fuel-soluble compounds in the supply tank or as water-soluble compounds in synthetic sea water. The latter is introduced into the fuel immediately prior to combustion.

The standard combustor exit nozzle is 2.5 cm in diameter. During initial calibration tests were also made using a 5 cm diameter nozzle. Metal temperatures in the specimen reached 1043°C with maximum cooling air flow.

2.6 BOND STRENGTH

The bond strength of the thermal barrier was determined using the ASTM C633-69 method. The test specimens are shown in Figure 10. Each test specimen is coated with the system under test. Two specimens are then bonded together for each test with a high-strength epoxy adhesive. After curing the adhesive, the specimens are mounted in a tensile testing machine. They are then subjected to a tensile pull to failure at a rate of 0.25 mm/minute.

2.7 COATING TENSILE STRENGTHS

Tensile strength of the coating systems was determined using the fixture shown in Figure 11. A typical specimen is found in Figure 12. The bond coat was applied to a thickness of 0.13 mm and the ceramic to a thickness of 0.25 mm. After coating, the retaining bolt was removed and the specimens were examined for cracking or other flaws. Coating tensile strength was measured by pulling the specimen to failure and calculating the stress required using the failure load and the coating cross-sectional area as determined after test. Crosshead travel during the loading cycle was 0.25 mm/minute.

2.8 TBC TENSILE STRAIN TOLERANCE

The strain tolerance or ability of the TBC's to accept mechanical elongation of the substrate was also determined. The specimens used in this test were standard 6.4 cm tensile bars. The bars were first pulled to provide a slight yield and ensure a uniform loading without bending. Specimens were coated with the TBC and tested at a loading rate of 0.005 mm/mm/minute. The specimens were monitored visually during the test to determine when coating failure occurred.

2.9 AIRFOIL SCREENING TESTS

Prior to coating turbine blades for engine installation, burner rig tests were conducted on airfoil shaped specimens to confirm coating uniformity and reliability of the coatings on non-cylindrical configurations.

The airfoil specimens were nickel-base superalloys B1900 and IN-100. Four TBC systems were tested with NiCrAlY bond coats and these four ceramics: (1) sintered $ZrO_2 \cdot 8Y_2O_3$; (2) fused $ZrO_2 \cdot 8Y_2O_3$; (3) $2CaO \cdot SiO_2$; and (4) $CaO \cdot TiO_2$.

Three TBC samples and a fourth uncoated instrumented sample were tested in a burner rig using clean Diesel No. 2 fuel. The rotating samples were cycled into a 1030° to 1060°C flame (57 minutes in flame, 3 minutes out per hour) each hour to provide thermal shock from a modified 5 cm diameter orifice plate which allowed flame coverage over the full width of each sample.

Thermocouples in an uncoated airfoil bar at locations at the leading and trailing edges indicated surface temperatures of 815° and 670°C, respectively. The variation is believed to be due to the proximity of the leading edge to the combustor exhaust nozzle plate. An optical pyrometer focused on the leading edge indicated a temperature (uncorrected for emissivity) of 860°C on the rotating samples.

After 50 hours of testing the test bars were removed and visually examined for coating spallation. Dimensional measurements were taken at areas where obvious spallation had occurred.

Each sample was sectioned through two areas exposed to the burner rig combustor effluent for determination of coating thickness and integrity.

2.10 BURNER RIG, 1000-HOUR TESTS

The 1000-hour tests were conducted in the same manner as the previous screening tests. They differed in the time of exposure. Ten specimens were installed in each of two test rigs and the two tests were run concurrently. After 697 hours of operation, four specimens in each test were replaced. This gave specimens that had been subjected to 303, 697 and 1000 hours of testing. Evaluation was by visual examination of the specimens during test and metallographic examination upon test completion. Temperature was controlled by optical measurement of the specimen surface temperature and by thermocouples installed in the specimen substrate.

2.11 ENGINE ENDURANCE TESTS

The engine endurance test was performed on first-stage turbine blades. Two blades were coated with each TBC to be evaluated. These blades were then installed in the disc in the normal manner. A 550-hour cyclic accelerated engine life endurance test was run on the test engine. Borescope examination of engine condition was performed every 50 hours with a partial teardown after 150 hours of operation and a complete teardown and evaluation was made at the end of the test run.

This Page Intentionally Left Blank

3

RESULTS OF LABORATORY TESTING

Testing was performed on the four coating arrangements (duplex, triplex, graded and diffused) described previously. Twenty-one coating systems were evaluated. These are reported in Table 3. One concept (reaction sintering and aluminizing) was found to spall excessively during the diffusion treatment. This approach was discontinued early in the program.

3.1 FURNACE CYCLIC TEST RESULTS

The 50-hour furnace cyclic test at 1150°C produced some degree of failure in all of the TBC's. The first specimen, Figure 13, is the baseline coating. The bond coat proved to be 0.19 mm rather than the target 0.23 mm. This discrepancy between direct measurement during coating and that obtained by metallographic sectioning is consistent in these coatings and was allowed for in subsequent coating applications. Coating failure occurred in the zirconia portion adjacent to the ceramic-bond coat interface.

System 1, a graded zirconia-NiCrAlY structure, is shown in Figure 14. A failure occurred in the ceramic face that is not evident in the photograph. A layer of the ceramic top coat spalled during handling after 12 hours of testing. The remainder of the specimen remained intact. The gradual transition from metallic to ceramic phase was not achieved. The ceramic and metallic phases tended to produce layers with the continuity of the metallic phase diminishing as the ratio of ceramic-to-metallic material increased. Overall integrity of the coating was good.

The coating applied to a CoCrAlY bond coat separated in the ceramic phase. Performance was similar to the equivalent NiCrAlY-base coating in System 1.

The graded zirconia-CoCrAlY coating of System 5 evidenced complete loss of the ceramic phase. Only the initial CoCrAlY layer remained. All of the zirconia-containing structure was lost during test.

The coating applied as System 8, zirconia-NiCrAlY, differed from the baseline in that yttrium content of the NiCrAlY was decreased from 0.5 to 0.2 percent. No effect related to the change in yttrium content was observed; loss of the ceramic phase near the metal-ceramic interface occurred as in the baseline coating.

Table 3

Advanced Ceramic Coatings for Industrial Turbine Blades, Vanes and Combustors

	Composition			Structure (Thickness)**		
Coating	Bond Layer	Intermediate Layer	Ceramic Layer	Bond Layer (mils)	Intermediate Layer (mils)	Ceramic Layer (mils)
Baseline	Ni-19Cr-6Al-0 5Y		ZrO_2 $8Y_2O_3$	3 - 5	-	12 - 14
1	Ni-19Cr-6Al-0 5Y	Graded	ZrO_2 $8Y_2O_3$	-	18 - 20	-
2	Ni-19Cr-6Al-0 5Y	Ni-17Cr-20Al-0 4Y * ZrO_2 $8Y_2O_3$	ZrO_2 $8Y_2O_3$	3 - 5	1 - 2	12 - 14
3	Ni-19Cr-6Al-0 5Y	Graded plus Ni-17Cr-20Al-0 4Y * ZrO_2 $8Y_2O_3$	ZrO_2 $8Y_2O_3$	-	18 - 20	-
4	Co-19Cr-6Al-0 8Y		ZrO_2 $8Y_2O_3$	3 - 5	-	12 - 14
5	Co-19Cr-6Al-0 8Y	Graded	ZrO_2 $8Y_2O_3$	-	18 - 20	-
6	Co-19Cr-6Al-0 8Y	Co-18Cr-15Al-0 6Y * ZrO_2 $8Y_2O_3$	ZrO_2 $8Y_2O_3$	3 - 5	1 - 2	12 - 14
7	Co-19Cr-6Al-0 8Y	Graded plus Co-18Cr-15Al-0 6Y * ZrO_2 $8Y_2O_3$	ZrO_2 $8Y_2O_3$	-	18 - 20	-
8	Ni-19Cr-6Al-0 2Y		ZrO_2 $8Y_2O_3$	3 - 5	-	12 - 14
9	Ni-19Cr-6Al-0 2Y	Graded	ZrO_2 $8Y_2O_3$	-	18 - 20	-
10	Ni-19Cr-6Al-0 2Y	Ni-17Cr-20Al * ZrO_2-$8Y_2O_3$	ZrO_2 $8Y_2O_3$	3 - 5	1 - 2	12 - 14
11	Ni-19Cr-6Al-0 2Y	Graded plus Ni-17Cr-20Al * ZrO_2 $8Y_2O_3$	ZrO_2 $8Y_2O_3$	-	18 - 20	-
12	Ni-19Cr-6Al-0 5Y	$MgAl_2O_4$ 33 (Ni-19Cr-6Al-0 5Y)	$MgAl_2O_4$	3 - 5	3 - 5	9 - 11
13	Ni-19Cr-6Al-0 5Y	$MgAl_2O_4$ 33 (Ni-19Cr-6Al-0 5Y) + Ni-17Cr-20Al-0 4Y * $MgAl_2O_4$	$MgAl_2O_4$	3 - 5	3 - 5	9 - 11
14	Co-19Cr-6Al-0 8Y	$MgAl_2O_4$ 33 (Co-19Cr-6Al-0 8Y)	$MgAl_2O_4$*	3 - 5	3 - 5	9 - 11
15	Co-19Cr-6Al-0 8Y	$MgAl_2O_4$ 33 (Co-19Cr-6Al-0 8Y) + Co-18Cr-15Al-0 6Y $MgAl_2O_4$	$MgAl_2O_4$	3 - 5	3 - 5	9 - 11
16	Ni-19Cr-6Al-0 2Y	$MgAl_2O_4$ 33 (Ni-19Cr-6Al)	$MgAl_2O_4$	3 - 5	3 - 5	9 - 11
17	Ni-19Cr-6Al-0 2Y	$MgAl_2O_4$ 33 (Ni-19Cr-6Al) + Ni-17Cr-20Al * $MgAl_2O_4$	$MgAl_2O_4$	3 - 5	3 - 5	9 - 11
18	Ni-19Cr-6Al-0 5Y	$CaTiO_3$ 33 (Ni-19Cr-6Al-0 5Y)	$CaTiO_3$	3 - 5	3 - 5	9 - 11
19	Co-19Cr-6Al-0 8Y	$CaTiO_3$ (Co-19Cr-6Al-0 8Y)	$CaTiO_3$	3 - 5	3 - 5	9 - 11
20	Ni-19Cr-6Al-0 2Y	$CaTiO_3$ (Ni-19Cr-6Al)	$CaTiO_3$	3 - 5	3 - 5	9 - 11
21	Ni-19Cr-6Al	ZrO_2 24MgO 33 (Ni-19Cr-6Al)	ZrO_2 24MgO	3 - 5	3 - 5	9 - 11

* Plasma sprayed coating will be reaction sintered for 4 hours at 1080°C in low activity aluminizing pack to form Ni-17Cr-20Al(Y) bonds with ZrO_2 $8Y_2O_3$ or $MgAl_2O_4$, the bond in case of CoCrAlY will have approximate composition Co-18Cr-15Al-0 6Y

** Where only a single layer is tabulated coating is graded

A graded zirconia-NiCrAlY coating, System 9, was more successful. Except for cracking normal to the surface the coating remained intact. The ytrrium content is lower, otherwise, the coating is equivalent to System 1.

The first of the spinel structures, System 12, incorporated an intermediate layer. The intermediate layer, a spinel-NiCrAlY mixture, separated from the bond coat adjacent to the interface. As in the previous specimens, no evidence of bond coat to substrate failure was observed. The spinel-CoCrAlY three-layer System 14 is one of the few that failed at the bondline rather than in the adjacent ceramic or metal-ceramic structure.

A calcium titanate-CoCrAlY coating (System 19) and a calcium-titanate-NiCrAlY coating (System 20) have remained intact. The CoCrAlY in the intermediate layer developed an intense blue color that diffused through the ceramic portion of this layer. The NiCrAlY analogue was free of discoloration and had a more uniform dispersion of the metallic phase.

Visual appearance of the furnace cyclic test at 1032°C is summarized in Table 4. The overall performance of the TBC's applied to nickel-base bond coats was better than that of those applied to cobalt-base bond coats. The yttria-stabilized zirconia adhered to the nickel-base bond coat but failed within 22 hours when tested on a cobalt-base alloy. Decreasing the yttrium content of the bond coat from 0.8 to 0.5 percent or less was also beneficial in this test. The calcium titanate coatings also proved to be less subject to spallation than the zirconia systems. All of the spinel coatings failed early in the test cycle.

Photomicrographs of some exposed coatings are shown in Figures 15 through 19. In Figure 15 the yttria-stabilized zirconia applied to a NiCrAlY bond coat is shown. No evidence of failure was observed. Oxides are visible at the bond coat-substrate interface. These have been observed in specimens sectioned prior to test and are associated primarily with the deposition process rather than the testing.

A section of the calcium titanate triplex coating is shown in Figure 16. This observed coating has larger pores than the zirconia coating previously shown. The bond coat is also more uniform with less oxide entrapment at the bond-substrate interface. A uniform distribution of the metallic phase was not achieved in the intermediate or transition zone and the coating closely resembles a duplex structure. The same coating system using a CoCrAlY bond coat is shown in Figure 17. Again, there is non-uniform metallic-ceramic distribution in the transition zone. The oxide content of the bond layer is equivalent to that observed in the NiCrAlY bond coats. In Figure 18 the triplex magnesium-zirconate coating is shown. This coating is more porous than either the zirconia or calcium titanate coatings. No evidence of a bond coat is visible. A 500X magnification of the bond/substrate zone is shown in Figure 19. The coating in this area is a mixture of ceramic and metallic phases associated with the intermediate layer. Oxidation attack on the unprotected base metal, MAR-M421, is visible to a depth of 0.02 mm.

Table 4

Visual Appearance of Specimens From Second Screening Test Conducted at 1032°C

Coating System Desig.	Time* (hrs) 5	22	30	50	Description**
Baseline	No effect	Circum-ferential cracks	No change	No change	NiCrAl 0.5Y/8Y_2O_3.ZrO_2 duplex coating
2	No effect	Ceramic spalled			Baseline, as above, but triplex coating
4	Edge chipped	Ceramic spalled			CoCrAl 0.8Y/8Y_2O_3.ZrO_2 duplex coating
6	Edge chipped	No change	Ceramic spalled		CoCrAl 0.8Y/8Y_2O_3.ZrO_2 triplex coating
8	No change	Surface spall	No change	Ceramic spalled	NiCrAl 0.8Y/8Y_2O_3.ZrO_2 duplex coating
10	No change	Edge cracks	No change	No change	NiCrAl 0.2Y/8Y_2O_3.ZrO_2 triplex coating
12	No change	Ceramic spalled			NiCrAl 0.5Y/MgO.Al_2O_3 triplex coating
14	No change	Slight chipping	Ceramic spalled		CoCrAl 0.8Y/MgO.Al_2O_3 triplex coating
16	Surface spall	No change	Edge chip	Ceramic spalled	NiCrAl 0.2Y/MgO.Al_2O_3 triplex coating
18	No change	No change	No change	No change	NiCrAl 0.5Y/CaO.TiO_2 triplex coating
19	No change	No change	No change	No change	CoCrAl 0.5Y/CaO.TiO_2 triplex coating
20	Surface spall	No change	No change	No change	NiCrAl 0.2Y/CaO.TiO_2 triplex coating
21	No change	No change	No change	No change	NiCrAl/ZrO_2.MgO triplex coating

* Time at which specimen removed for examination after start of test and cooled to 93-260°C.

** Duplex coatings have single component base and finish layers. Triplex coatings include an intermediate layer made from a mixture of 35 percent (by weight) bond coat and 65 percent ceramic.

In the third furnace oxidation test at 871°C the exposure time was 100 hours. Photomicrographs of the exposed specimens are seen in Figures 20 through 23. The visual appearance of specimens from this test are summarized in Table 5. As in the previous tests, zirconia and calcium titanate coatings applied to NiCrAlY bond coats were the least affected by the test environment. A photomicrograph of the yttria-stabilized zirconia duplex coating is shown in Figure 20. The ceramic phase is of uniform structure with numerous small voids. A zirconia coated specimen with a CoCrAlY bond coat is shown in Figure 21. This coating system was subjected to the same test as the specimen with the NiCrAlY bond coat in Figure 20. However, the coating using the cobalt bond coat failed after 47 hours of test while similar specimens using a NiCrAlY bond coat were intact after 100 hours of testing. The failure occurred at the bond coat/ceramic interface and resulted in complete loss of the insulating layer.

Table 5

Visual Appearance of Specimens Thermal Cycled at 871°C

Coating System Desig	Time* (hrs)									Description**
	6	23	30	47	50	67	74	90	100	
Baseline	No change	←	←	←	→	No change	Possible crack	No change	No change	NiCrAl 0.5Y/8Y_2O_3 ZrO_2 duplex coating
2	No change	←	←	←	←	←	←	→	No change	Baseline, as above, but triplex coating
4	No change	←	→	No change	Spalled					CoCrAl 0.8Y/8Y_2O_3 ZrO_2 duplex coating
6	Spalled									CoCrAl 0.8Y/8Y_2O_3.ZrO_2 triplex coating
8	No change	←	→	No change	Partial delamination	No change	←	No change	Separated	NiCrAl 0.8Y/8Y_2O3.ZrO_2 duplex coating
10	No change	←	←	←	←	←	←	→	No change	NiCrAl 0.2Y/8Y_2O_3.ZrO_2 triplex coating
12	Slight edge chip	No change	←	→	No change	Cracked & partial separation	No change	No change	Spall	NiCrAl 0.5Y/MgO.Al_2O_3 triplex coating
14	No change	←	→	No change	Co visible on surface	Chipped	Cracked	No change	Spall	CoCrAl 0.8Y/MgO.Al_2O_3 triplex coating
16	No change	←	→	No change	Small spall	No change	←	No change	Spall	NiCrAl 0.2Y/MgO.Al_2O_3 triplex coating
18	No change	←	←	←	←	←	←	→	No change	NiCrAl 0.5Y/CaO.TiO_2 triplex coating
19	No change	←	←	←	←	←	→	No change	Co visible	CoCrAl 0.5Y/CaO TiO_2 triplex coating
20	No change	←	←	←	←	←	←	→	No change	NiCrAl 0.2Y/CaO.TiO_2 triplex coating
21	No change	←	←	←	←	←	←	→	No change	NiCrAl/ZrO_2.MgO triplex coating

* Time at which specimen was removed for examination after start of test and cooled to 93-260°C

** Duplex coatings have single component base and finish layers. Triplex coatings include an intermediate layer made from a mixture of 35 percent (by weight) base alloy and 65 percent ceramic

The appearance of a triplex calcium titanate coating is shown in Figure 22. This coating differs structurally from the zirconia coatings. The zirconia-base coatings tend to have a more uniform dispersion of smaller voids. In contrast, the calcium titanate coatings contain relatively isolated large voids combined with areas that are nearly void-free. The intermediate metal-ceramic layer is visible in the area adjacent to the bondline as a region of dispersed metal particles.

The triplex magnesium zirconate specimen from this series of tests is shown in Figure 23. A continuous void is evident. It was not possible, at the time, to determine if this void developed during test or was the result of damage during specimen preparation. The dispersion of the metallic phase is more uniform in the intermediate layer than that of the specimen (Fig. 18) used in the previous test. This change had no visible effect on coating life.

3.2 FURNACE CORROSION TEST RESULTS

The furnace corrosion tests provided data on the response of the TBC's to various contaminants. Microstructures of coatings subjected to this test are shown in Figures 24 and 25. The triplex calcium titanate coating shown in Figure 24 also incorporated a metal-ceramic intermediate layer to reduce thermal stress on the coating. No evidence of coating attack by the sodium or sulfate ions is evident. The zirconia-base coating, Figure 25, is also intact. The results of the corrosion tests are summarized in Table 6.

Table 6

Destabilization Effect by Selected Elements in a 871°C Furnace Corrosion Test

Coating System	Cubic CaO TiO_2 (%)	Cubic ZrO_2 (%)	Mono-clinic ZrO_2 (%)	Tetra-gonal ZrO_3 (%)
$CaTiO_2$ as-deposited	96-97	-	-	-
$CaO.TiO_2$ + V and S*	84-93	-	-	-
$CaO.TiO_2$ + V, S and P*	83-87	-	-	-
Sintered ZrO_3 as-deposited	-	87	4	9
Sintered ZrO_2. $8Y_2O_3$ + V, S and P*	-	26	64	5
Fused $ZrO_2.8Y_2O_3$ as-deposited	-	89	-	-
Fused $ZrO_2.8Y_2O_3$ + V and S*	-	89	-	-
Fused $ZrO_2.8Y_2O_3$ + V, S and P*	-	50	-	-
$MgO.ZrO_2$ as-deposited	-	79	-	-
$MgO.ZrO_2$ + V and S*	-	12	49	12

* Na plus these elements as were used as corrodents.

Some loss of the cubic structure in the calcium titanate was observed after exposure to salts containing vanadium and sulfur. This amounted to between 4 and 8 percent. Similar data for zirconia-base coatings illustrate the rapidity with which magnesia-stabilized zirconia is attacked when compared with yttria-stabilized zirconia. For the magnesium-zirconate coating the cubic structure dropped from 79 to 12 percent. The monoclinic rose from undetected to 49 percent. The yttria-stabilized zirconia remained stable under the test conditions. The addition of phosphorus to the test affected the performance of some coatings. The calcium titanate coatings retained better than 80 percent (83 and 79%) cubic, which is close to that of previous tests. The magnesium zirconate coating was destabilized as before. The $ZrO_2.8Y_2O_3$ coating deposited from the sintered powder, used as a baseline at the initiation of the program, decreased in cubic phase to 26 percent while an equivalent composition processed from fused material decreased to 50 percent cubic.

3.3 BURNER RIG TEST RESULTS

Four ceramics were burner rig tested, to confirm furnace screening test results, in a 50-hour calibration test. The specimens are shown in Figure 26. The first coating, $ZrO_2.24$ MgO, exhibits severe spallation in the hot zone. In the same figure is the baseline coating $ZrO_2.8Y_2O_3$. The latter specimen is free of spallation and shows no evidence of spallation. The $CaO.TiO_2$ coating system in Figure 26B is also spall-free while all of the $MgO.Al_2O_3$ coating has been lost with spallation occurring at the bond-ceramic interface.

Based on cyclic furnace and burner rig calibration tests, five coating systems were selected for the initial 500-hour burner rig test using a 2.5 cm nozzle.

1. Fused yttria-stabilized zirconia with a NiCrAlY bond coat.
2. Sintered yttria-stabilized zirconia with a NiCrAly bond coat.
3. Calcium titanate with a NiCrAlY bond coat.
4. Calcium titanate with a CoCrAlY bond coat.
5. Calcium titanate with a NiCrAlY bond coat, applied as a multi-layer structure.

The first four coatings were conventional duplex structures using a nominal 0.13 mm bond coat and a 0.31 mm ceramic overlay. The two zirconia coatings differed in that one was plasma sprayed from fused zirconia and the other from a sintered grade. Both cobalt- and nickel-base bond coats were used with the calcium titanate coating. Furnace testing had shown that the nickel-base bond coat gave a more thermal shock-resistant system. This selection was made to determine if the more severe burner rig test would give similar results. The final selection, a graded multi-layer coating, was included for purposes of comparing duplex and more complex structures.

The fuel used in this test was doped to the following levels of contamination in the combustion gases:

V.....50 ppm
Na+K..... 1 ppm
Ca..... 0.5 ppm
Pb..... 0.5 ppm
Mg.....150 ppm

and a 0.5 percent sulfur level was maintained in the fuel. This fuel simulates water washed and treated residual fuel oil. Except for sodium the additives were incorporated as fuel-soluble additives. The sodium content was derived from synthetic sea water emulsified with the oil by a gear pump in the fuel line. The impurity level far exceeds that normally accepted in turbine engine fuels. During test heavy deposits were formed on combustor components, Figures 27 and 28. These deposits interferred with normal combustor operation and frequent stops for disassembly and cleaning were required. Heavy deposits were also formed on the test bars with the heaviest buildup occurring on the cooler area near the specimen holder, as shown in Figure 29.

Test conditions were monitored by a thermocouple installed in an uncoated MAR-M421 specimen. Metal temperature was controlled at an indicated temperature, 871°C, using a 1159°C flame temperature.

A summary of the test results, as indicated by the visual appearance of the test specimens, is given in Table 7. Two burner rig nozzles were used, a 2.5 and a 5 cm, during this test. The change to a 5 cm nozzle was made after 325 hours of operation to increase test severity and reduce problems encountered with fouling of the combustor and subsequent temperature drop. This test was found to be severe and the remainder of the tests used the 2.5 cm nozzle. Due to the heavy deposits from the contaminated fuel, visual evaluation of the test specimens was of limited value. Circumferential cracking was observed in the specimens with a cobalt-base bond coat.

The duplex coated $ZrO_2.8Y_2O_3$/NiCrAlY test bars were checked for crystal structure after 324 hours and 514 hours of test. At 324 hours little change was found, as indicated below:

- fused zirconia 85 percent cubic
- sintered zirconia 81 percent cubic.

However, after an additional 190 hours (514 total) the surface, as determined by X-ray diffracton of the zirconia, was largely destabilized, as given below:

- fused zirconia 50 percent cubic
- sintered zirconia 28 percent cubic.

This determination is limited to a depth of 0.02 mm and does not necessarily indicate change in the bulk of the ceramic coating.

Table 7

Specimens Removed at Completion of First Burner Rig Test
With High Vanadium Fuel

Holder (Mount)	Hours		Coating/Bond[3]	Comments
	2.5 cm Nozzle[1]	5.0 cm Nozzle[2]		
1(882)	210	190	$ZrO_2.8Y_2O_3$ (Fused)/ NiCrAlY	Good retention of dense ceramic with same laminar cracking.
2(907)	0	190	$CaO.TiO_2$/NiCrAlY	Porous ceramic structure with good adherence but openings in ceramic to bond coat.
3(906)	210	190	$CaO.TiO_2$/NiCrAlY	Bond coat thin and irregular. Dense ceramic phase and visible environmental reaction.
4(883)	0	190	$ZrO_2.8Y_2O_3$ (Fused)/ NiCrAlY	Dense adherent ceramic phase.
5(884)	0	190	(Uncoated MAR-M421)	Mild oxidation with visible fuel deposits.
6(908)	325	190	$CaO.TiO_2$/NiCrAlY	Denser than previous ceramics. Bond coat irregular with poor coating retention.
7(909)	325	190	$CaO.TiO_2$/CoCrAlY	Numerous circumferential cracks with dense coating.
8(885)	325	190	$ZrO_2.8Y_2O_3$ (Fused)/ NiCrAlY	Good coating retention with minimal bond coat.
9(886)	210	190	$ZrO_2.8Y_2O_3$ (Sintered)/ NiCrAlY	Porous coating with good retention.

(1) Initial surface temperature 870°C. As combustor fouled temperature dropped to below 730°C.
(2) Surface temperature 920°C.
(3) Coating thickness 0.25 mm, bond coat 0.05-0.1 mm.

In Figure 30 a portion of the specimen duplex coated with a NiCrAlY bond coat and a fused $ZrO_2.8Y_2O_3$ TBC is shown. This specimen was installed after the first 100 hours of burner rig operation, giving it an exposure time of 400 hours. The area shown exhibits a short laminar crack parallel to the bond coat. At this time the overall coating surface is intact. Short, discontinuous separations of this type probably account for the small localized spall areas noted on similar specimens under test.

A duplex $CaTiO_3$/NiCrAlY burner specimen after 190 hours of test (2.5 cm nozzle) is shown in Figure 31. This specimen was installed for the final 190 hours of the test and illustrates the intended coating structure. X-ray diffraction data (0.02 mm penetration) indicates that the surface reaction formed $MgTiO_3$ in the hottest section with a deposit of $Mg_3V_2O_8$ being built up in cooler areas (below 800°C). Although it cannot be distinguished in the photomicrograph, close visual examination of the specimen shows a thin surface reaction zone. EDX analysis confirms that the magnesium and vanadium are retained on the surface and do not penetrate into the bulk of the coating.

A photomicrograph of a duplex $CaTiO_3$/NiCrAlY coating with 400 hours exposure is shown in Figure 32. The coating is denser than that shown in Figure 31 and the bond coat is inconsistent. Metallographic visual examination of this specimen shows a zone 0.02 mm thick of darker material. X-ray diffraction analysis shows this area to be $CaTiO_3$ that has reacted with the fuel impurities to form $MgTiO_3$.

A second fused $ZrO_2.8Y_2O_3$/NiCrAlY duplex system after 400 hours of testing is documented in Figure 33. The section is similar to that shown in Figure 30 with the characteristic small pore structure normally obtained with this ceramic. As in previous specimens, destabilization of the surface was detected by X-ray diffraction but the underlying coating was not.

A section from an uncoated MAR-M421 test bar used for temperature control is shown in Figure 34. A higher magnification photomicrograph of this specimen is given in Figure 35 showing the mild oxidation that has occurred during test. The heavy deposit of $Mg_3V_2O_8$ is evident in this photograph. These tend to insulate the thermocouple, giving low-temperature readings and may also contaminate the thermocouple junction.

In Figure 36 a third $CaTiO_3$/NiCrAlY duplex system is shown. This specimen has had 515 hours of testing. The bulk of the TBC has been lost during test. The coating that remains is denser than normal and exhibits the $MgO.TiO_2$ surface reaction zone previously observed on this material after 400 hours of testing. Some of the coating loss seen in this photograph developed during metallography, as evidenced by the coating particles and voids in the mounting material near the surface of the remaining coating.

The next specimen, Figure 37, is a duplex $CaTiO_3$/CoCrAlY system tested for 515 hours. This coating specimen exhibits delamination, both from the bond coat and within the ceramic phase. Generally, the adherence of the coatings to CoCrAlY bond coats has been less reliable than to NiCrAlY bond coats. It has been observed that the cobalt tends to migrate through the ceramic phase.

In Figure 38 a third duplex fused $ZrO_2.8Y_2O_3$/NiCrAlY specimen is shown. This specimen has been tested for 515 hours. As with the other specimens, areas of coating loss exist. The void or dark area adjacent to the outer coating surface is due to pullout during metallgraphy, indicating loose deposits were on the surface initially that were subsequently lost during the polishing operation. The bond coat is inconsistent circumferentially; thicknesses varied from 0.00 to 0.08 mm. Ceramic retention was not affected by this variation.

The baseline coating, duplex sintered $ZrO_2.8Y_2O_3$/NiCrAlY, is shown in Figure 33 after 400 hours exposure. As with other $ZrO_2.8Y_2O_3$ coatings, destabilization of the surface is indicated by X-ray diffraction. The limited penetration (0.02 mm) of X-ray diffraction makes it impractical to determine the depth and amount of the destabilization.

3.3.1 Second Burner Rig Test

Based upon the results of the first 513 hours of burner rig testing, five coating systems were selected for additional evaluation. These coatings are given in Table 8.

Table 8

TBC's Selected for Second Series of Burner Rig Tests

Bond Coat*	Ceramic Coat**
NiCrAl-0.2Y	Fused $ZrO_2.8Y_2O_3$
NiCrAl-0.8Y	Fused $ZrO_2.8Y_2O_3$
NiCrAl-0.5Y	Sintered $ZrO_2.8Y_2O_3$
NiCrAl-0.5Y	$CaO.TiO_2$
CoCrAlY	$CaO.TiO_2$

* Nominal 0.13 mm
** Nominal 0.25 mm

The first two coating systems were selected for determining the effect of yttrium content in the bond coat. Both used $ZrO_2.8Y_2O_3$ for the ceramic overlay. The third coating employed an intermediate yttrium level in the bond coat. The ceramic phase was plasma sprayed using sintered rather than the fused material of the first two coating systems. The last two coatings employed calcium titanate as the ceramic phase. They differed in that the first incorporated a nickel-base bond coat and the latter a cobalt-base material.

Fuel composition also differed from the previous test, as shown in Table 9 and test conditions in Table 10. The test conditions also differ in that sulfur and sodium levels have been increased while the vanadium content is lower. Magnesium, added in the first test to inhibit attack by vanadium, has been eliminated. The high levels of vanadium and magnesium used in the first test were in excess of fuels generally being considered and heavy deposits fouled combustors and test specimens. Visual inspection and temperature control during the test cycle was difficult and errors may exist due to these deposits.

Table 9

Second Burner Rig Test Fuel Composition

Sulfur	2 percent
Vanadium	2 ppm
Sodium	2 ppm

Table 10

Test Conditions for Second Burner Rig Test

Gas temperature	1066°C
Metal temperature	871°C
Surface temperature	932°C

The specimens and their total exposure time are summarized in Table 11. The initial time to first spallation is also noted. This spallation was the first visual observation of any coating loss. Six specimens were replaced after 2.5 hours of initial operation due to thermocouple failure and massive coating loss due to overheat from erroneous temperature indications.

Table 11

Second Burner Rig TBC's

Specimen Number	Coating	Time to Spall* (hrs)	Total Exposure Time (hrs)
S1-1	NiCrAl-0.2Y/	2.5	2.5
S1-2	Fused $8Y_2O_3.ZrO_2$	17.5	158.7
S1-3		98.5	156.2
S1-4		**	341.5
S1-5		**	341.5
S2-1	NiCrAl-0.8Y/	2.5	2.5
S2-2	Fused $8Y_2O_3.ZrO_2$	2.5	2.5
S2-3		73.6	497.7
S2-4		**	341.5
S2-5		**	341.5
S3-1	NiCrAlY/$8Y_2O_3.ZrO_2$	2.5	2.5
S3-2	(NASA Baseline)	98.5	156.2
S4-1	NiCrAl-0.5Y/	2.5	497.7
S4-2	$CaO.TiO_2$	2.5	2.5
S4-3		73.6	156.2
S4-4		**	341.5
S4-5		10.0	341.5
S5-1	CoCrAlY/$CaO.TiO_2$	2.5	156.2
S5-2		2.5	2.5
S5-3		15.0	497.7
S6-1	Base	NA	341.5

* Defined as first observable coating loss times less 10 hours due to overheat at beginning of test.

** Not discernible - increasingly heavy deposits made it difficult to distinguish between deposit spall and coating spall.

NA Not applicable.

After 76 hours of test the specimens were removed from the flame and examined visually. Specimen metal temperature at this time varied between 749° and 813°C with an average surface temperature of 843°C. The specimen coated with NiCrAl/0.2Y and fused $ZrO_2 \cdot 8Y_2O_3$ was undamaged. The remaining specimens exhibited some spallation.

At 92 hours the specimens were again inspected. Except for a small chip on the tip, no damage was observed in the NiCrAl/0.2Y fused $ZrO_2 \cdot 8Y_2O_3$ specimen. Specimen temperatures were slightly higher, 760° to 832°C metal and 849°C surface, than previously. After 139 hours, testing was stopped and the combustor dismantled, cleaned, inspected and reassembled. The fuel nozzle was found to be clogged with the fuel contaminants which had led to the instability of combustion.

After 159 hours of test, five coated specimens were removed for evaluation. The specimens are shown in Figure 39. The first specimen, duplex fused $ZrO_2 \cdot 8Y_2O_3$/NiCrAl0.2Y, has the section subjected to the burner flame blackened. At the transition zone (flame edge) heavy fuel deposits are evident while in the flame path only a few deposits are evident. Some spallation of the deposits is visible as small whitish areas about 2 mm in diameter.

In the case of the second sample (0.8Y bond coat) heavy deposits are evident in the transition zone and the test area is blackened. Visual examination indicates that greater coating loss has occurred in this specimen than in the specimen using 0.2Y in the bond coat. This difference is not visible in the photograph due to the spallation of the black deposits which masks the areas where coating loss has occurred.

The duplex coated specimen, sintered $ZrO_2 \cdot 8Y_2O_3$/NiCrAl0.5Y, has deposits at the transition zone that appear to be greater than on the two previous specimens. Coating condition was indeterminate due to the fuel deposits and blackened condition of the exposed portion of the specimen that masked coating performance.

The fourth specimen, a duplex coated $CaTiO_3$/NiCrAl0.5Y specimen, also has fuel deposits that mask coating performance. Visual examination indicated that the deposits are heavier than those found on the sintered $ZrO_2 \cdot 8Y_2O_3$ specimens.

The fifth specimen is a duplex coating of $CaTiO_3$/CoCrAlY. As in previous tests, the cobalt-base bond coat was less effective than the nickel-base analogue. Its visual appearance indicated that coating loss rather than deposit buildup has occurred near the transition zone.

In all five specimens, visual examination of the specimens during test was of limited value. Fuel deposits and blackening of the specimens made it impractical to establish coating loss. This was done later on metallurgical specimens. The specimens removed at 159 hours were replaced for the remainder of the test with duplex-coated spcimens using $ZrO_2 \cdot 8Y_2O_3$ and $CaTiO_3$ ceramic coatings applied to NiCrAlY base coats.

The appearance of pairs of specimens at the completion of the 932°C burner rig test are shown in Figure 40. In the first pair the appearance of the fused $ZrO_2 \cdot 8Y_2O_3$ N-CrAl0.2Y shows heavy fuel deposits on the surface as well as small, light areas where the deposits have separated from the coating. The TBC has remained intact for 314 hours.

Next is an uncoated specimen and one with a fused $ZrO_2 \cdot 8Y_2O_3$/NiCrAl0.8Y exhibit fuel deposits and, except for the larger diameter of the coated bar, the specimens appear to be equivalent with no observable loss of coating on the TBC specimen.

The next pair of specimens are both fused $ZrO_2 \cdot 8Y_2O_3$/NiCrAl-0.8Y coatings after 341 hours of test. As with the previous coatings, no major coating loss has occurred. Shown next are $CaO \cdot TiO_2$ coated specimens that are intact. However, heavier fuel deposits were developed than were found on the $ZrO_2 \cdot 8Y_2O_3$ coatings. Next, a $CaO \cdot TiO_2$ coating with a CoCrAlY bond coat is compared with a NiCrAlY-base coating tested for 341 hours. The NiCrAlY is intact with heavy fuel deposits, while the specimen with the CoCrAlY bond coat is spalled to the bond coat/ceramic interface.

Metallurgical sections were taken 6 mm from the tip of three specimens coated with $ZrO_2 \cdot 8Y_2O_3$. The specimens had bond coats ranging from 0.2 to 0.8 percent yttrium (Figs 41, 42 and 43). One specimen was exposed for 497 hours and two were exposed for 341 hours. No effect resulting from changing the bond coat yttrium level was observed. The specimens exposed for 341 hours had no fractures while the 497-hour specimens had fractures parallel to the surface.

In Figure 44 the $CaO \cdot TiO_2$/NiCrAl-0.5Y coating is shown. The coating has larger pores than the zirconia-base system. The surface is also more irregular than the zirconia specimen subjected to the same test. The effect of using a CoCrAlY bond coat with this TBC is shown in Figure 45. Spallation of the ceramic occurred early.

3.3.2 Third 500-Hour Burner Rig Test

The third 500-hour burner rig test was initiated using the following test parameters:

Flame temperature - 1010°-1093°C
Specimen surface temperature - 793°C
Fuel - Diesel No. 2
Fuel additive - Synthetic sea salt (3 ppm)

These conditions are those used previously for an in-house materials development program. The fuel simulated a clean fuel with accelerated sea salt ingestion and the sample temperature was that at which a high rate of attack had developed on superalloys being tested at Solar for use in turbine hot components.

Ten MAR-M421 hollow bar specimens were put into test. These are listed below:

System	Bond Coat (0.13 mm)	Finish Coat (0.25 mm)
1	Ni-19Cr-6Al-0.2Y	$ZrO_2 \cdot 8Y_2O_3$
2*	"	"
3	Ni-19Cr-6Al-0.8Y	"
4*	"	"
5	Ni-19Cr-6Al-0.2Y	$CaO \cdot TiO_2$
6*	"	"
7	Ni-19Cr-6Al-0.8Y	"
8*	"	"
9	Ni-19Cr-6Al-0.5Y	None
10	None	"

* Polished ceramic surface

The eight TBC's tested used bond coats with two levels of yttrium, 0.2 and 0.8 percent, and two ceramic compositions, $ZrO_2 \cdot 8Y_2O_3$ and $CaO \cdot TiO_2$. One NiCrAlY coated specimen was installed without the ceramic overlay and an uncoated bar was included as a control.

The coatings tested were applied by plasma spray to a nomimal thickness of 0.13 mm (0.005") for the bond coat and 0.25 mm (0.010") for the ceramic overlay. After coating, one specimen of each composition was hand polished on the outer surface after plasma spray to provide a smooth outer surface.

After 175 hours of exposure six specimens, listed below, were removed for examination:

MAR-M421 control bar
NiCrAlY coated bar
NiCrAl-0.2Y/$ZrO_2 \cdot 8Y_2O_3$ duplex coated bar
NiCrAl-0.8Y/$ZrO_2 \cdot 8Y_2O_3$ duplex coated bar
NiCrAl-0.2Y/$CaTiO_3$ duplex coated bar

There was limited hot corrosion of the control bar. Some corrosion, as shown in Figure 46, developed during test but overall attack was less than anticipated.

During the test heavy deposits were formed on the specimens, Figure 47. A NiCrAlY/$ZrO_2 \cdot 8Y_2O_3$ duplex coated specimen is shown after removal from the rig. The heavy deposits developed separated from the underlying ceramic coating during removal from the test rig.

In Figure 48 a photomicrograph of the specimen is presented, polished and duplex coated with NiCrAlY/$ZrO_2 \cdot 8Y_2O_3$. The coating was not affected by the test conditions and is free of the circumferential cracking observed in other test specimens.

Another polished specimen, duplex coated with NiCrAlY/$CaTiO_3$, is presented in Figure 49. This coating also remained stable throughout the test. No cracks were observed that could be attributed to thermal stresses developed during the first 175 hours of evaluation. During metallographic preparation of the specimens it was observed that the $CaTiO_3$ coating was weaker than the $ZrO_2 \cdot 8Y_2O_3$ coating and more susceptible to mechanical damage, such as pullout.

The specimens at 175 hours were replaced with similar test bars and the 500-hour burner rig endurance test was continued. At this time the test temperature was raised 56°C (specimen surface 849°C) to increase the rate of hot corrosion and overall test severity.

A second change in test conditions was made after 400 hours of testing. The uncoated MAR-M421 specimen installed at 175 hours was removed and sectioned for metallurgical examination. Very little hot corrosion had occurred. A new base control specimen was installed and the specimen test temperature was increased an additional 56°C to 905°C for the final 100 hours of testing.

At completion of the 500-hour test all of the remaining specimens were removed for metallurgical examination. This provided specimens with nominal 335 and 500 hours exposure in addition to the 175-hour specimens previously replaced.

All of the $ZrO_2 \cdot 8Y_2O_3$ specimens exhibited a similar appearance and structure after testing. A typical example after 335 hours of test is shown in Figure 50. The as-tested bar has moderate deposits from the fuel contaminants. The coating structure is intact, as shown in the photomicrograph, except for some radial cracking. The radial cracking was only observed on one specimen and was limited to approximately one-fourth of the total circumference. A similar section taken from a test system ($ZrO_2 \cdot 8Y_2O_3$) after 500 hours of testing is shown in Figure 51. This specimen has a slightly less dense structure and is free of cracks. The small change in structure may account for the improved crack resistance of the second specimen.

As was the case with the $ZrO_2 \cdot 8Y_2O_3$ coating, all of the $CaO \cdot TiO_3$ coatings gave similar results. The variation in yttrium in the bond coat did not measurably affect performance. A typical specimen ($CaO \cdot TiO_2$) is presented in Figure 52 after 500 hours of testing. The surface deposits are slightly heavier than those observed with the $ZrO_2 \cdot 8Y_2O_3$ specimens. The majority of the coating is intact although local cracked areas did develop, as shown in Figure 53. Generally, the results of the 500-hour burner rig test indicated that both the $ZrO_2 \cdot 8Y_2O_3$ and $CaO \cdot TiO_2$ coatings warranted further development.

An uncoated specimen run for 100 hours at 905°C, Figure 54, exhibited surface oxidation to a depth of 0.025 mm and typical evidence of internal sulfidation extending for an additional 0.025 mm. None of the TBC specimens exhibited a similar penetration at the conclusion of the test.

3.4 BURNER RIG AIRFOIL SCREENING TEST RESULTS

As noted earlier, burner rig airfoil tests were conducted to determine the effect of part geometry on coating performance. Table 12 summarizes the results of these tests and Figure 55 presents typical specimens. A typical cross section is shown in Figure 56.

The TBC's, based on sintered $ZrO_2.8Y_2O_3$, tended to develop separations in the ceramic approximately 0.02-0.07 mm from the bond coat. These paralleled the substrate surface and were not evident on the exterior surfaces. The fused $ZrO_2.8Y_3O_3$ specimens tended to crack in a more nearly radial direction. Spallation was observed with these specimens at both the leading and trailing edges. Cracking was normal, in most instances, to the bondline and little spallation occurred. A representative structure with this type of crack was shown in Figure 50. Some radial cracks were developed during the deposition process, as shown. Subsequent examination of the specimens after burner rig testing did not establish any relationship between these initial cracks and coating life.

The most successful coating in this test was $2CaO.SiO_2$. No evidence of coating failure was observed. After testing, metallurgical sections showed an adherent crack-free coating.

The photomicrograph in Figure 56 illustrated some of the problems encountered in plasma spraying these specimens. The coating is flawed in two locations; one is near the leading edge. The appearance indicates that the coating application was initiated at this point. Overlap is visible and an irregularity appears at this point. On the trailing edge an uncoated area is visible. Variations in coating thickness are also evident with the maximum thickness being developed on the trailing suction face and the minimum at the center of the pressure face. Ceramic thickness also varied on individual specimens over the range of 0.23 to 0.30 mm. A thickness of 0.25 $\pm$0.02 mm was selected for ceramic coating thickness on test engine blades.

3.5 BURNER RIG 1000-HOUR ENDURANCE TEST

The first burner rig endurance test used the following test parameters:

Fuel	Diesel No. 2
Fuel/air ratio	0.020
Flame temperature	1204°C (2199°F)
Substrate temperature	927°C (1700°F)
Surface temperature	1038°C (1900°F)
Nozzle diameter	2.5 cm

The ten coated specimens listed in Table 13 were installed. Calcium titanate and fused yttria-stabilized zirconia were applied to MAR-M421, Hastelloy X and X-45M substrates. Sintered yttria-stabilized zirconia and calcium titanate were applied to MAR-M421. One MAR-M421 bar was left uncoated. These coatings are shown in Figures 57 to 61 after the 1000-hour endurance test.

Table 12

Summary of Metallographic Examination of Coated Airfoil Bars Exposed to 50-Hour Burner Rig Testing at 815°C Leading Edge

Sample (Mount Number)	Coating	Location From Tip (mm)	Appearance
3-7 (917)	Sintered $ZrO_2.8Y_2O_3$	25	Circumferential crack through ceramic just above bond coat around trailing edge and covering over 40% of convex surface. Circumferential cracks around leading edge and continuing over 40% of concave surface.
		12	Circumferential crack at leading edge No crack in concave surface except small area towards trailing edge. Crack at trailing edge and convex surface with crack covering over 75% of convex surface.
3-1 (914)	Sintered	25	Crack appearing to start at concave side of trailing edge and continuing around trailing edge. Coating removed, popped off or very thin at concave side, trailing edge.
		12	Small amount of ceramic removed off of convex side, leading edge crack through ceramic on concave side by trailing edge and through trailing edge.
2-7 (915)	Fused $ZrO_2.8Y_2O_3$	12 & 25	Ceramic intact on concave surfaces, off at convex, trailing and leading edges.
3-5 (916)	$CaO.TiO_2$	12	Ceramic spalled off trailing edge, also on concave surface near trailing edges where bond coat thickness reached 0.3 mm.
		25	Crack through ceramic normal to bond coat at leading edge. Ceramic spalled off at trailing edge.
2-5 (913)	$CaO.TiO_2$	12	Ceramic has spalled off of leading and trailing edges.
		25	Ceramic at trailing edge cracked but intact. Spalled at leading edge.
2-1 (912)	$CaO.TiO_2$	12 & 25	Ceramic spalled from trailing edge and small area at leading edge.
102 (974)	Sintered ZrO_2	12	Interconnecting porosity, parallel to bond coat, circumferential crack on convex surface, trailing edge and over 40% of concave surface.
1-4 (975 & 976)	$2CaO.SiO_2$	12 & 25	Uniform bond coat and ceramic. No cracks. (NASA)

Table 13

Initial Test Specimens for 1000-Hour Endurance Test

Specimen	Base Metal	Bond Layer	Ceramic Layer
HX-1	Hastelloy X	Ni-19Cr-6Al-0.2Y	$CaO.TiO_2$
HX-2	Hastelloy X	Ni-19Cr-6Al-0.2Y	$ZrO_2.8Y_2O_3$
MM-2	MAR-M421	None	None
MM-4	MAR-M421	Ni-19Cr-6Al-02Y	None
MM-5	MAR-M421	Ni-19Cr-6Al-0.2Y	$CaO.TiO_2$
MM-6	MAR-M421	Ni-19Cr-6Al-0.2Y	$ZrO_2.8Y_2O_3$
NA-4	MAR-M421	Ni-14.3Cr-14.3Al-0.16Y	$ZrO_2.8Y_2O_3$
NA-6	MAR-M421	Ni-14.3Cr-14.3Al-0.16Y	$2CaO.SiO_2$
XM-2	X-45M	Ni-19Cr-6Al-0.2Y	$ZrO_2.8Y_2O_3$
SM-3	X-45M	Ni-19Cr-6Al-0.2Y	$CaO.TiO_3$

Metallurgical specimens were prepared from each test bar after test. In most cases the visual examination made during test was found to be unreliable since coating appearance was obscured by the fuel deposits. Figure 62 is a photomicrograph of the MAR-M421 specimen coated with NiCrAlY at the completion of the test. The NiCrAlY bond coat has been severely attacked and oxide penetration has occurred to a depth of 0.13 mm. In some areas oxidation of the NiCrAlY has led to loss of the coating. In Figure 63 the baseline $ZrO_2.8Y_2O_3$ TBC is shown after test. Approximately half of the ceramic coating thickness has been lost during test. A separation of the ceramic overlay from the bond coat is also visible. However, the attack on the substrate observed in the NiCrAlY coated specimen has not occurred. A MAR-M421 specimen coated with calcium silicate is shown in Figure 64. The retained ceramic is approximately 0.19 mm thick. The structure has less visible porosity than the $ZrO_2.8Y_2O_3$ specimen. A separation has occurred between the bond coat and the ceramic, as occurred with the $ZrO_2.8Y_2O_3$.

The cobalt-base alloy X-45M specimen with a $ZrO_2.8Y_2O_3$ TBC, is shown in Figure 65. The ceramic coating was lost early in the test and severe degradation of the substrate has occurred. The small amount of retained bond coat is fully oxidized, as is the X-45M. A specimen of MAR-M421 coated with the same $ZrO_2.8Y_2O_3$ TBC is shown in Figure 66 for comparison. This specimen provided the best resistance. The ceramic phase is free of cracks and no degradation of the substrate or bond coat has occurred. A second specimen after test retained 50 percent of the ceramic coating. The bond coat was not affected.

In these tests performace of calcium titanate coatings were similar to that of the zirconia coatings. The X-45M specimen, Figure 67, shows severe oxidation. None of the bond coat is visible as a discrete phase. A heavy oxide

layer has developed on the substrate and the coating has separated at the ceramicmetal interface. Numerous cracks have developed in the TBC and in some areas a total loss of coating has occurred. The coating performance on this alloy is similar to that previously observed with CoCrAlY bond coats.

3.6 BURNER RIG 1000-HOUR CORROSION TEST

This test differs from the test reported in Section 3.5 in that the substrate temperature was reduced to 816°C and the fuel was doped with an aqueous solution of sulfate and synthetic sea salt to produce the following levels of corrodents: sulfur - 0.5-1.0 percent; sodium - 5 ppm.

The specimens tested are given in Table 14. Two evaluations were made of each specimen. During and after test the specimens were examined visually. At the completion of the test a metallurgical section was made of each specimen. The visual examination was obscured by deposits of salt and unburned fuel residues deposited on the specimens. Spallation of these deposits could not be readily distinguished from loss of TBC. The external appearance of the specimens is shown in Figure 68. Figures 69 through 74 are photomicrographs of representative sections.

Table 14

Material Systems Evaluated in Corrosion Endurance Test

Specimen Number	Substrate	Bond Coat	Ceramic
MM-1	MAR-M421	-	-
MM-3	MAR-M421	NiCrAlY	-
MM-9	MAR-M421	NiCrAlY	$CaO.TiO_2$
MM-10	MAR-M421	NiCrAlY	$ZrO_2.8Y_2O_3$
NA-1*	MAR-M421	NiCrAlY	$ZrO_2.8Y_2O_3$
NA-5*	MAR-M421	NiCrAlY	$2CaO.SiO_2$
HX-6	Hastelloy X	NiCrAlY	$CaO.TiO_2$
HX-7	Hastelloy X	NiCrAlY	$ZrO_2.8Y_2O_3$
XM-4	X-45M	NiCrAlY	$CaO.TiO_2$
XM-5	X-45M	NiCrAlY	$ZrO_2.8Y_2O_3$

Two of the coatings, NA-1 and NA-5, were baseline TBC systems and are shown in Figure 68. The two Hastelloy X specimens, coated with $CaO.TiO_2$ and with $ZrO_2.8Y_2O_3$, have lost all of the ceramic coating. A typical metallurgical section of the coated Hastelloy X specimen is shown in Figure 69. The NiCrAlY

bond coating has been retained but oxidation is evident while the ceramic coating is in good condition. Combustion deposits have been retained to a thickness of approximately 0.6 mm.

X-45M specimens with the same TBC's had less spallation. However, heavy deposits were formed that gave the appearance of a spalled TBC. Figure 70 shows the bond coat and coating intact.

The bare MAR-M421 specimen and the specimen coated with NiCrAlY are severely oxidized, as shown in Figure 71. The calcium titanate TBC after test is shown in Figure 72. Some cracking is visible but the overall coating is intact. The MAR-M421-$ZrO_2 \cdot 8Y_2O_3$ baseline system is shown in Figure 73. Coating separation developed near the ceramic-bond coat interface. Bond coat oxidation was also greater than that of the calcium titanate TBC.

The MAR-M421-calcium siicate baseline TBC is shown in Figure 74. The ceramic coating has been lost and the NiCrAlY bond coat is severely oxidized. Slight evidence of the ceramic coating is visible at the ceramic-bond coat interface.

3.7 TBC BOND STRENGTH TEST RESULTS

The following average results for TBC adhesive strength at room temperature were obtained based on six tensile tests:

	Bond Strength
$ZrO_2 \cdot 8Y_2O_3$/NiCrAlY	61.9 MPa
$CaO \cdot TiO_2$/NiCrAlY	30.5 MPa

Coating failure developed in the ceramic-bond coat interface area.

3.8 TBC TENSILE STRENGTH

Tests were conducted on bond coated specimens with and without the ceramic overlay. It was found that the load required to fail the bond coat was equal to that required to fail the specimens with the TBC. Close examination indicated the ceramic failed in tension prior to bond coat failure. The TBC system fractured at an average load of 88,425 Pa for all specimens. After test, all of the specimens were found to exhibit uniform fracture.

3.9 TBC STRAIN TOLERANCE

Twelve Hastelloy X specimens were tested. All had NiCrAlY bond coats with six zirconia-8% yttria overlays and six calcium titanate overlays.

Target coating thicknesses were 0.13 mm for the bond and 0.25 mm for the ceramic overlay.

Visual examination at 100X for cracking or spalling was used to determine coating tensile strain limits. The calcium titanate was found to be the more strain-tolerant of the two coating systems. Visible evidence of cracking for the titanate coating, occurred at 10 percent total tensile strain while the zirconia TBC failed at an average value of 0.5 percent total tensile strain. In all cases the cracks were in the form of parallel circumferential cracks, as shown in Figure 75.

Further stressing of the coatings resulted in spallation. This occurred at 1.4 percent total tensile strain for the zirconia coatings and 1.7 percent for the calcium titanate coating. A typical spallation is shown in Figure 76. Both coatings remained adherent throughout the tensile specimens elastic limits, although cracks developed in the ceramic coating.

4

ENGINE TEST OF THERMAL BARRIER COATINGS

Engine testing of TBC's was incorporated into the program as a separate item to verify laboratory test results with a practical demonstration. Eight TBC first-stage turbine blades were subjected to engine test. This was a development accelerated life endurance test of the Mars engine encompassing operation on liquid and gaseous fuels with at least one stop-start cycle every 24 hours of operation.

4.1 ENGINE TEST PROCEDURE

Four TBC systems were run in a 550-hour engine endurance test. Each TBC listed in Table 15 was applied to two Mars firststage turbine blades. Coating thicknesses are target values; true thicknesses could not be determined prior to test. Post-test measurements were not considered reliable since coating loss might have occurred during operation. The eight coated blades were installed in pairs at 90-degree spacings.

The spacing and pairing of the blades was selected to minimize rotor imbalance due to possible loss of the coatings. Calculation of coating weight effects indicated that 100 percent ceramic coating loss from more than two adjacent blades would exceed the design values for rotor imbalance at maximum operating speed. In addition, positioning the blades with identical (e.g., fused $ZrO_2 \cdot 8Y_2O_3$) coatings at 180-degree intervals further reduced the probability of imbalance due to coating loss since equivalent coatings were expected to provide similar weight losses in the event of failure by a given TBC under test. Cooling airflow for coated and uncoated blades was maintained at the design level, as established by flow checking, to further guard against problems generated by coating failure. Engine conditions during test are given in Table 16. During test an optical pyrometer was used to monitor blade temperature. The resulting data indicated that TBC's increased the average surface temperature 83°C. The increase in surface temperature was attributed to the insulative effect of the TBC's. As the heat flow through the blade is reduced, a greater temperature gradient is developed. As a result, the surface temperature of the blade more nearly approaches that of the gas stream and the internal surfaces tend toward that of the cooling air. A simplified thermal model is presented in the analytical section. Quantitative values for thermal gradients cannot be made at this time since coating variables, i.e., the amount and effect of porosity, interfacial thermal resistance, etc., are not known.

Table 15

TBC's Applied to First-Stage Turbine Blades

Composition	Thickness (cm)	Composition	Thickness (cm)	Source
Ni-14Cr-14Al-0.2Y	0.013	$2CaO.SiO_2$	0.025	NASA
Ni-14Cr-14Al-0.2Y	0.013	$ZrO_2.8Y_2O_3$	0.025	NASA
Ni-19Cr-6Al-0.2Y	0.013	$CaO.TiO_2$	0.025	Solar
Ni-19Cr-6Al-0.2Y	0.013	$ZrO_2.8Y_2O_3$	0.025	Solar

Table 16

Mars Cyclic Endurance Engine Test

Duration: Calibration Run	50 hours 500 hours
Rotor inlet temperature	1010° to 1113°C
Blade thermal cycle (surface)	316° to 910°C (hot restart)
Blade temperature (bulk)	810°C (maximum)
Blade tip speed	427 mps
Tip shoe rub depth (design)	0.76 mm
Restarts (hot or cold)	Every 24 hours
Time to maximum blade temperature	Cold, 120 secs; hot, 50 secs.
Inspection	50, 100, 250 and 550 hours
Fuel	50% diesel, 50% natural gas

4.2 CALCIUM SILICATE TBC BLADE TEST RESULTS

The overall appearance of the calcium silicate TBC blade after engine test is shown in Figure 77. Three types of coating loss were observed. On the pressure face, spallation occurred to a maximum distance from the tip of 0.96 cm (0.38"). The spalled area approximates that of the region of maximum thermal stress (exclusive of leading edge) on the blade surface. The fracture edges are clean and sharp to the bond coat, indicating that the full coating thickness was lost through spallation late in the engine test. The bond coat is fully exposed, retaining only a few embedded ceramic particles rather than the thin layer frequently observed in spalled coatings from burner rig test.

Coating loss on the leading edge of the blade appears to be a combination of erosion and spallation. A photomicrograph of the leading edge cross section 0.64 mm (0.25") from the tip is shown in Figure 78. On the pressure side the edge of the coating is tapered, indicating that erosion may have occurred after the initial coating loss. A small spalled area, possibly lost during specimen preparation, is also evident, as is the initiation of a crack in the ceramic near the bond coat.

The third area of coating loss was at the blade tip, suction side. This loss appears to have been initiated by tip rub. The loss is limited and occurred to some degree in all coated blades. The test engine was assembled to tolerances that would intentionally generate rub between the blade tips and the solid tip shoes. During rub, metal temperatures at the tip approached the melting point. Coating loss in this region is unavoidable as the substrate is deformed to provide tip clearance. A minor defect, a local area with insufficient bond coat, is also apparent in Figure 78. This defect is probably the junction point of the pressure face-suction face bond coats. This variation, along with the adjacent heavier bond coat, is the result of first-time manual spraying of a complex shape.

In Figure 79 a higher magnification of the leading edge and bond coat structure is seen. The laminar appearance is typical of plasma sprayed coatings. No evidence of ceramic retention was observed in this area.

A typical photomicrograph of the retained calcium silicate coating is shown in Figure 80. This section was taken of the pressure face 0.64 cm (0.25") from the blade tip. A dot map of the calcium concentration is included. The calcium concentration was not affected by the test. Near the exposed surface a crack parallel to the surface has developed. It is believed that this fracture occurred during sectioning since coating loss would be expected if it were present during engine operation. Of greater significance are the microcracks perpendicular to the surface. These may serve to reduce the thermal stress during engine operation.

4.3 SINTERED $ZrO_2 \cdot 8Y_2O_3$ TBC BLADE TEST RESULTS

In Figure 81 the appearance of a sintered $ZrO_2 \cdot 8Y_2O_3$ TBC blade is shown. Spallation is largely confined to the leading edge area. On the pressure side coating loss is bounded by a clean fracture, indicating failure by spallation. On the suction side the coating feathers out to expose bond coat, indicating coating loss early in the test through spallation or a continuous erosion in this area. The sintered zirconia coating is free of the large spalled area observed on the pressure face of the calcium silicate coated blade.

A thin layer of the ceramic overcoat was retained on the leading edge of this blade, as seen in Figure 82. The bond coat exhibits the same variation in thickness as the previous blade, with the greater thickness being on the pressure side of the leading edge. The zirconia coating is slightly more porous than the calcium silicate coating.

A photomicrograph taken at the leading edge 0.64 cm (0.25") from the tip is shown in Figure 83. As mentioned previously, some evidence of ceramic retention is visible. In comparison of the bond coat structure shown in Figures 79 and 82, the bond coat used with the $2CaO \cdot SiO_2$ coating appears to be more oxidized than the bond coat used with the zirconia coating.

A typical coating section is shown in Figure 84. The laminar crack is believed to have developed during specimen preparation. The coating is somewhat more porous in the vicinity of the bond coat than it is near the exposed surface. This characteristic was also observed with the $2CaO \cdot SiO_2$ coating. Whether this variation in porosity developed during coating application or is the result of the test environment could not be determined.

4.4 CALCIUM TITANATE TBC BLADE TEST RESULTS

A calcium titanate TBC blade is shown in Figure 85. Coating loss was primarily in the leading edge area where a combination of spallation and erosion occurred. One blade (shown) had a limited spall at the trailing edge cooling holes. Exposed coating edges are rounded to a greater degree than the previous blades, indicating that significant erosion may have occurred during test. A scan was made for calcium content in the coating. No evidence of calcium depletion was observed, as is evident in the dot map of Figure 86.

A section taken 0.64 cm (0.25") from the tip, Figures 87 and 88, show some ceramic to have been retained in this area. In Figure 87 the variation in coating thickness from the leading edge to the suction face is visible. Figure 88 is a photomicrograph taken at the tip of the leading edge.

Problems encountered with manual spraying are evident. In this area the bond coat is extremely thin, well below acceptable limits. The coating also exhibits an abnormal fused structure of the type developed where excessive heat is applied during deposition due to a slow traverse rate or insufficient

cooling. These conditions result in excessive coating stress, as is indicated by the numerous cracks. Some coating was retained in spite of the numerous fractures, indicating that the cohesive strength of the coating is high. A more typical coating section is shown in Figure 89. This section was taken approximately 0.25 cm (0.1") from the leading edge on the pressure face. Some microcracking is evident, but the massive laminar cracks observed on the leading edge are absent. Coating integrity has been maintained and an adequate bond coat was applied. A calcium concentration dot map, Figure 90, of this section does not show the calcium depletion observed in burner rig test bars.

4.5 FUSED $ZrO_2 \cdot 8Y_2O_3$ TBC BLADE TEST RESULTS

A fused $ZrO_2 \cdot 8Y_2O_3$ TBC blade is shown in Figure 91. This blade had minimal coating loss. The exposed bond coat is limited to the tip of the leading edge. A small spalled area is located in this position. A photomicrograph of the leading edge, 0.64 cm (0.25") from the tip, is shown in Figure 92. The TBC has spalled off, leaving only the bond coat in this area. A metallographic section showing the bond coat is included as Figure 93. A few particles of the ceramic overlay have been retained. As was the case with the previous blade, the bond coat is thin in this area.

A more representative coating section after test is shown in Figure 94. This section was taken from the pressure face approximately 0.25 cm (0.1") behind the leading edge. It possesses a uniform structure and bond coat. No evidence of coating deterioration due to engine test is visible.

This Page Intentionally Left Blank

5

ANALYTICAL EVALUATION OF THERMAL BARRIER COATINGS

During the program various analytical studies were performed. These were related to the stresses developed during TBC deposition and the effects on engine performance.

5.1 STRESSES IN TBC's DUE TO DEPOSITION VARIABLES AND FLAWS

The approximate physical condition of the plasma sprayed TBC is shown in Figure 95. The bond coat is thin and conforms to the substrate. Its effects may be neglected in this calculation.

At the instant the plasma sprayed oxide adheres rigidly to the surface (effective bond temperature) the strain must necessarily be zero. However, with any change in temperature from the effective bond temperature, a strain will develop due to the difference in the coeffiient of thermal expansion between the oxide and the MAR-M421.

The coefficient of thermal expansion is defined as

$$\alpha = \frac{d\ell}{L_o dT} \quad \text{or} \quad = \frac{\Delta L}{L_o \Delta T}$$

where L^o is a reference length usually taken at room temperature (21°C). However, the zero strain temperature is well above room temperature.

Therefore, starting with

$$\frac{\Delta L}{L_o} = \alpha \Delta T$$

it is necessary to convert L_o to L_{SF} (i.e., L is stress-free). Let the superscript $^{(1)}$ identify the oxide and the superscript $^{(2)}$ identify the substrate (MAR-M421).

At the stress-free temperature T_{SF}

$$\alpha^{(1)} = \frac{L_{SF}^{(1)} - L_o^{(1)}}{L_o^{(1)} \times (T_{SF}-21)}$$

$$\text{and} \quad \bar{\alpha}^{(2)} = \frac{L_{SF}^{(2)} - L_o^{(2)}}{L_o^{(2)} \ (T_{SF}-21)}$$

where $\bar{\alpha}$ is the average coefficient of thermal expansion from room temperature (21°C) to T_{SF}. Since $L_{SF}^{(1)} = L_{SF}^{(2)} = L_{SF}$, this leads to

$$L_o^{(1)} = \frac{L_{SF}}{\bar{\alpha}^{(1)} \times (T_{SF}-21) + 1}$$

$$\text{and} \quad L_o^{(2)} = \frac{L_{SF}}{\bar{\alpha}^{(2)} \times (T_{SF}-21) + 1}$$

This allows an L_{SF} to be defined, from which the appropriate L_o may be calculated.

Because the strain induced in the materials comes about from a relative change in dimension between the TBC and the substrate, it is necessary to determine this difference. This can be done from the equation:

$$\Delta L_{(T_{SF} \rightarrow T)} = \Delta L_{(21 \rightarrow T)} - \Delta L_{(21 \rightarrow T_{SF})}$$

since the data on coefficients of thermal expansion refer to 21°C:

$$\frac{\Delta L^{(1)}_{(T_{SF} \rightarrow T)}}{L_o^{(1)}} = \frac{\bar{\alpha}^{(1)} \times (T-21)}{L_o^{(1)}} - \frac{\bar{\alpha}^{(1)} \times (T_{SF}-21)}{L_o^{(1)}}$$

$$\text{and} \quad \frac{\Delta L^{(2)}_{(T_{SF} \rightarrow T)}}{L_o^{(2)}} = \frac{\bar{\alpha}^{(2)} \times (T-21)}{L_o^{(2)}} - \frac{\bar{\alpha}^{(2)} \times T_{SF}-21)}{L_o^{(2)}}$$

Assuming the TBC and the substrate are not attached, thus allowing them to expand or contract independently. The new dimension at temperature T will be:

$$L^{(1)} = L_{SF} + \Delta L^{(1)}_{(T_{SF} \longrightarrow T)}$$

$$\text{and} \quad L^{(2)} = L_{SF} + \Delta L^{(2)}_{(T_{SF} \longrightarrow T)}$$

Now, it is necessary to re-attach the TBC to the substrate. The total strain will be the relative difference in dimension between the TBC and the substrate, i.e.:

$$\epsilon_T = \frac{L^{(2)} - L^{(1)}}{L^{(2)}}$$

The strain can be positioned between the two materials as follows.

Prior to re-attaching the material the situation is:

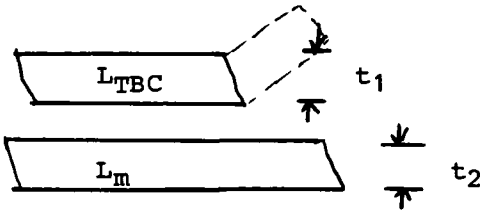

In order to re-attach, the forces $F^{(1)}$ and $F^{(2)}$ are required:

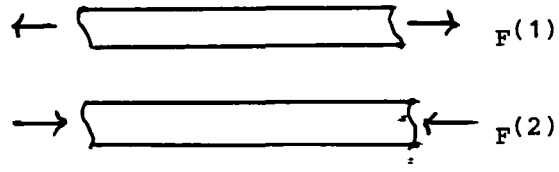

To produce a uniaxial state of stress, equilibrium requires:

$$F^{(1)} + F^{(2)} = 0$$

or $$\sigma^{(1)}A^{(1)} = -\sigma^{(2)}A^{(2)}$$

Therefore,

$$\epsilon^{(1)}E^{(1)}A^{(1)} = -\epsilon^{(2)}E^{(2)}A^{(2)}$$

and $$\frac{\epsilon^{(1)}}{\epsilon^{(2)}} = -\frac{E^{(2)}A^{(2)}}{E^{(1)}A^{(1)}} = -\frac{E^{(2)}t^{(2)}}{E^{(1)}t^{(1)}}$$

since $E^{(2)} > E^{(1)}$ and $t^{(2)} >> t^{(1)}$

then $|\epsilon^{(1)}| >> |\epsilon^{(2)}|$

It is a good assumption that all of the strain is accommodated in the oxide layer and that any stress in the metal can be neglected; therefore,

$$\epsilon^{(1)} = \epsilon_T$$

Hence, from $\epsilon_{TBC} = \epsilon_T E(T)_{TBC}$, the stress in the oxide layer may be calculated.

The information required is $\bar{\alpha}^{(1)}$, $\bar{\alpha}^{(2)}$, $E(T)^{(1)}$ and $E(T)^{(2)}$. In addition, due to the small value of Poisson's ratio of the TBC material (= 0.230) biaxial stress should be considered, i.e.,

$$\sigma_x = \frac{E}{1-\nu^2}(\epsilon_x + \nu\,\epsilon_y);\ \sigma_y = \frac{E}{1-1\nu^2}(\epsilon_y + \nu\,\epsilon_x)$$

Assuming circular symmetry $\epsilon_x = \epsilon_y$

then $$\sigma = E\epsilon_x \frac{1 + \nu}{1 - \nu^2}$$

and $$\frac{1 + \nu}{1 - \nu^2} = \frac{1 + .23}{1 - .23^2} = 1.30$$

Therefore,

$$\sigma_x \text{ biaxial} = 1.3\ \sigma_x \text{ uniaxial or } \sigma_x \text{ biaxial} = (1.3)E(T)_{TBC}\epsilon_T$$

The data used in the calculations were taken from INCO (Ref. 8) for MAR-M421 and from Sevik and Stoner, PWA (Ref. 9) for yttria-stabilized zirconia. The data used in the calculations are shown in Table 17.

Table 17

Thermal Property Data

Temperature Range (°C)	$\bar{\alpha} \times 10^6$		Temperature (°C)	$E \times 10^{-6}$	
	ZrO_2	MAR-M421		ZrO_2	MAR-M421
21- 371	4.6	8.0	21	6.6	29.4
21- 454	4.7	8.15	371	5.3	26.9
21- 538	4.8	8.3	538	4.7	25.5
21- 760	5.1	8.7	760	4.0	23.2
21- 871	5.2	9.1	871	3.7	21.9
21- 982	5.3	9.9	982	3.2	21.1
21-1093	5.5	11.0	1093	3.0	20.4

For simplicity, the previous calculation assumed that the substrate and ceramic coating are both at the same temperature. As the film is being sprayed down, this assumption is not necessarily valid. An alternate assumption is that the substrate is at a constant temperature. This assumption is based upon the plasma spray process where the substrate is held at a relatively low temperature (e.g., 120°-370°C) during coating application and the ceramic is deposited near its melting point.

The method is the same in principle to the previous technique; however, the substrate and stress-free temperature differ.

Results of the calculations, assuming substrate and coating are constantly at the same temperature, are shown in Figure 96. Zero stress-strain temperatures from 371°to 1093°C were considered, as were test temperatures from 21° to 1093°C. The TBC is in tension for all temperatures above T_{SF} and in compression below T_{SF}. This is a consequence of the higher coefficient of thermal

expansion of the metal. If the coating fails by spalling this is a compressive failure and would occur during the cool-down cycle. Figure 96 indicates that spalling failures could be minimized by maintaining a low T_{SF}. Conversely, cracks running normal to the TBC-substrate interface are tensile failures which would be minimized by maintaining a high T_{SF}.

At the metal-ceramic interface, strain begins when the ceramic has adhered and resumed a rigid structure. This coating temperature (T_{SF}) is well above the average substrate temperature. Figure 97 shows the relationship between these temperatures and the resulting stress developed in the coating. As the coating cools to the substrate temperature it generates a tensile stress in the coating. Further simultaneous cooling of both the coating and the substrate reverses this trend. By varying T_{SF} and the substrate temperatures, the residual stress can be brought to a pre-determined value.

TBC's are a poor thermal conductor. This may reduce the substrate temperature as successive layers are deposited. As indicated in Figure 96, this would have the effect of increasing the compressive loading on the outer layers when temperatures are below T_{SF}. Evidence of this happening would be the presence of cracks parallel to the TBC-substrate interface but at a distance from the interface.

Thin materials (i.e., columns) loaded in compression can experience instabilities well before the ultimate compressive strength is exceeded. A TBC is a thin oxide layer that can be faced with relatively high compressive loads. A calculation of the critical compressive loads for various oxide coating parameters aids in understanding the conditions to cause spalling, assuming the idealized condition shown in Figure 98.

With a pre-existing crack of length ℓ, a distance h below the surface, the Euler buckling load equation is the simplest method for calculating the critical load for instability on a column (P_e). This method has been applied to estimate the flaw sensitivity in a TBC. The Euler equation is:

$$(P_e)\text{critical} = \frac{\pi^2 EI}{\ell^2}$$

where $$I = \frac{bh^3}{12}$$

and $$\sigma_e = hb$$

This becomes

$$\frac{(\sigma_e)\text{critical}}{E} = \left(\frac{\pi^2}{\ell^2}\right)\left(\frac{bh^3}{12}\right)\left(\frac{1}{hb}\right)$$

is $$\frac{(\sigma_e)\text{critical}}{E} = \left(\frac{\pi^2}{12}\right)\left(\frac{h}{\ell}\right)^2$$

This equation (shown in dimensionless form) is plotted in Figure 99. Also shown are the room-temperature normalized stresses corresponding to the various zero stress-strain temperatures. Figure 99 indicates that as the critical stress decreases, the flaw size, ℓ, will increase if the film thickness remains constant, again showing spalling is less likely for lower T_{SF}'s.

The figure also points out that for a constant critical stress, as the film thickness decreases the flaw size necessary for instability decreases. If T_{SF} is increasing as successive layers are sprayed, then the instability can become more of a problem. Higher compressive loads coupled with thinner effective thickness can significantly increase the flaw sensitivity.

This discussion assumes that flaws are present in the material, given the flaw of a certain dimension the conditions under which it will spall off have been calculated. The approach is approximate; however, the qualitative observations should be representative. The compressive strength of zirconia stabilized with either magnesia or calcia are reported to be as high as 300 x 10^3 psi and as low as 85 x 10^3 psi. Likewise, figures for the modulus of elasticity can be found as high as 19.2 x 10^6 psi and as low as 6.6 x 10^6. This gives a range in σ/E from 4.4 x 10^{-3} to 4.5 x 10^{-2}. Comparing this range with Figure 96 indicates the uncertainty present in the problem. The worst case suggests that the film is failing by pure compressive loading for T_{SF} > 450°F, whereas the best case indicates that the compressive loads are far too low to cause failure.

5.2 THERMO-ANALYTICAL EFFECTS OF TBC's

For this portion of the program the effects anticipated on the performance of the Solar Mars gas turbine engine were analyzed. Table 18 summarizes the engine ratings at two different rotor inlet temperatures. A third rotor inlet temperature, 1113°C, is being considered. Operating at these temperatures requires the use of large amounts of cooling air in the gas producer and turbine sections. The management of this cooling air is shown in Figure 100. The first- and second-stage vanes and blades (V1, V2, B1, B2) are air cooled. TBC analyses were based on coating these items. The affected airflows are boxed in the diagram. The remaining airflows cannot be reduced since, in addition to cooling, they provide a buffer to control the flow path of the hot gases.

The cooling airflow expenditure of TBC Mars turbine blading is 50 to 55 percent of the flow required by the present convection and film-cooled airfoils for the same metal temperatures. The first- and second-stage coated vanes would use less air, ejected entirely through the trailing edges (film holes would be troublesome and the film inefficient) and would require new casting tooling while eliminating the hole drilling operations. From the heat trans=-fer standpoint, the stator end shrouds should be coated only if backside

Table 18

Mars Gas Turbine Engine Rating, Present and Proposed

Rotor Inlet Temperature	Present Rating 982°C	Proposed Rating 1057°C
Engine airflow (kg)	36.7	36.7
Pressure ratio (15 stages)	15.63	16.10
Burner outlet temperature (°C)	1016	1095
Horsepower (hp)	10,929	12,915
S.F.C. (Btu/hp/hr)	7,770	7,466
Thermal efficiency (%)	32.75	34.08

convective cooling is used, which is not yet the case for the Mars turbine. The first-stage blades could be readily coated without casting modifications, it being sufficient to specify a smaller metering orifice hole.

5.2.1 Simplified Thermal Model of the Airfoils

Assumptions

The model (Fig. 101) is representative of the suction side of the airfoils, and is used to evaluate the effect of TBC's on both the first- and second-stage vanes. The results derived for the extreme cases are valid for the convectively-cooled first-stage blades.

Dimensions:

Span - 1.8 cm

Developed surface length - 7.1 cm for the first vanes
- 6.1 cm for the second vanes

Wall - 0.13 cm MAR-M421

Bond coat - 0.10 mm NiCrAlY

Overcoat - variable around 0.38 mm $ZrO_2 \cdot 8Y_2O_3$

Thermal Properties:

Thermal conductivities - per Figure 102

Specific heats - per Figure 103 and 0.26 cal/gm °C for the air

Densities - 6.98 g/cc for NiCrAlY
- 5.67 g/cc for $ZrO2_2 \cdot 8Y_2O_3$
- 8.98 g/cc for MAR-M421

The thin bond coat of NiCrAlY offers a negligible resistance to heat conduction.

Neglect conduction in the coating along the gas flow direction.

Convective cooling and trailing edge ejection only.

This means replacing the present film-cooled first-stage vanes by a convective cooling scheme and modifying the present second-stage vanes to include trailing edge ejection instead of the present pressure side ejection.

- Variable external and internal heat transfer coefficients (Figs. 104 and 105) and baseline coolant flow rates yield uncoated metal maximum temperatures typical of those prevailing in the present 982°C engine.

- Baseline airflows: 0.0075 lb/s for the first vane model
  0.0009 lb/s for the second vane model

Corresponding Coolant-to-Gas Flow Ratios for the Cascades

ϕ = 0.0396 and 0.00762, respectively.

The internal heat transfer coefficient varies with the 0.705 power of the cooling air flow; this assumes that the coolant passages are identical for the coated and uncoated cases.

5.2.2 Results

First-Stage Vanes

Figure 106 shows that the same outer skin metal temperatures are obtained with an uncoated airfoil using a coolant-to-gas flow ratio of ϕ = 0.0396 and with the same airfoil coated with a 0.38 mm thick TBC but using only a ϕ = 0.0158, i.e., 60 percent less cooling air.

The present Mars engine vanes are actually cooled with ϕ = 0.0354 to a higher effectiveness than the baseline vanes used in this analysis. The net cooling air savings due to coating amounts to 55 percent. Figure 107 illustrates the effect of coolant-to-gas flow ratio on various parameters such as local cooling effectiveness, temperature differentials, and coolant temperature rise. At the proposed flow ratio of 0.0158, we note a differential of 166°C across the TBC, i.e., a gradient of 4430°C/cm. In contrast, the metal shell differential and gradient amount to only 36° and 289°C/cm.

Figures 108 and 109 provide the average time constants for the uncoated and coated airfoils as 0.8 and 1.75, respectively.

Figure 110 shows the effect of TBC thickness on the cooling effectiveness at $\phi = 0.0396$. Doubling the overcoat thickness from 0.38 to 0.76 mm further reduces the metal temperature by 64°C.

Figure 111 shows that a coated Mars first-stage vane cooled with $\phi = 0.0158$ could tolerate a burner hot spot of 1329°C while not exceeding 982°C metal temperature at its hottest point.

Another factor that influences the performance of the TBC's is surface roughness. Normally these coatings are applied in such a manner that they produce a rough surface finish. The calculated requirements are shown in Figure 112. This figure shows that a polished surface is required and that additional finishing operations will be required on the coated components.

Some further analytical results based on the Mars engine design are summarized below. The first-stage turbine blade has an airfoil length of 31.50 mm. During normal engine operation the blade length will increase 0.318 mm due to thermal growth and 0.0304 mm elastically for a total growth of 0.348 mm. This results in a total blade growth of 0.011 mm/mm that must be accommodated by the TBC.

The rate of blade growth as the engine stabilizes is less well defined. From the data available, the calculated average rate of blade growth will be 0.013 mm/sec. This indicates that steady-state conditions of blade growth will be achieved after 27 seconds of operation.

The results of these studies are summarized below.

In the present uncoated vane and blade engine design the following requirements exist for cooling air from the compressor discharge:

- First-stage blades - 1.3 percent
- First-stage nozzle vanes - 3.96 percent
- Second-stage nozzle vanes - 0.76 percent.

Use of a TBC on these components will result in the following approximate reductions in coolant requirements:

- First-stage blades - 50 percent
- First-stage vanes - 55 percent
- Second-stage vanes - 50 percent.

With regard to engine performance, this provides the following improvements. The specific fuel consumption would be reduced by 1.4 percent and shaft horsepower would be increased 2.76 percent. A secondary, but important, benefit

is the hot spot tolerance. Heat transfer calculations show that this will be increased by 347°C, allowing a maximum surface hot spot temperature of 1330°C while metal temperature would not exceed 982°C. This allows design values closer to the maximum limits of the blade and vane alloys, giving a potential for further increases in engine performance.

6

CONCLUSIONS

The following conclusions were drawn from the program evaluations of thermal barrier coating systems:

1. The $CaO.TiO_2$ was found to be stable in the presence of vanadium, sulfur and other contaminants found in low-grade fuels.

2. The $ZrO_2.8Y_2O_3$ performed well in tests using clean fuel but was unstable in the presence of vanadium.

3. The $2CaO.SiO_2$ did not spall during burner rig testing but a considerable loss of the coating occurred during engine test.

4. The $MgO.Al_2O_3$ coatings were susceptible to attack by fuel contaminants and had poor thermal shock resistance.

5. Once coating optimization was achieved, duplex coating performance was superior to that of the more complex graded and multi-layer structures.

6. Coatings using CoCrAlY bond coats were more likely to spall than those using NiCrAlY bond coats.

7. Small variations in the starting material, e.g., fused versus sintered stabilized zirconia powders, had significant effects on coating performance.

8. Substrate composition affected coating performance and optimization of deposition parameters is required for each specific application.

9. When tested for tensile strain tolerance, $CaO.TiO_2$ coatings were able to withstand greater substrate elongation without cracking than were $ZrO_2.8Y_2O_3$ coatings.

10. Visual examination after 550-hour engine testing indicated that the $ZrO_2.8Y_2O_3$ coatings were more erosion resistant than were $CaO.TiO_2$ coatings. However, neither coating degraded due to thermomechanical exposure.

11. Coating spallation did not occur at an interface but in the ceramic phase, leaving a thin retained ceramic layer.

12. The successful application of TBC's to the Mars engine would give a 2.76 percent increase in horsepower, a reduction of 4.7 percent in specific fuel consumption, and would reduce the stresses generated by thermal transients.

13. TBC's applied to engines using low-grade fuels would reduce their susceptibility to attack by impurities in the fuel.

7

RECOMMENDATIONS

Additional development work should be performed on the thermal barrier coatings studied in this program. Some recommendations are given below:

1. Modify the coating system to improve the strain tolerance using techniques such as laser scribing and/or compliant, low-modulus layers.

2. Additional engine tests should be performed by coating non-critical hot components of production engines and maintaining the necessary records for determination of coating performance over long periods of time in an operating gas turbine.

3. Additional data is needed relating composition and structure of the TBC's to the attack by contaminants in low-grade fuels.

4. An engine test should be performed using reduced cooling air and thermal barrier coated components to determine if the predicted performance increase can be achieved through the use of TBC's.

5. Detailed deposition process parameter studies need to be performed to ensure optimization of present coatings and consistant application.

6. Tests for individual TBC characteristics need to be performed in the laboratory. These would cover items such as particulate erosion by carbon in a high-velocity hot gas stream, coating life prediction data, reliability, and other relevant coating characteristics that would meet the requirements of engine designers.

This Page Intentionally Left Blank

REFERENCES

1. Stephens, G.E., "Cost/Benefit Analysis of Advanced Materials Technologies for Future Aircraft Turbine Engines," NASA-CR-16525, PWA Report PWA-5755 (August 1980).

2. Wilkins, C.R., Wallace, F.J. and Zajchoinski, P.H., "Ceramic/Metallic Thermal Barrier Caotings for Gas Turbines," 8th International Thermal Spraying Conference (1976).

3. Stepka, F., et al, "Summary of NASA Research on Thermal Barrier Coatings," NASA TM-X-73584 (1977).

4. Stepka, F.S., "NASA Thermal Barrier Coatings - Summary and Update," NASA Tech. Memorandum 79053, presented at Project SQUID (ONR) Workshop on Cooling Problems in Aircraft Gas Turbines, Monterey, CA (Sept. 27-28, 1978).

5. Levine, S.R., "Adhesive/Cohesive Strength of a ZrO_2/NiCrAlY Thermal Barrier Coating," NASA TM-73792 (1978).

6. Andress, D.E., "An Analytical Study of Thermal Barrier Coated First-Stage Blades in an F100 Engine,: United Technologies Corp., Pratt & Whitney Aircraft Group Report FR-9609 on NASA Contract NAS3-31032 (February 1978).

7. Grisaffe, S.J., Levine, S.R. and Clark, J.S., Technical Paper presented at ASME 23rd Annual International Gas Turbine Conference, London, England, NASA TM-78848 (April 1978).

8. High Temperature High Strength Nickel Base Alloys, The International Nickel Company, Inc., 3rd. Ed. (July 1977).

9. Sevick, W.R. and Stoner, B.L., "An Analytical Study of Thermal Barrier Coated First-Stage Blades ina JT9D Engine," United Technologyies Corp., Pratt & Whitney, Contract NAS3-21033.

This Page Intentionally Left Blank

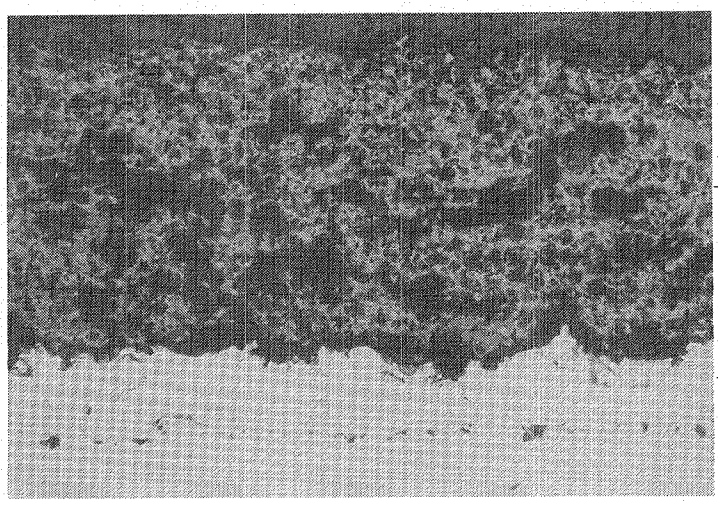

Figure 1.

Initial $ZrO_2 \cdot 8Y_2O_3$ TBC Desired

Magnification: 100X

Mount No. 9683

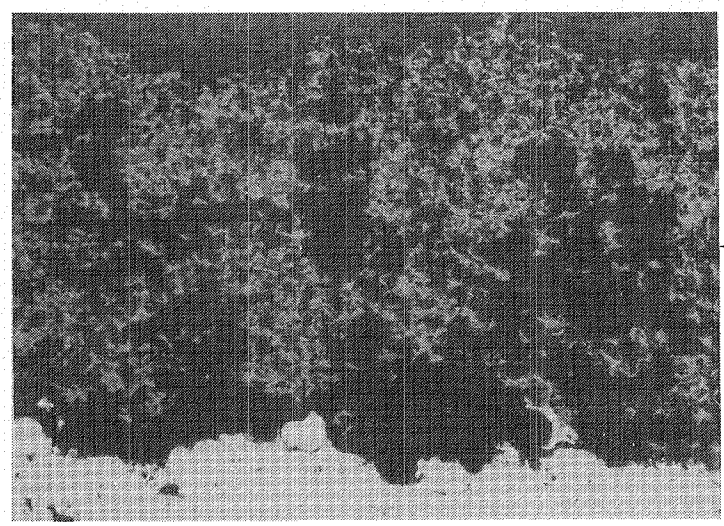

Figure 2.

Vendor Applied $ZrO_2 \cdot 8Y_2O_3$ TBC

Magnification: 100X

Mount No. 9685

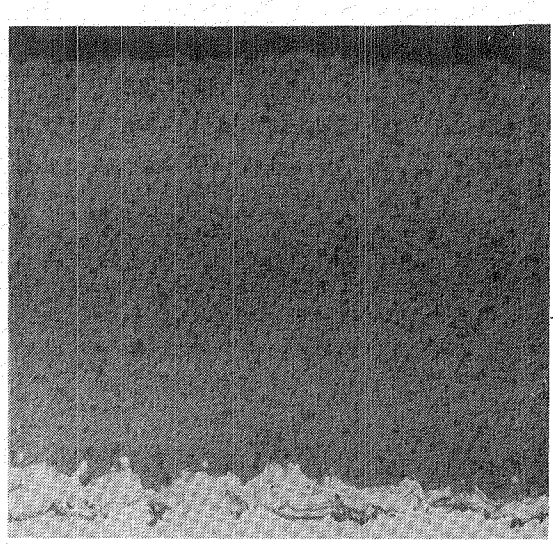

Figure 3.

Representative $ZrO_2 \cdot 8Y_2O_3$ TBC Using Fused Powder

Magnification: 100X

Mount No. 9683

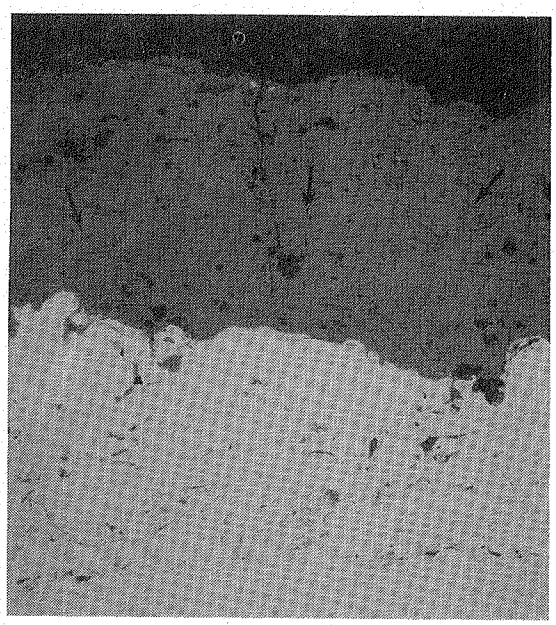

Figure 4.

Calcium Titanate Applied at 450 amps

Magnification: 150X

Mount No. 843

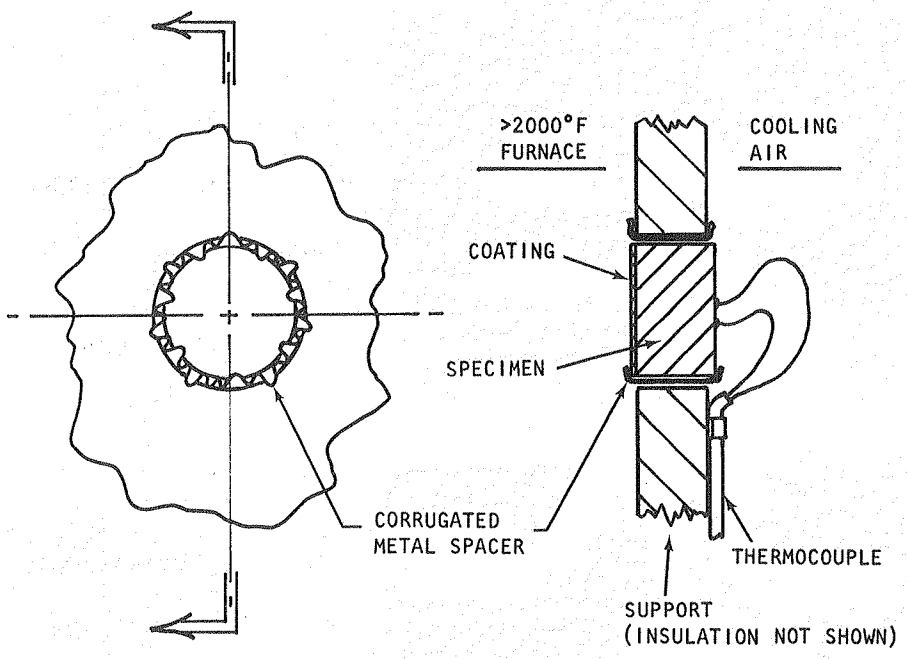

Figure 5. Typical Screening Specimen Support (Approximately 2X)

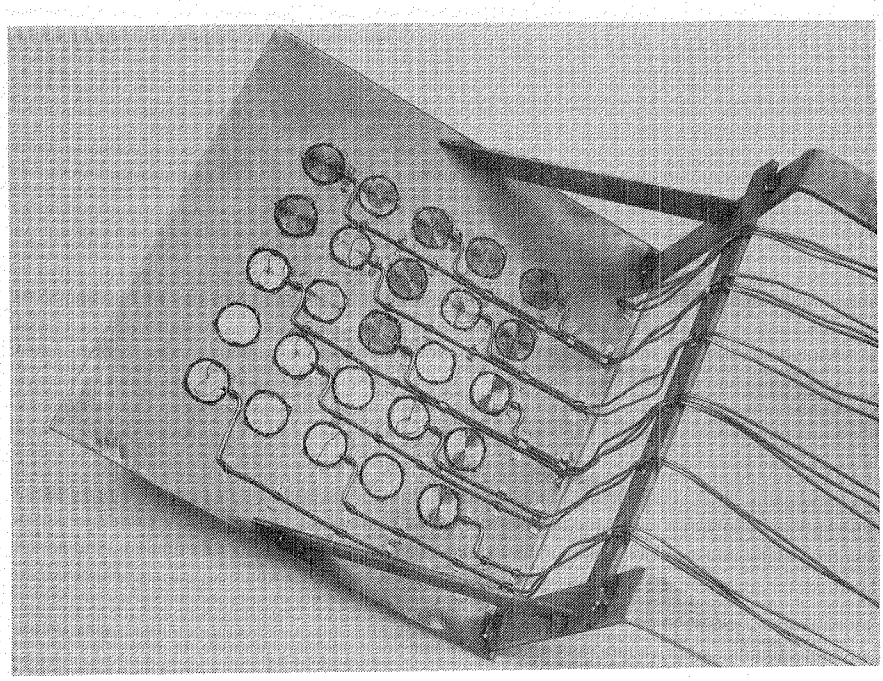

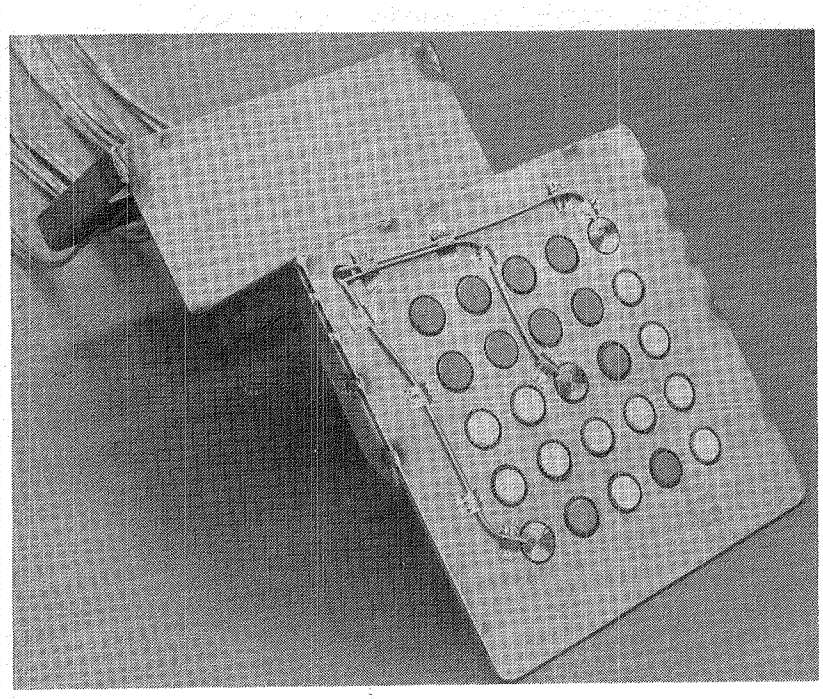

Figure 6. Furnace Test Panels for Material Screening Tests

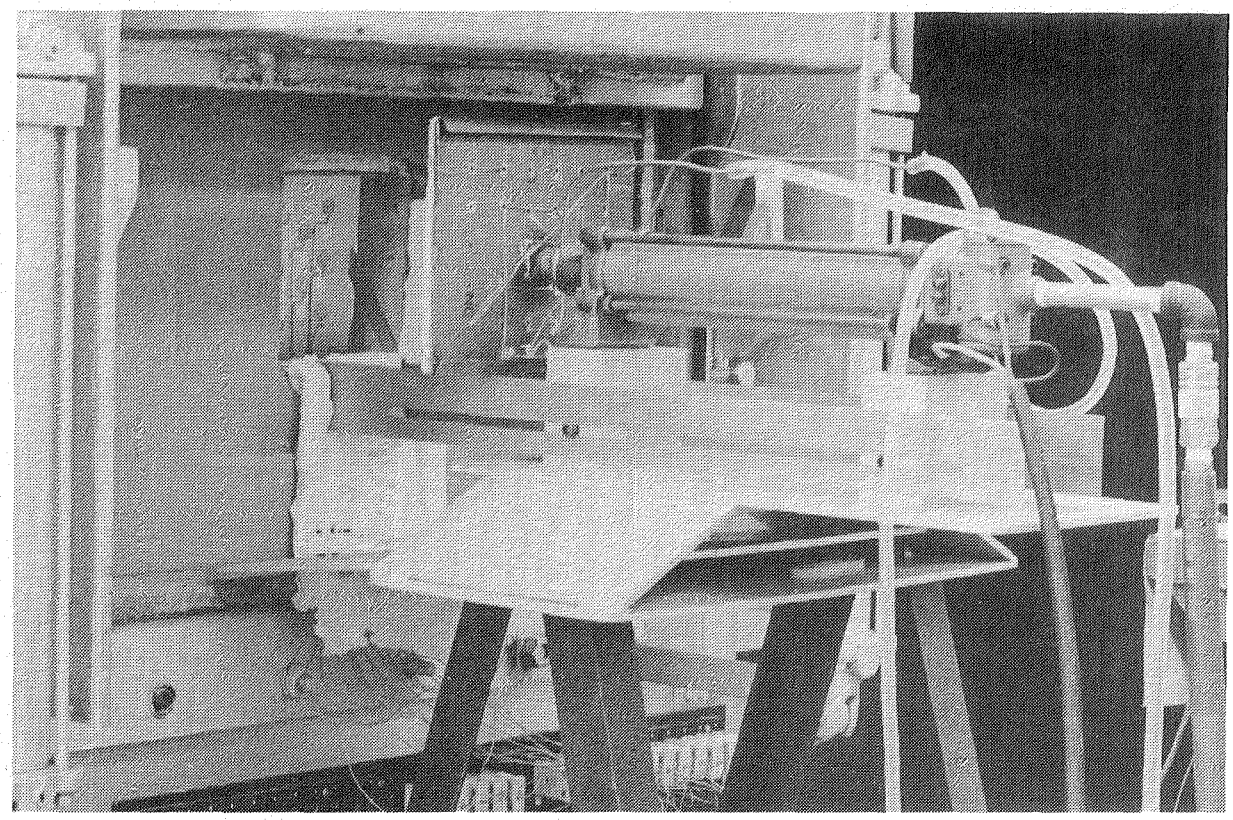

Figure 7. Screening Test Panel Installed in the Furnace Door Opening

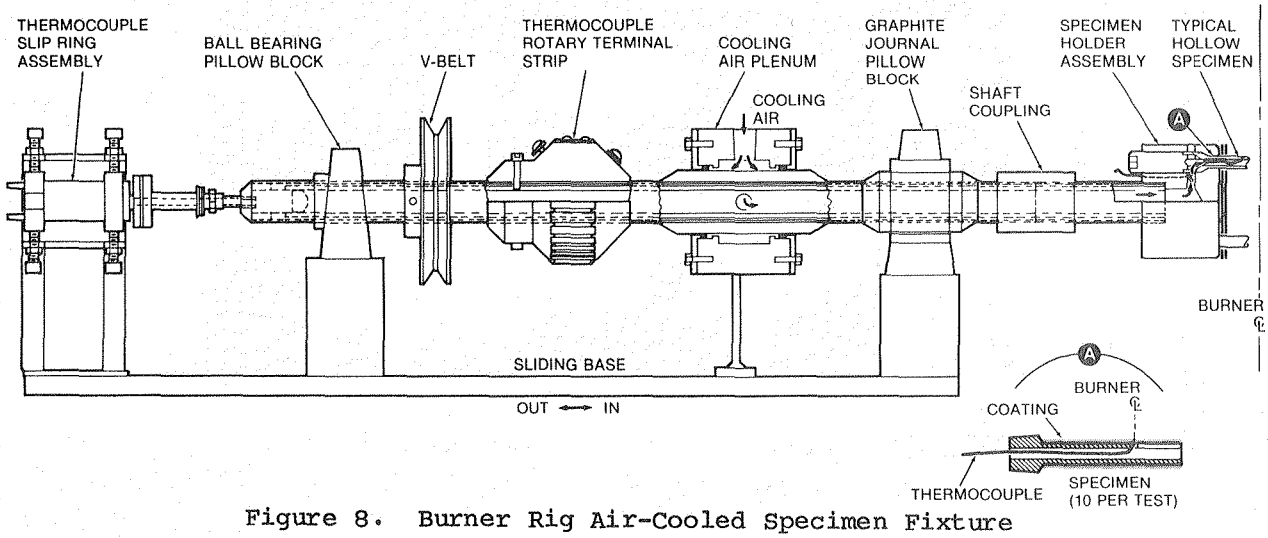

Figure 8. Burner Rig Air-Cooled Specimen Fixture

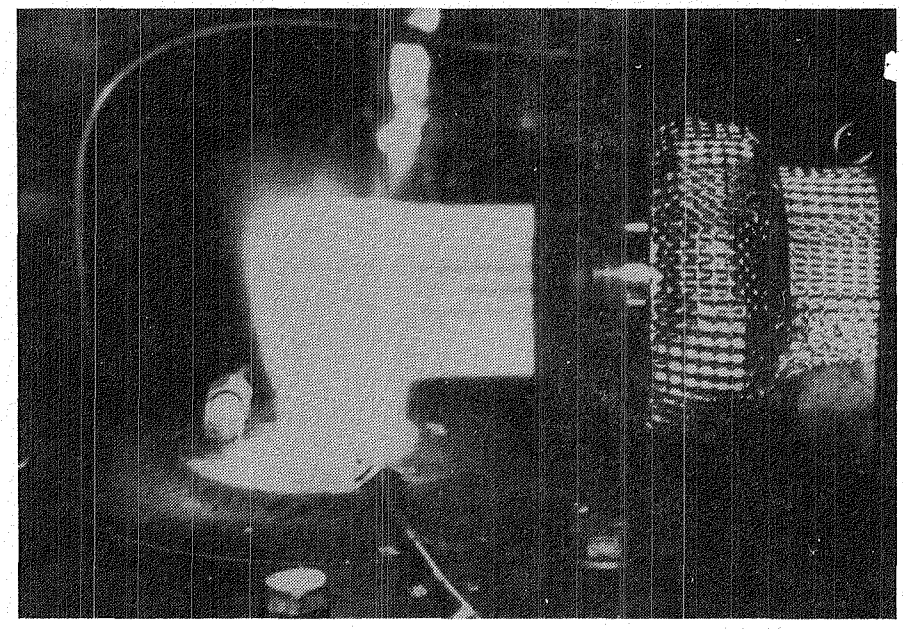

Figure 9. Burner Rig Operation

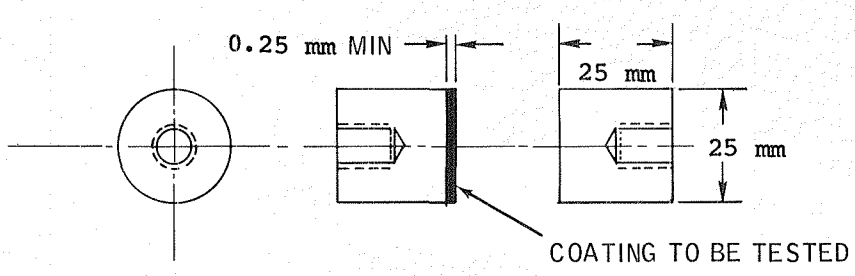

Figure 10. Tensile Bond Test Specimens

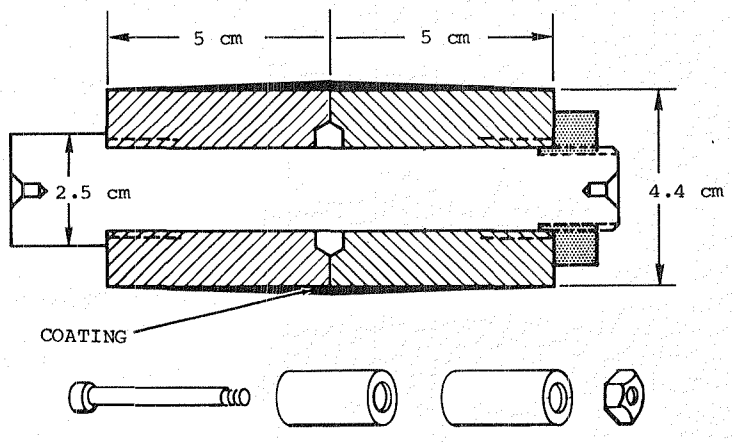

Figure 11. Cylindrical Coating Tensile Test Specimen

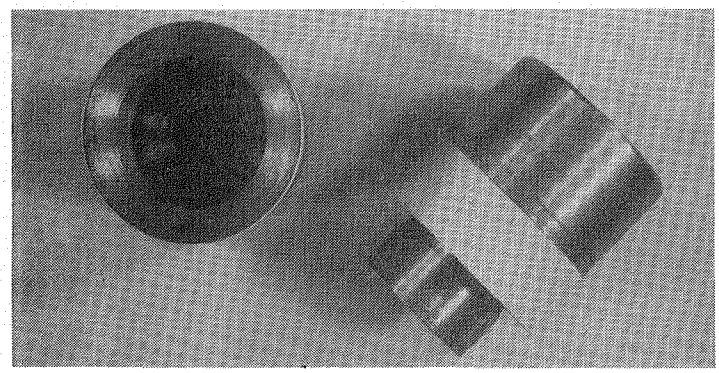

Figure 12.

Tensile Specimen After Test

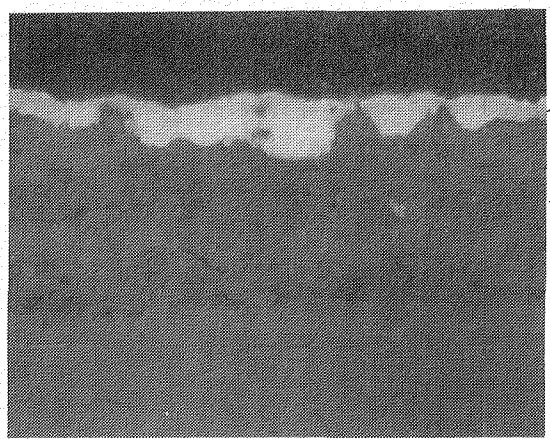

Figure 13. Baseline Coating - Yttria-Stabilized Zirconia on NiCrAlY (0.5%Y) Bond Coat Tested at 1150°C

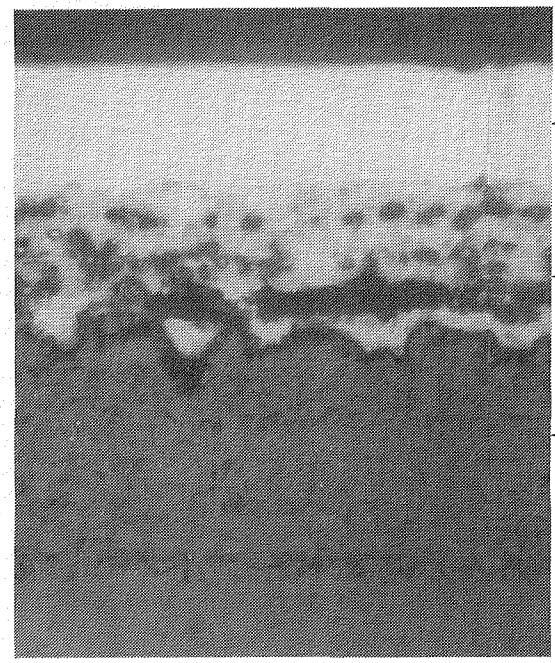

Figure 14. Graded Yttria-Stabilized Zirconia-NiCrAlY Coating (0.5%Y) Tested at 1150°C

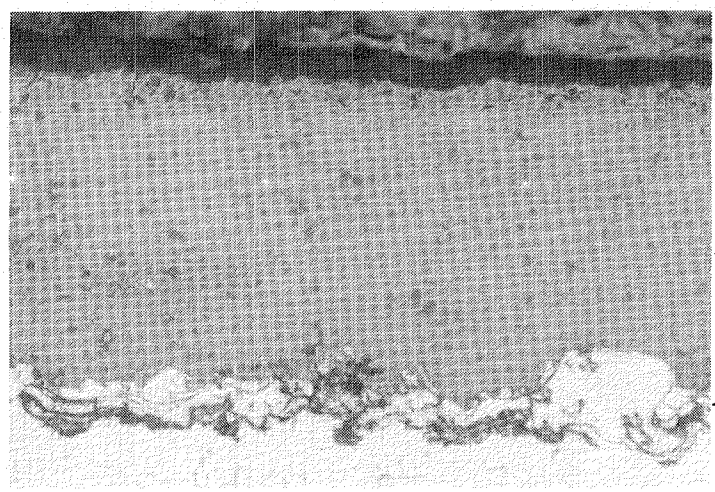

Figure 15.

Yttria-Stabilized Zirconia Coating After 50-Hour, 1032°C Furnace Thermal Cycle Test

Magnification: 100X

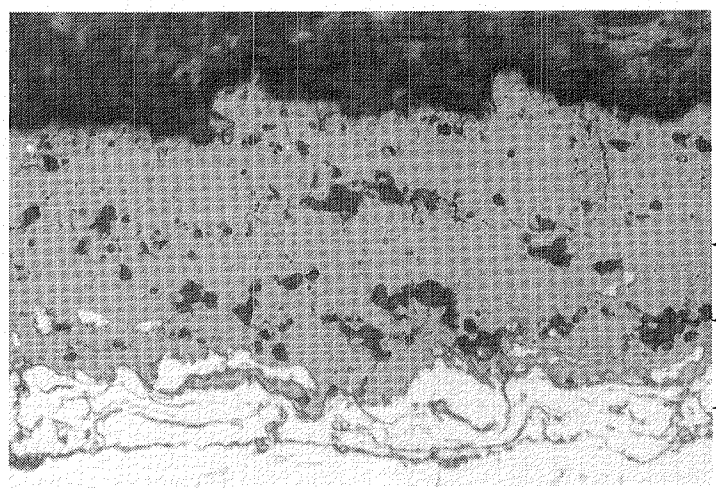

Figure 16.

Calcium Titanate Triplex Coating After 50-Hour, 1032°C Furnace Thermal Cycle Test

Magnification: 100X

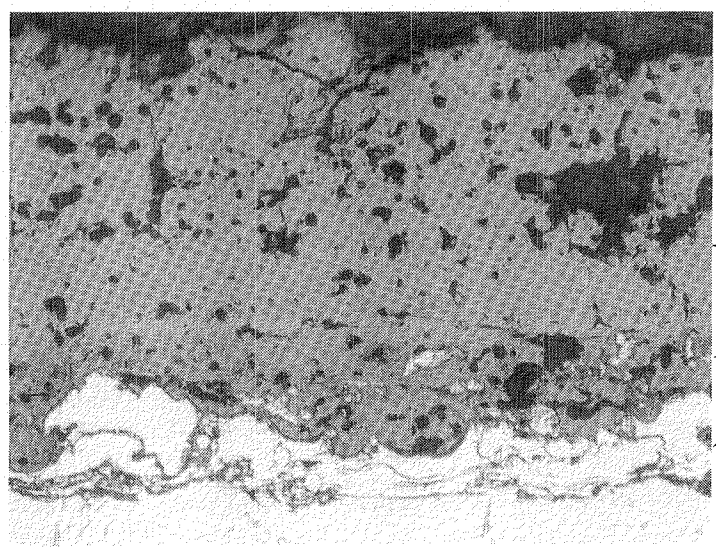

Figure 17.

Calcium Titanate Triplex Coating After 50-Hour, 1032°C Furnace Thermal Cycle Test Using CoCrAlY Bond Coat

Magnification: 100X

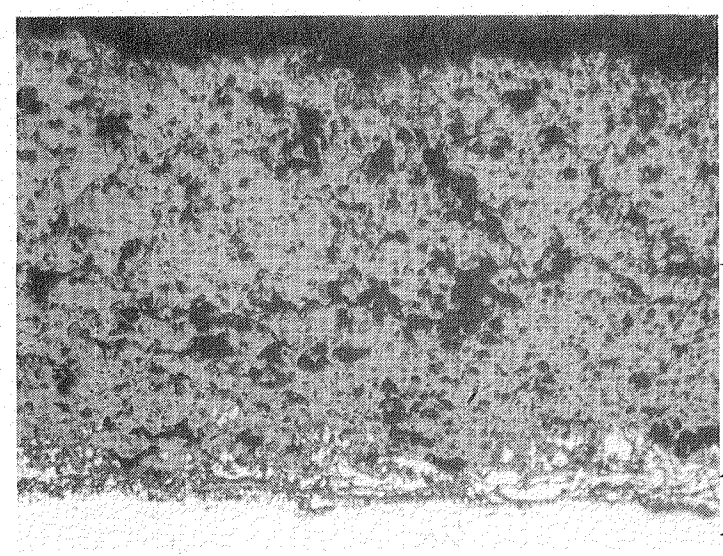

Figure 18.

Magnesium Zirconate Triplex Coating After 50-Hour, 1032°C Furnace Thermal Cycle Test

Magnification: 100X

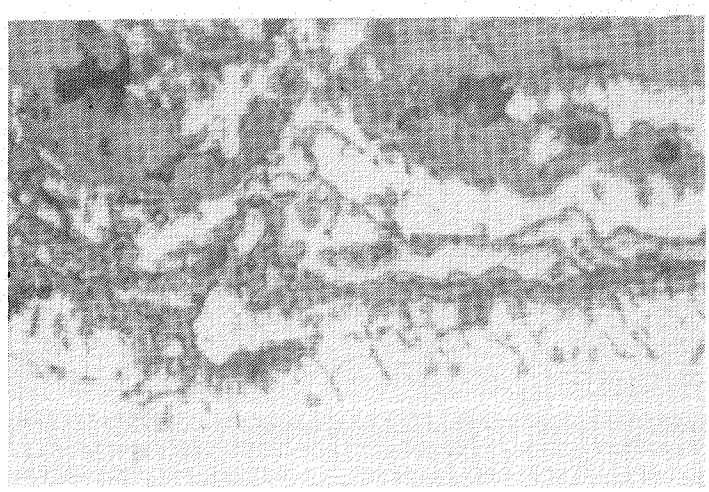

Figure 19.

Bond Coat - Substrate Interface From Magnesium Zirconate Triplex Coating

Magnification: 500X

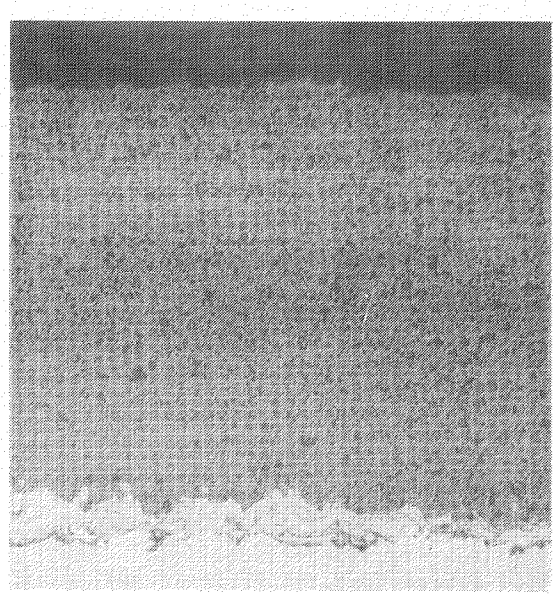

Figure 20.

Baseline $ZrO_2 \cdot 8Y_2O_3$ NiCrAlY Coating After 100-Hour Furnace Cyclic Test at 871°C

Magnification: 75X

Mount No. 9647

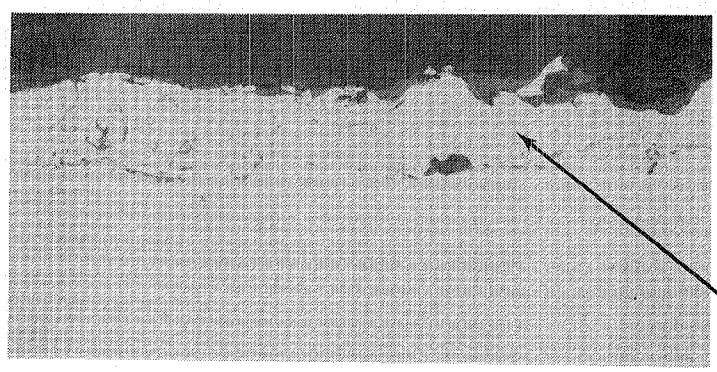

Figure 21.

Duplex CoCrAlY-$ZrO_2.8Y_2O_3$ Coating After 100-Hour Furnace Cyclic Test at 871°C

Magnification: 150X

Mount No. 9647

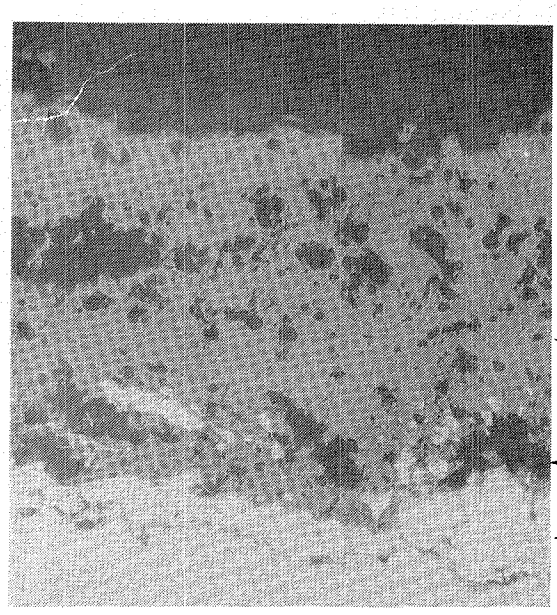

Figure 22.

CoCrAlY-$CaO.TiO_2$ Triplex Coating After 100-Hour Furnace Cyclic Test at 871°C

Magnification: 150X

Mount No. 9648

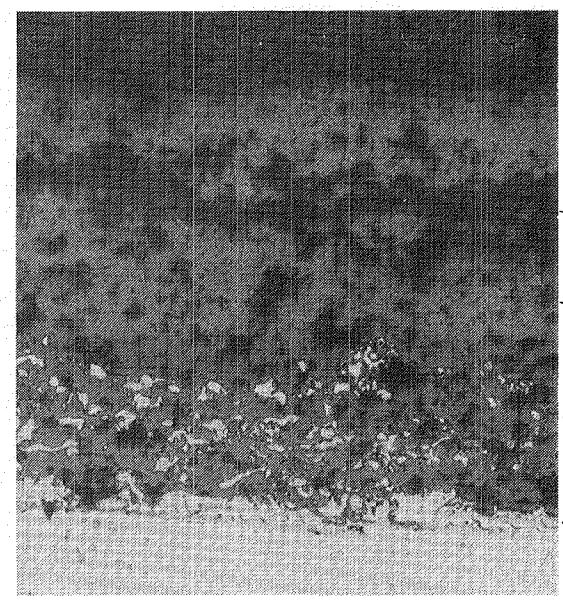

Figure 23.

Magnesium Zirconate Triplex Coating After 100-Hour Furnace Cyclic Test at 871°C

Magnification: 100X

Mount No. 9648

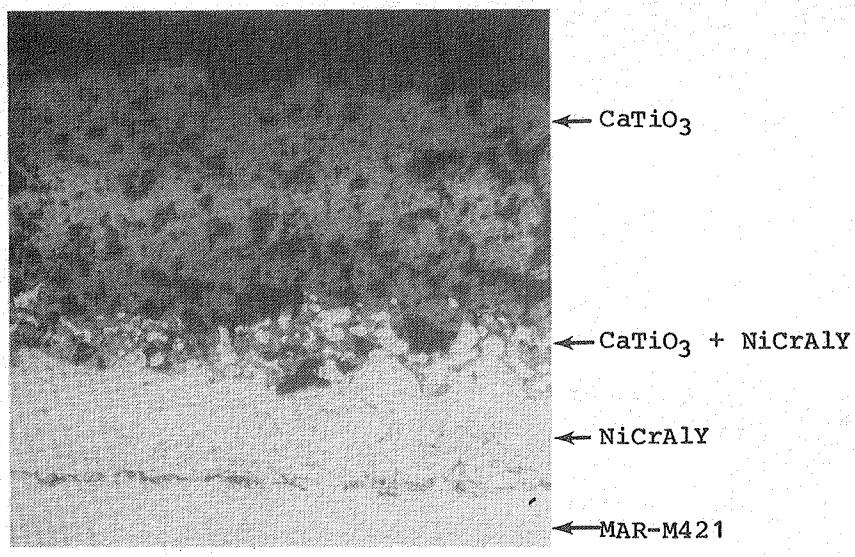

Figure 24. Calcium Titante Triplex Coating After Hot Corrosion Testing at 760°C
Magnification: 100X; Mount No. 9532

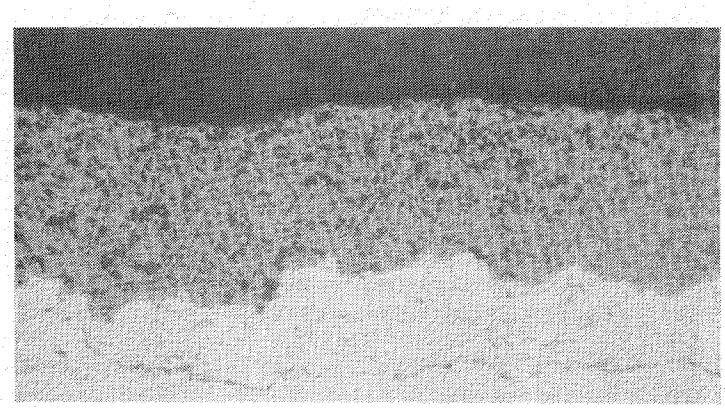

Figure 25. Baseline Coating ($ZrO_2 \cdot 8Y_2O_3$) After Hot Corrosion Testing at 816°C
Magnification: 100X

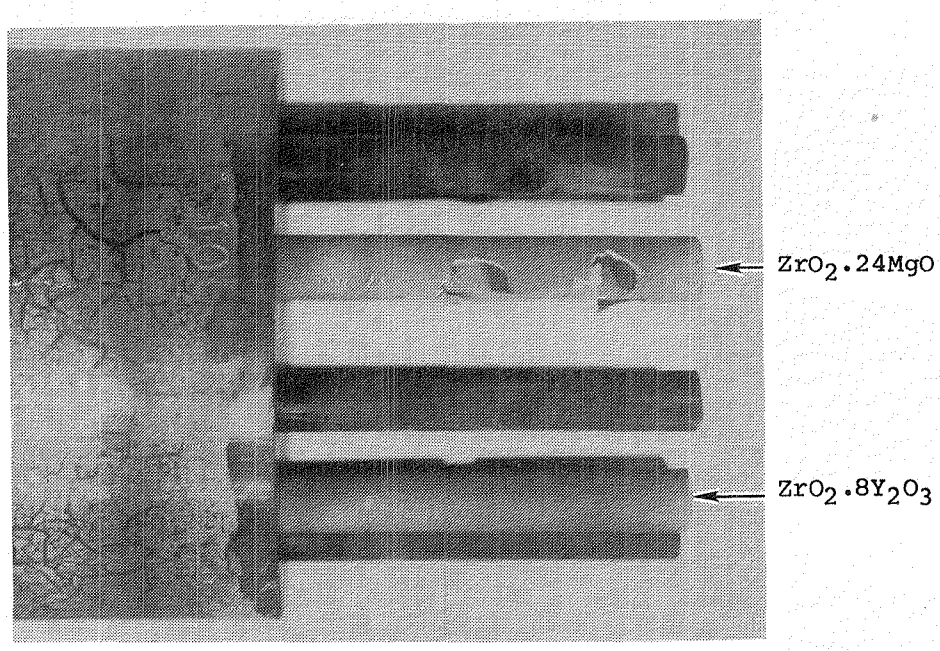

Figure 26A. Yttria-Stabilized Zirconia (Baseline) and Magnesium Zirconate After Burner Rig Exposure at 1043°C Specimen Temperature (5 cm Diameter Rig Nozzle)

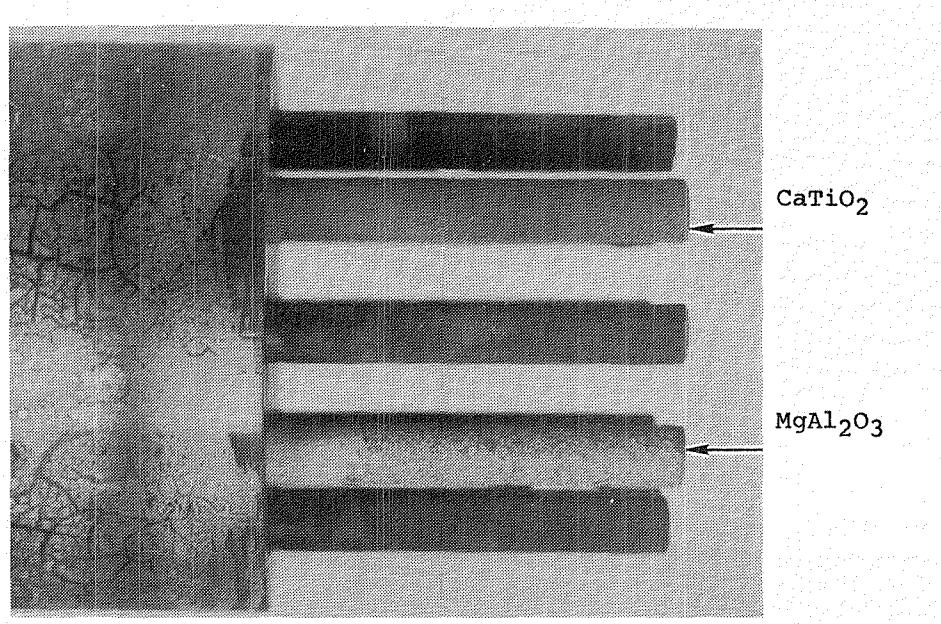

Figure 26B. Calcium Titanate and Spinel Specimens After Burner Burner Rig Exposure at 1043°C Specimen Temperature (5 cm Diametr Rig Nozzle)

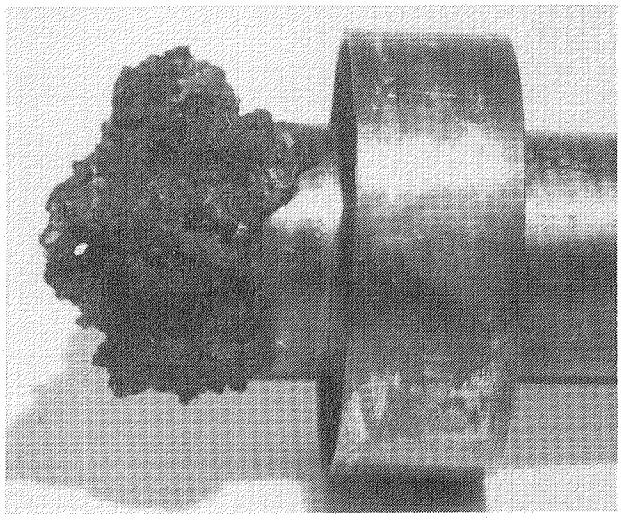

Figure 27.

Fuel Nozzle After 170 Hours Operation With High Vanadium Fuel

Magnification: Approx. 2X

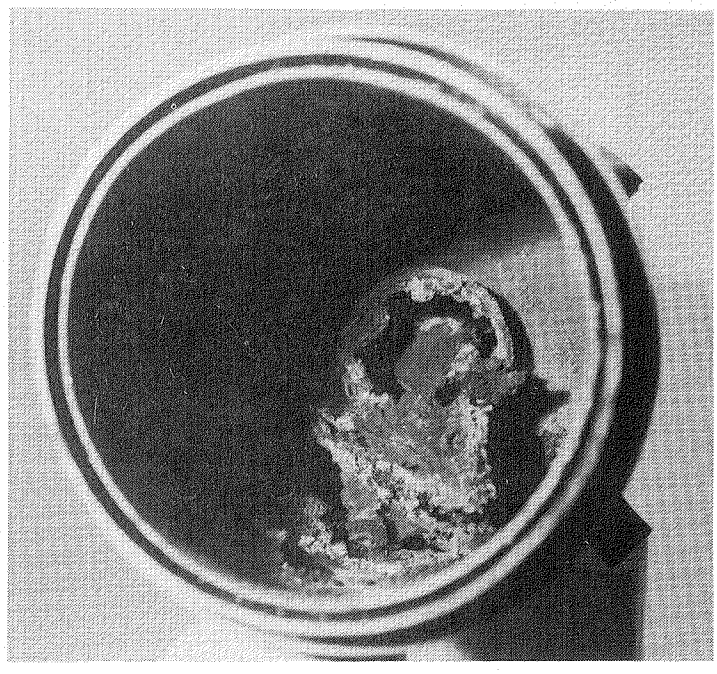

Figure 28.

Combustor After 170 Hours Operation on High Vanadium Fuel

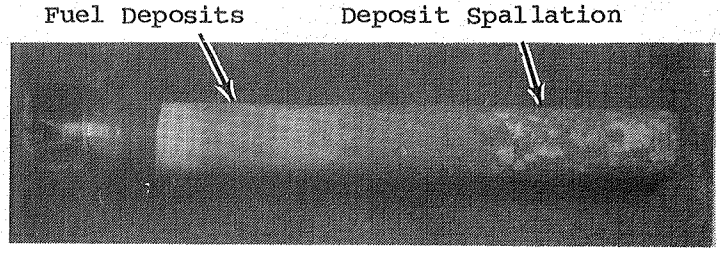

Figure 29.

Typical Burner Rig Specimen After Test With High Vanadium Fuel

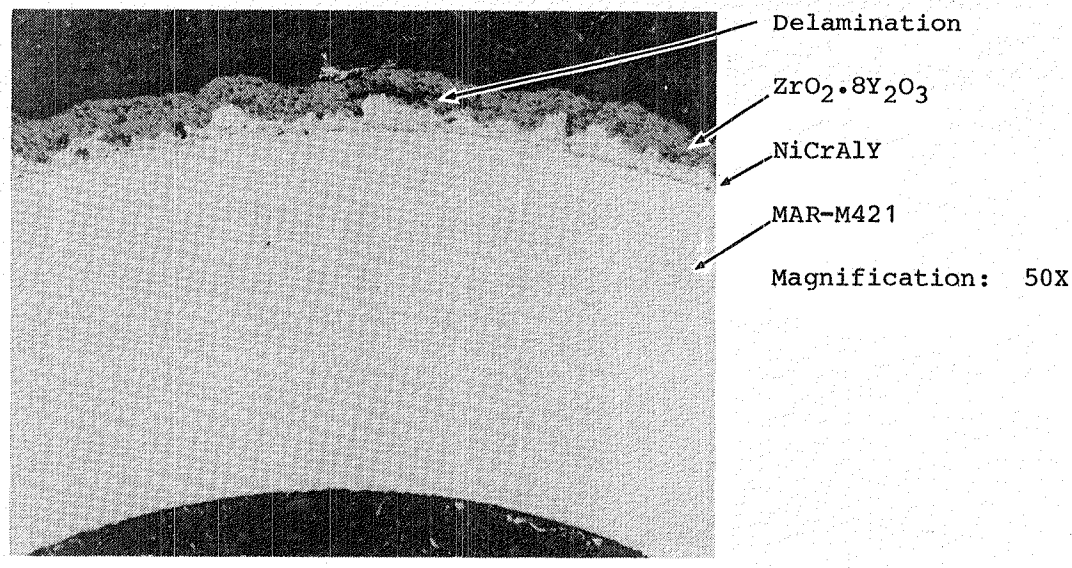

Figure 30. Duplex Fused $ZrO_2 \cdot 8Y_2O_3$/NiCrAlY After 400 Hours Burner Rig Exposure Using High Vanadium Fuel

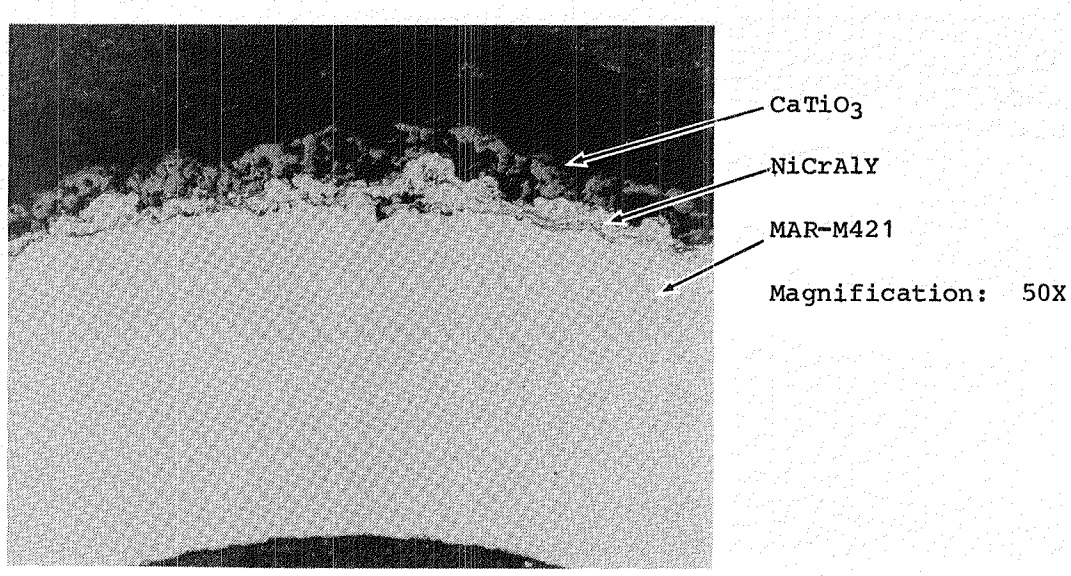

Figure 31. Duplex $CaTiO_3$/NiCrAlY Coating After 190 Hours Burner Rig Exposure Using High Vanadium Fuel

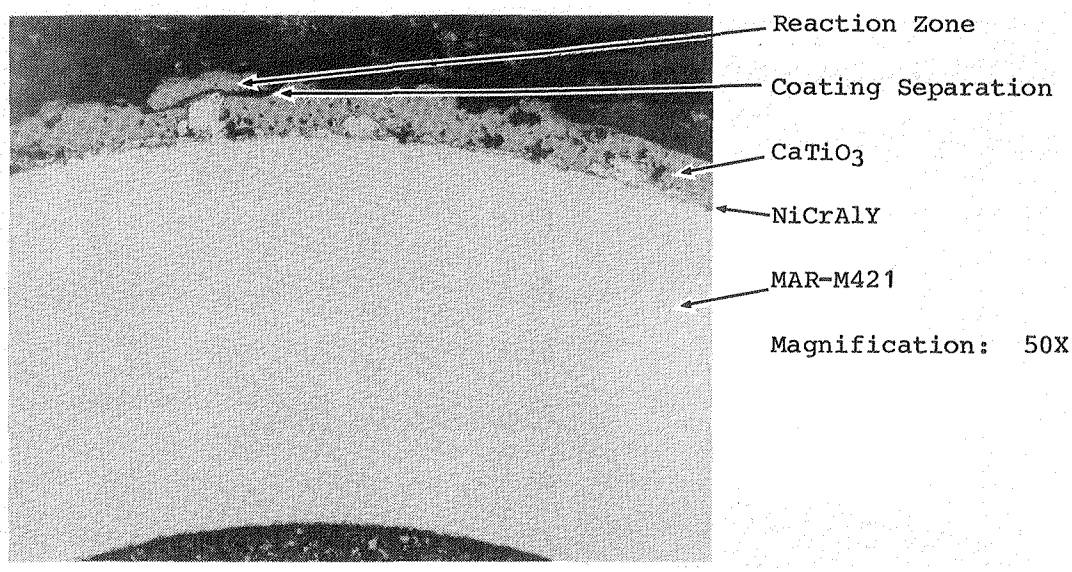

Figure 32. Duplex $CaTiO_3$/NiCrAlY Coating With Defecting Bond Coat After 400 Hours Burner Rig Exposure

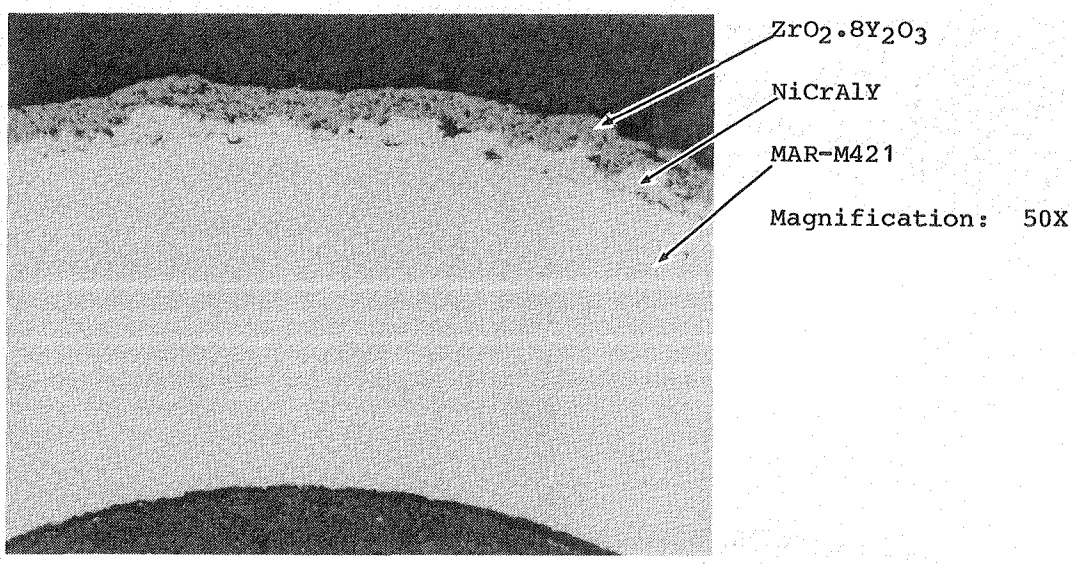

Figure 33. Duplex Fused $ZrO_2 \cdot 8Y_2O_3$/NiCrAlY Coating After 400 Hours Burner Rig Exposure Using High Vanadium Fuel

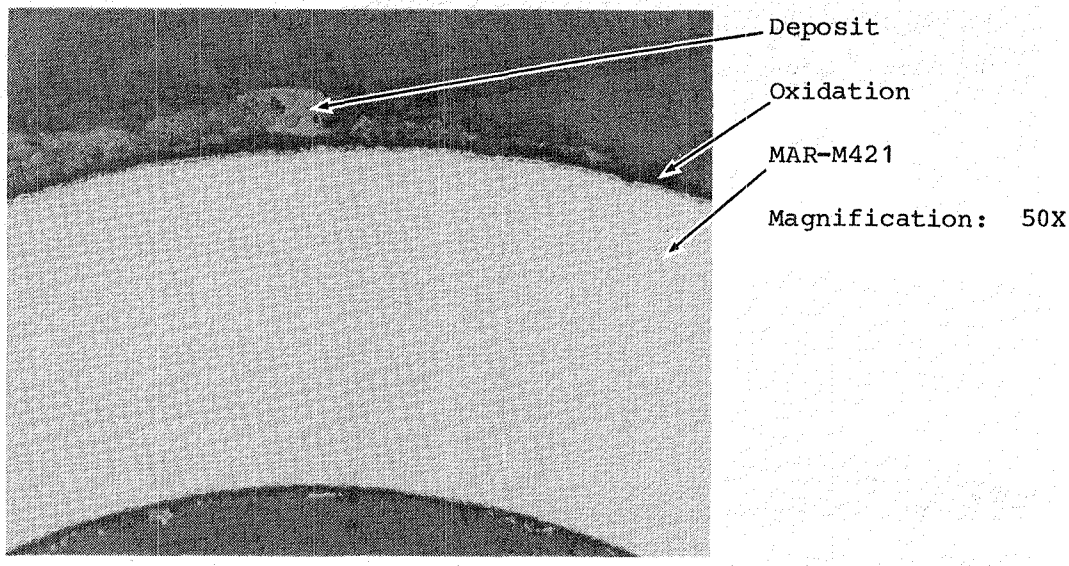

Figure 34. Uncoated MAR-M421 Test Specimen After 400 Hours Burner Rig Exposure Using High Vanadium Fuel

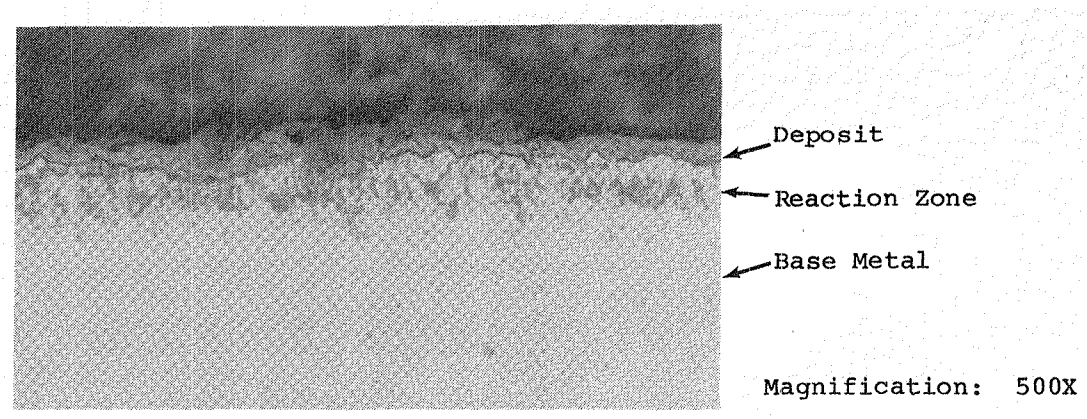

Figure 35. Attack on Uncoated MAR-M421 After 190 Hours Burner Rig Exposure With High Vanadium Fuel

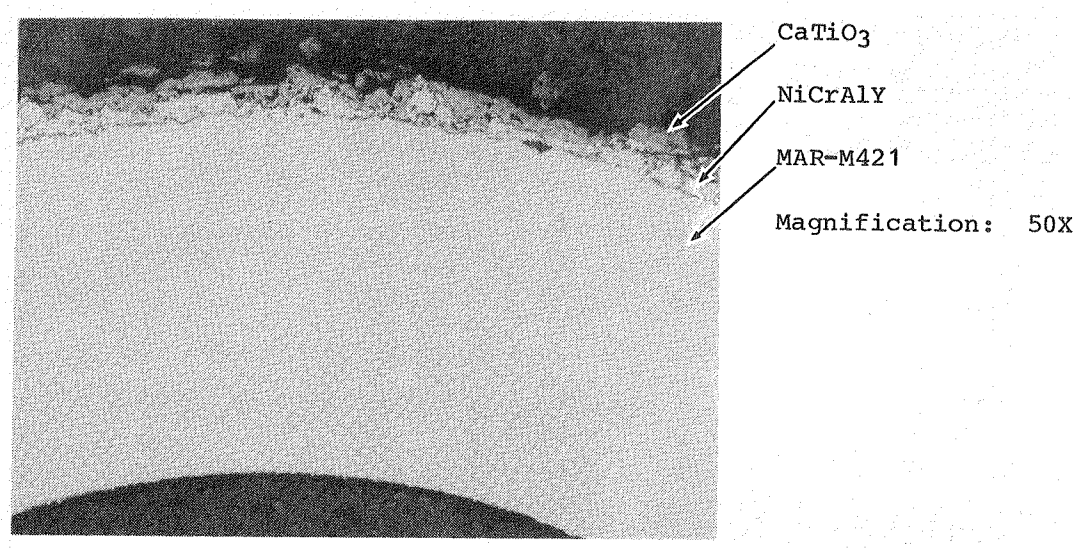

Figure 36. Duplex $CaTiO_3$/NiCrAlY Coating System After 515 Hours of Burner Rig Testing Using High Vanadium Fuel

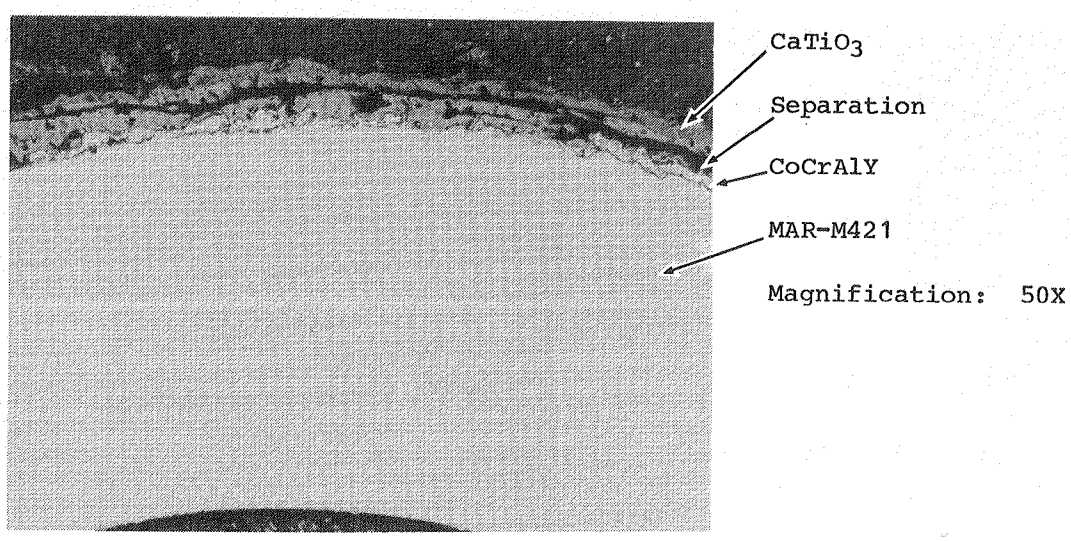

Figure 37. Duplex $CaTiO_3$/CoCrAlY Coating System After 515 Hours of Burner Rig Testing Using High Vanadium Fuel

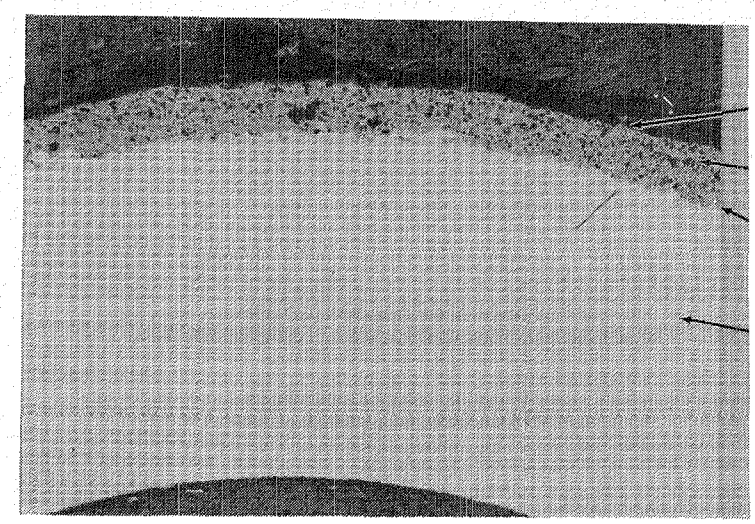

Figure 38. Duplex Fused $ZrO_2 \cdot 8Y_2O_3$/NiCrAlY Coating System After 515 Hours of Burner Rig Testing Using High Vanadium Fuel

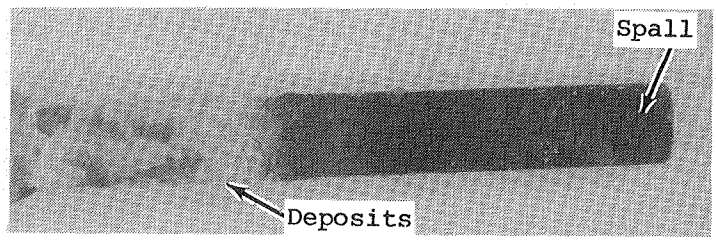

Fused $ZrO_2 \cdot 8Y_2O_3$/NiCrAl-0.2Y Duplex Coated Specimen After 159 Hours of Testing

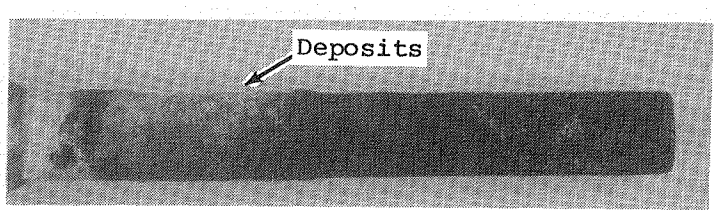

Fused $ZrO_2 \cdot 8Y_2O_3$/NiCrAl-0.8Y Duplex Specimen After 159 Hours of Testing

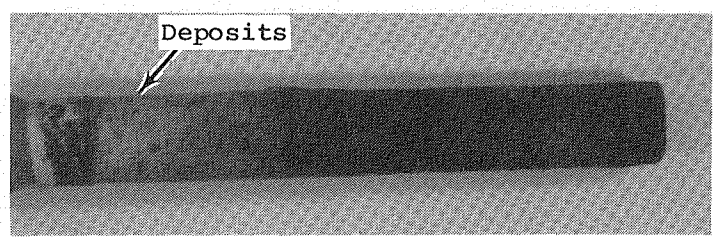

Sintered $ZrO_2 \cdot 8Y_2O_3$/NiCrAl-0.5Y Duplex Specimen After 159 Hours of Testing

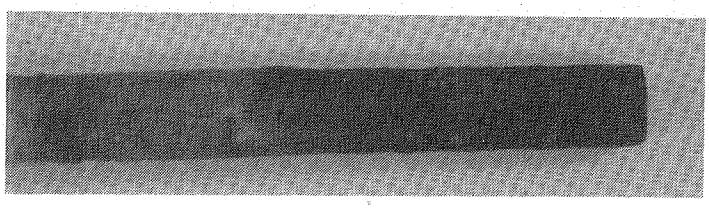

Duplex $CaTiO_3$/NiCrAl-0.5Y Coated Specimen

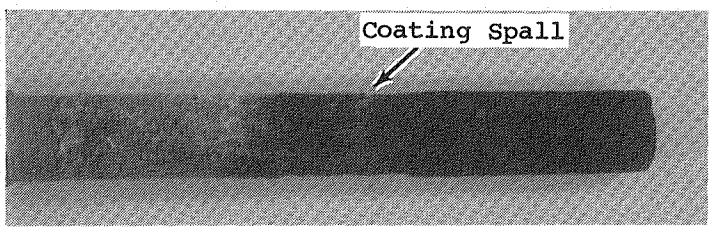

Duplex $CaTiO_3$/CoCrAlY Specimen

Figure 39. Test Specimens After 150 Hours of Burner Rig Testing at 932°C Using Fuel Containing Sulfur, Sodium and Vanadium

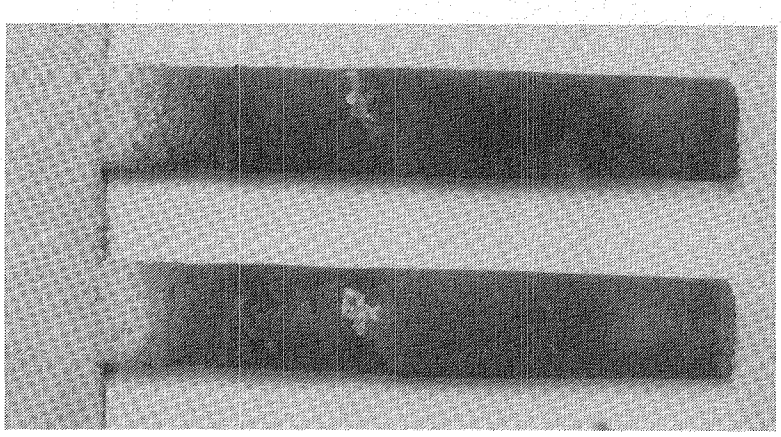

Fused $ZrO_2 \cdot 8Y_2O_3$/
NiCrAl-0.2Y - 341 Hours

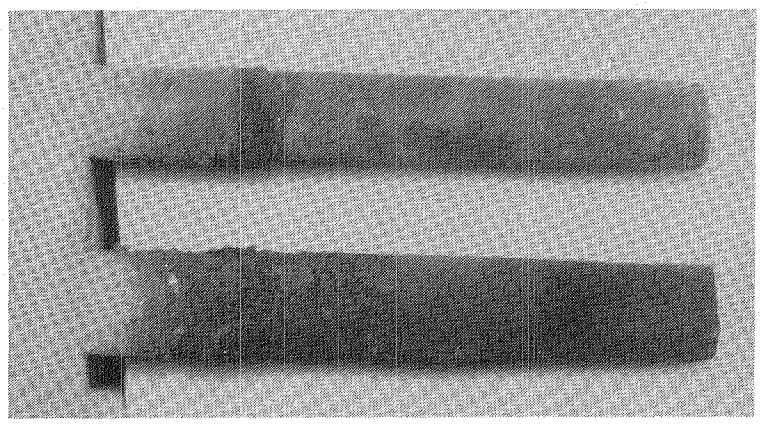

Fused $ZrO_2 \cdot 8Y_2O_3$/
NiCrAl-0.2Y - 341 hours

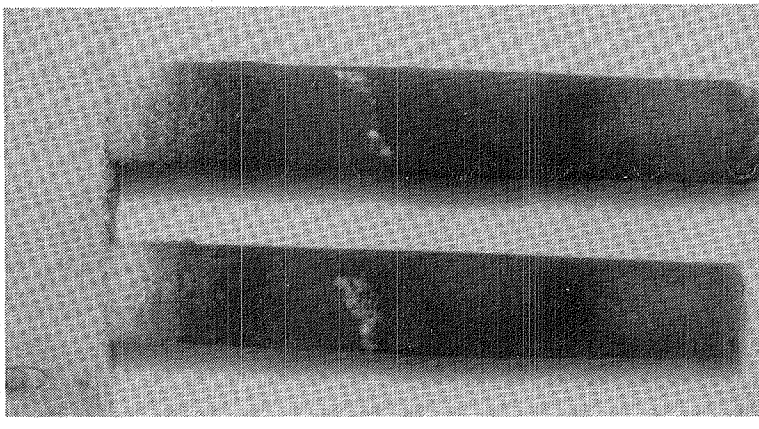

Uncoated - 341 Hours

Fused $ZrO_2 \cdot 8Y_2O_3$/
NiCrAl-0.8Y - 497 Hours

Fused $ZrO_2 \cdot 8Y_2O_3$/
NiCrAl-0.8Y - 341 Hours

Figure 40. Test Specimens at Completion of 500-Hour Burner Rig Test at 932°C Using Fuel Containing Sulfur, Sodium and Vanadium (Sheet 1 of 2)

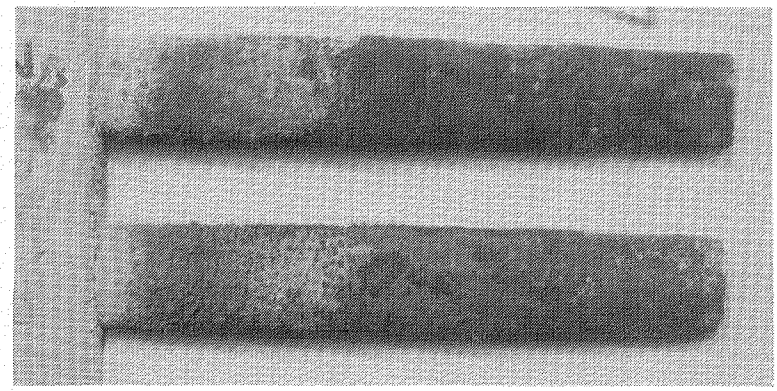

$CaO.TiO_2$/NiCrAl-0.5Y - 497 Hours

$CaO.TiO_2$/NiCrAl-0.5Y - 341 Hours

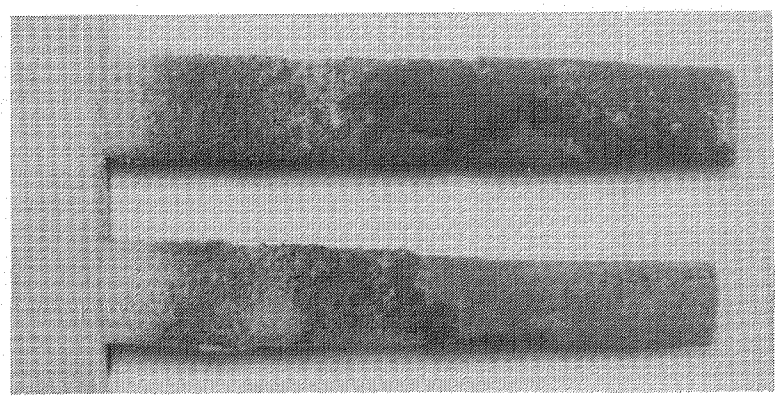

$CaO.TiO_2$/NiCrAlY - 341 Hours

$CaO.TiO_2$/CoCrAlY - 497 Hours

Figure 40. Test Specimens at Completion of 500-Hour Burner Rig Test at 932°C Using Fuel Containing Sulfur, Sodium and Vanadium (Sheet 2 of 2)

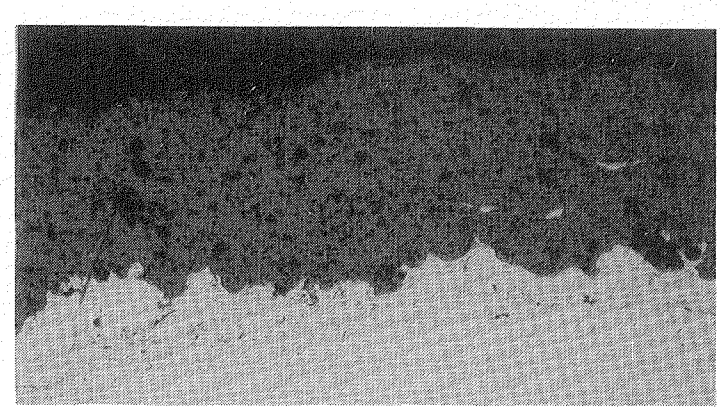

Figure 41.

Fused $ZrO_2.8Y_2O_3$/NiCrAl-0.2Y TBC After 341 Hours of Burner Rig Testing at 932°C With Sodium, Sulfur and Vanadium in the Fuel

Magnification: 100X

Mount No. 1319

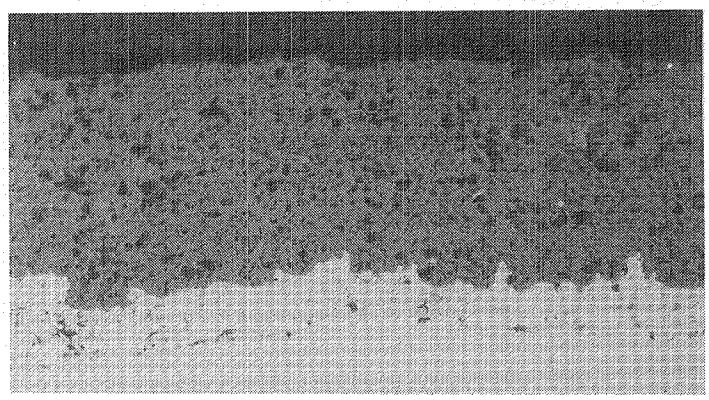

Figure 42.

Fused $ZrO_2.8Y_2O_3$/NiCrAl-0.5Y TBC After 341 Hours of Burner Rig Testing at 932°C With Sodium, Sulfur and Vanadium in the Fuel

Magnification: 100X

Mount No. 1320

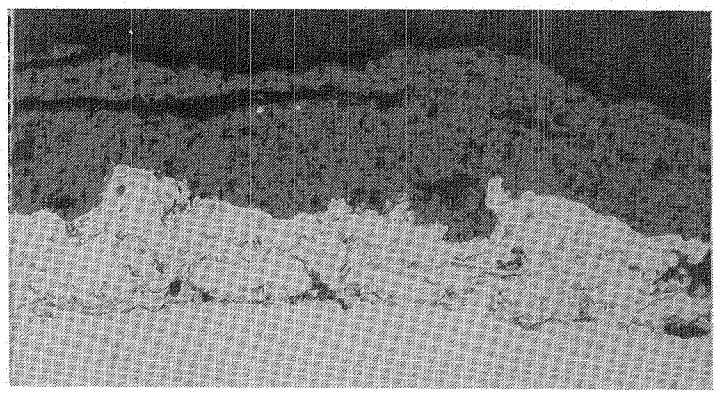

Figure 43.

Fused $ZrO_2.8Y_2O_3$/NiCrAl-0.8Y TBC After 497 Hours of Burner Rig Testing at 932°C With Sodium, Sulfur and Vanadium in the Fuel

Magnification: 100X

Mount No. 1320

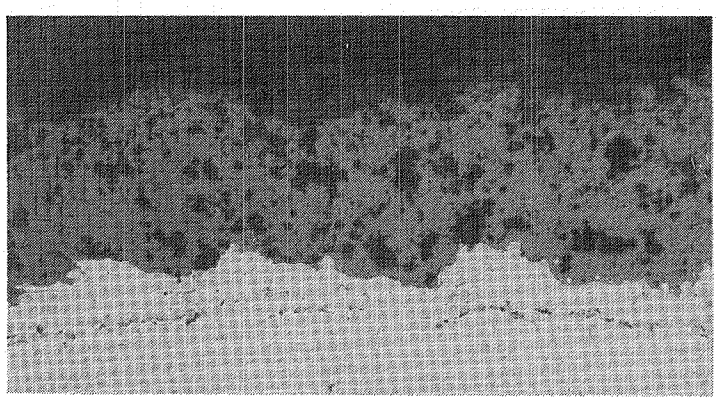

Figure 44.

$CaO.TiO_2$/NiCrAl-0.5Y TBC After 341 Hours of Burner Rig Testing at 932°C With Sodium, Sulfur and Vanadium in the Fuel

Magnification: 100X

Mount No. 1321

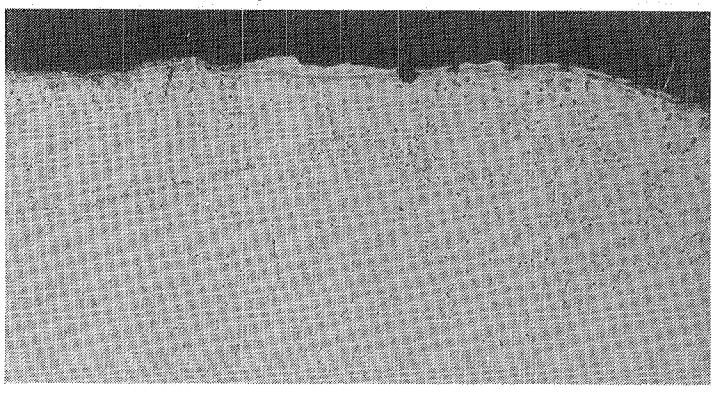

Figure 45.

$CaO.TiO_2$/CoCrAlY TBC After 497 Hours of Burner Rig Testing at 932°C With Sodium, Sulfur and Vanadium in the Fuel

Magnification: 100X

Mount No. 1321

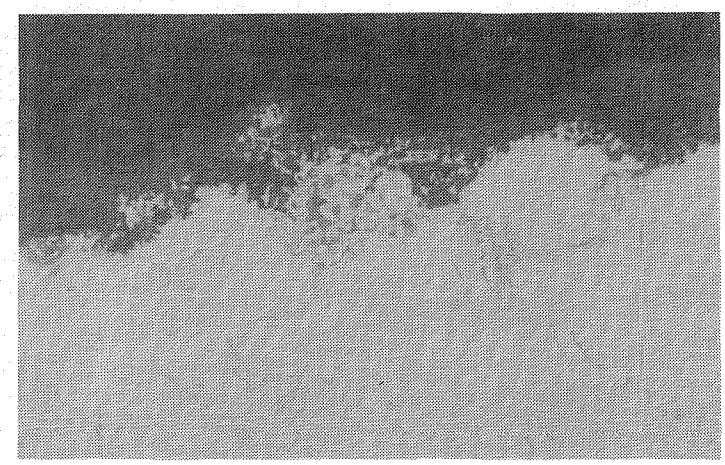

Figure 46.

Uncoated MAR-M421 Control Bar After 175 Hours of Testing at 793°C With 3 ppm Salt

Magnification: 500X

Mount No. 1837

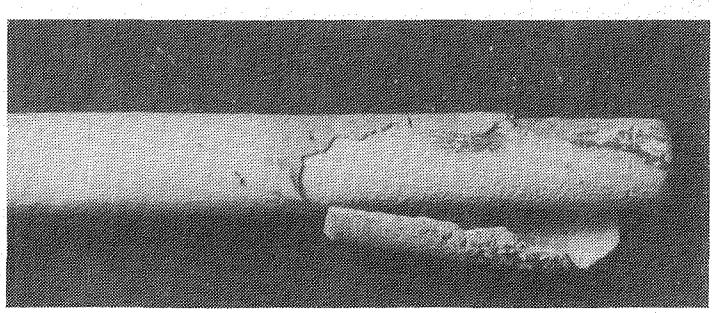

Figure 47.

Duplex Coated NiCrAlY/ $ZrO_2 \cdot 8Y_2O_3$ After 175 Hours of Burner Rig Testing at 793°C and 3 ppm Sea Salt

Fuel Deposit

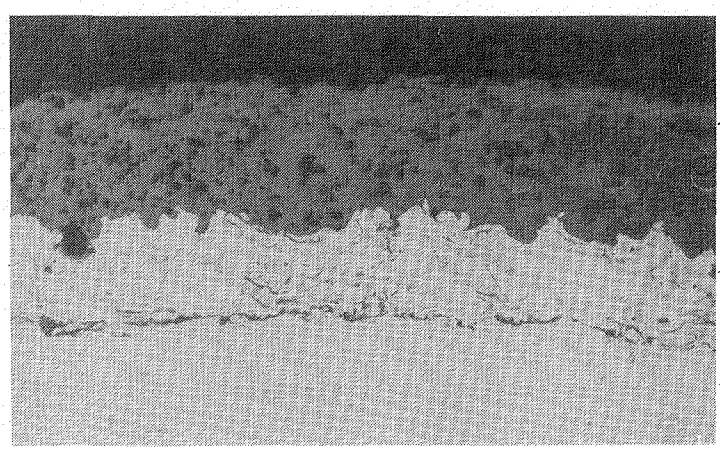

Magnification: 100X

Figure 48. Duplex Coated NiCrAlY/$ZrO_2 \cdot 8Y_2O_3$ Specimen After 175 Hours of Testing at 793°C and 3 ppm Sea Salt

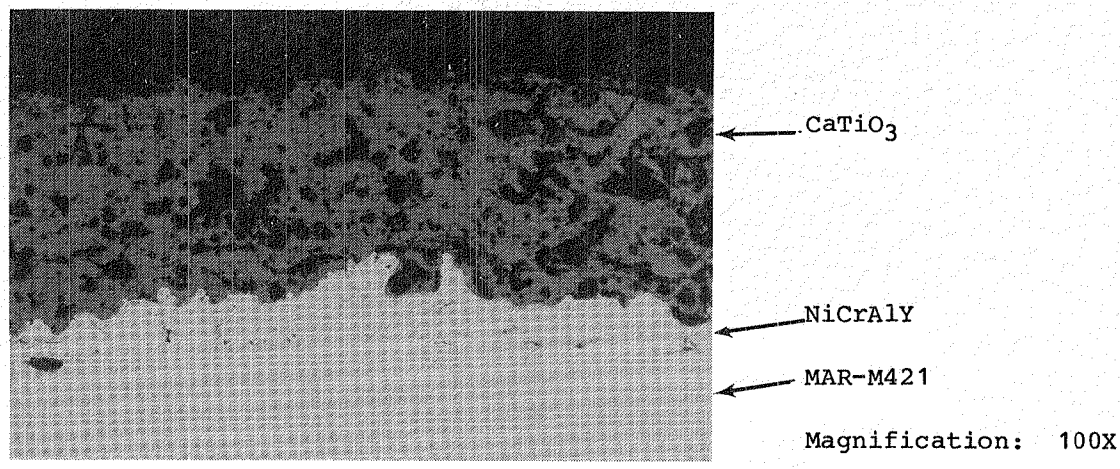

Figure 49. Duplex Coated NiCrAlY/$CaTiO_3$ Coating After 175 Hours Testing at 793°C and 3 ppm Sea Salt

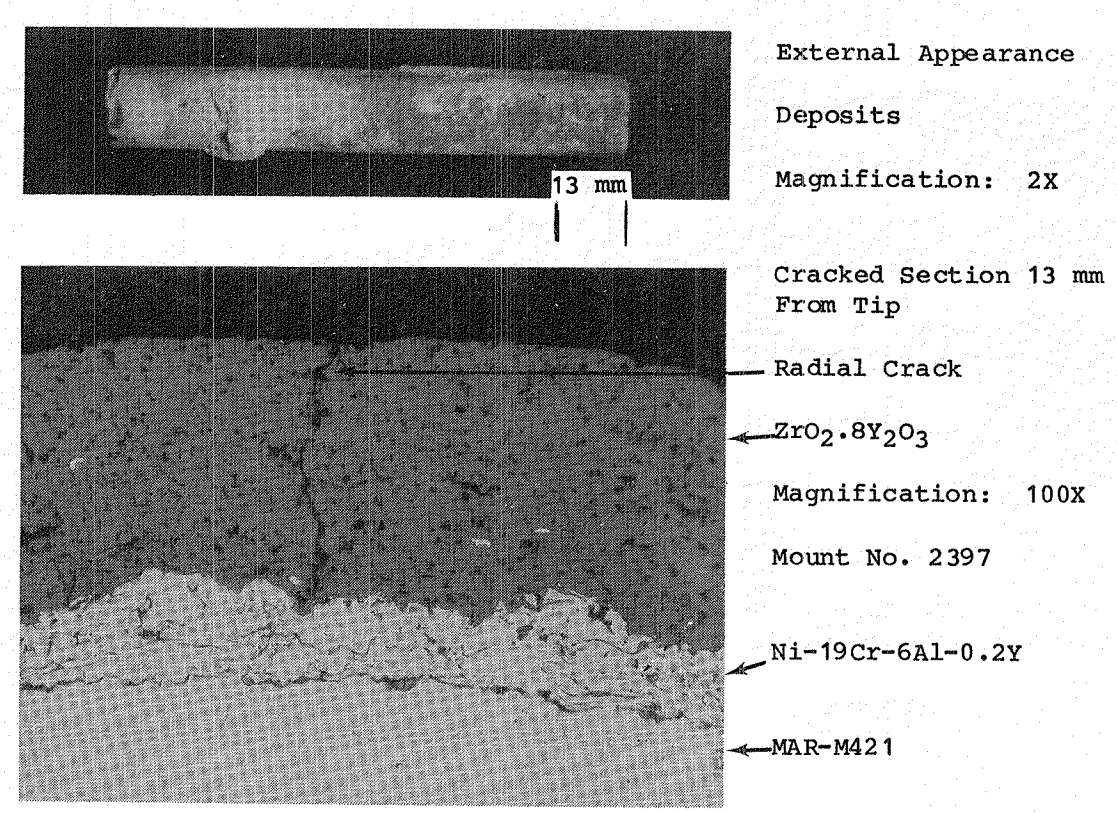

Figure 50. NiCrAlY/ZrO_2 TBC After 225-Hour Test at 849°C and 100 Hours at 905°C, 3 ppm Sea Salt

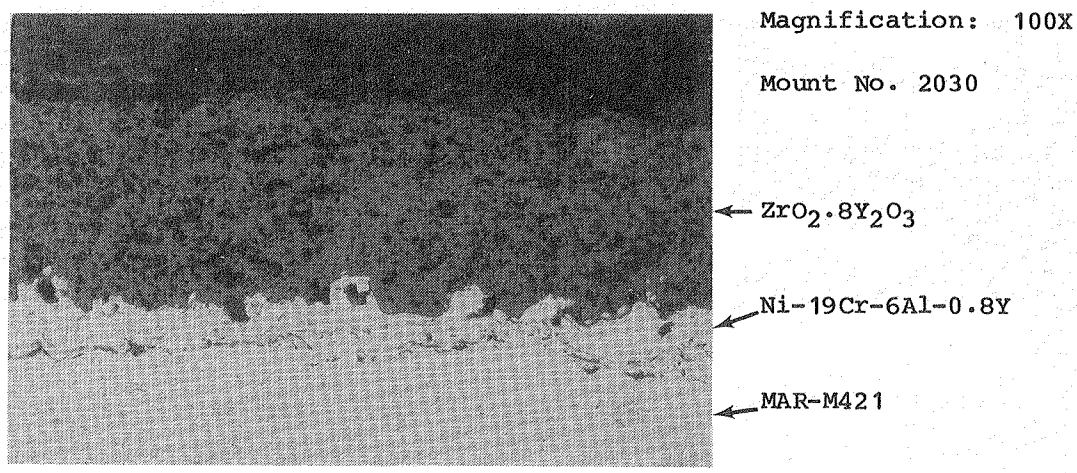

Figure 51. $ZrO_2 \cdot 8Y_2O_3$ Coating After 500-Hour Burner Rig Test; 175 Hours at 793°C, 225 Hours at 849°C and 100 Hours at 905°C, 3 ppm Sea Salt

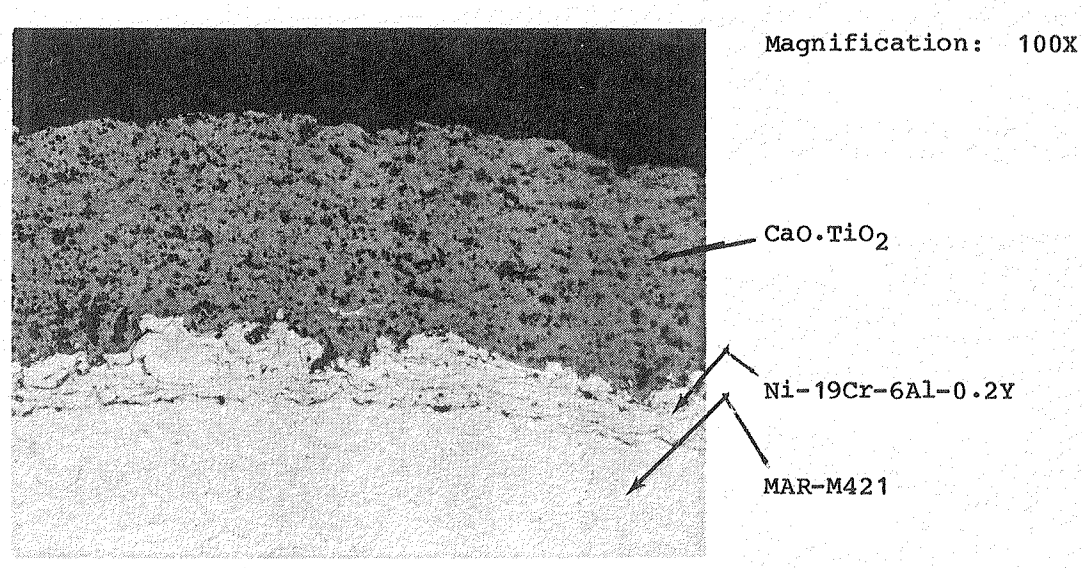

Figure 52. $CaO \cdot TiO_2$ Specimen After 500-Hour Burner Rig Test; 175 Hours at 793°C, 225 Hours at 849°C, and 100 Hours at 905°C, 3 ppm Sea Salt

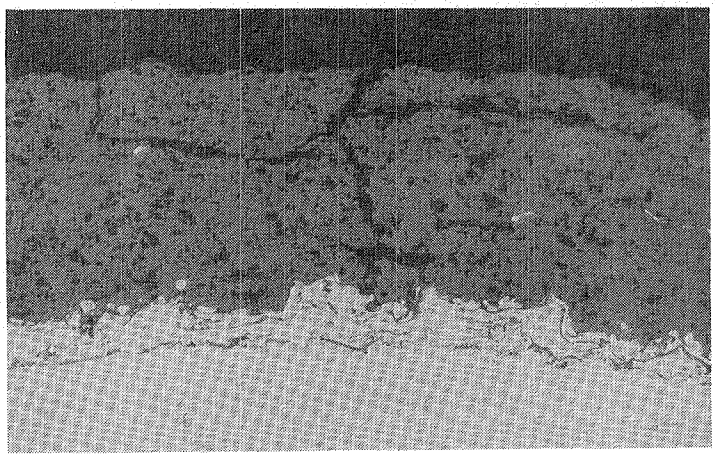

Figure 53.

Cracked Area of $CaO.TiO_2$ Coating After 500-Hour Test; 175 Hours at 793°C, 225 Hours at 849°C and 100 Hours at 905°C, 3 ppm Sea Salt

Magnification: 100X

Mount No. 2396

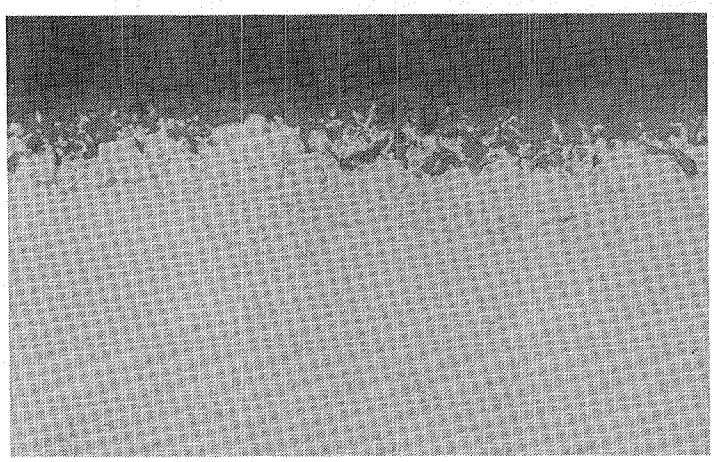

Figure 54.

Uncoated MAR-M421 Specimen After 100-Hour Burner Rig Test at 905°C and 3 ppm Sea Salt

Magnification: 500X

Mount No. 2020

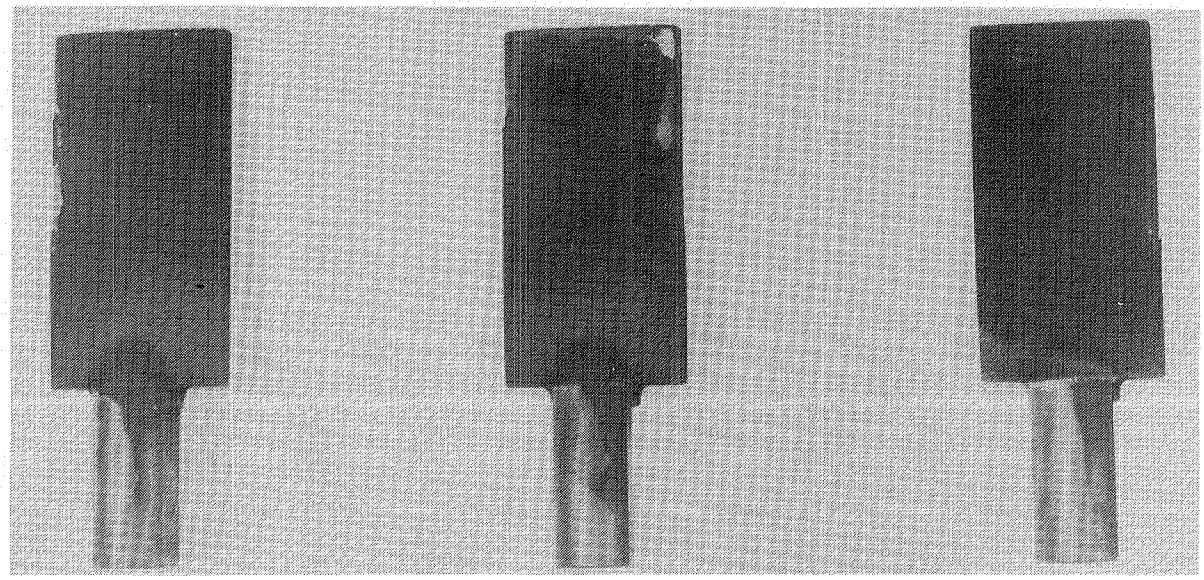

Figure 55. Airfoil or Paddle Shaped Samples After 50-Hour Test at 815°C Leading Edge

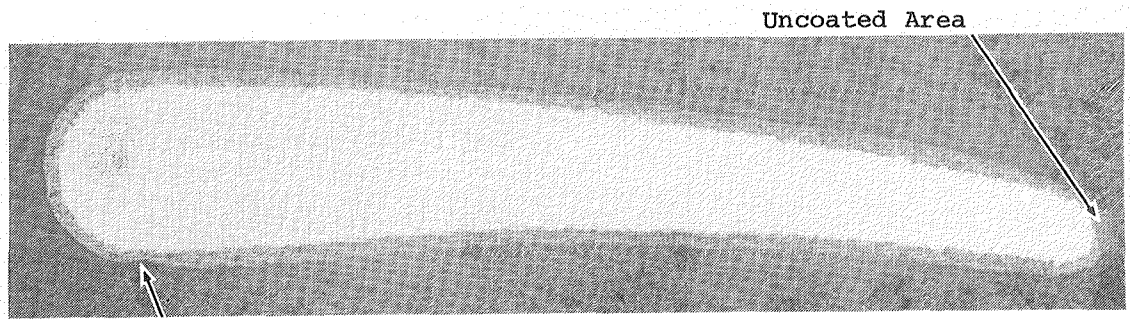

Figure 56. As-Coated Airfoil Section; Coating System Sintered $ZrO_2 \cdot 8Y_2O_3$ Applied to a NiCrAlY Bond Coat (Magnification: 5X)

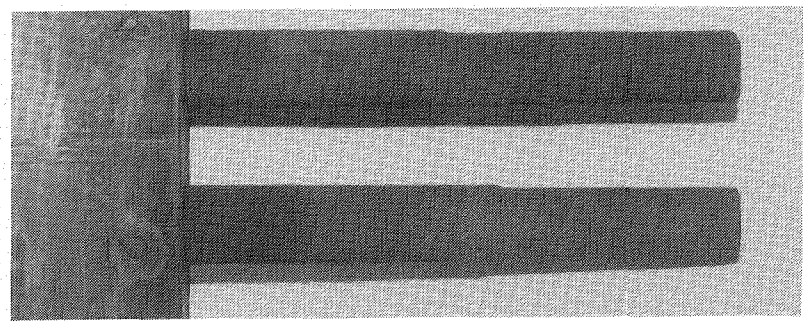

Figure 57. Calcium Titanate and Baseline Coated MAR-M421 Bars After 1000-Hour Endurance Test

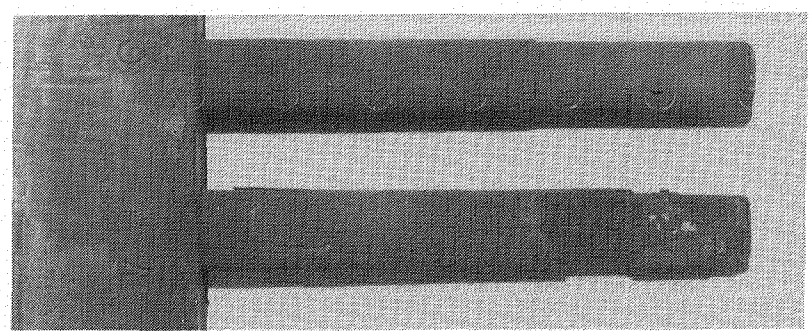

Figure 58. Calcium Silicate Coated MAR-M421 and Calcium Titanate Coated X-45M Bars After 1000-Hour Endurance Test

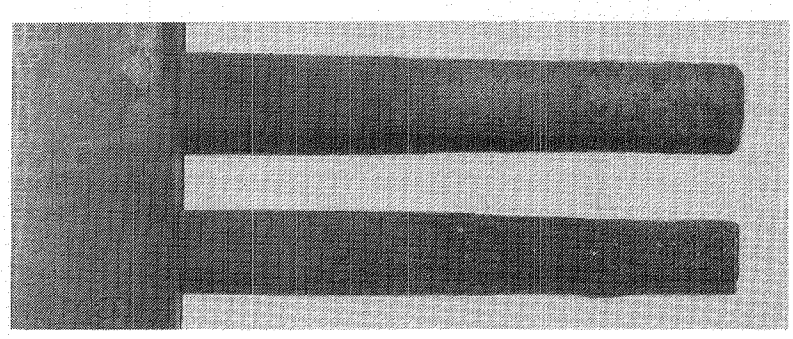

$ZrO_2 \cdot 8Y_2O_3$/MAR-M421

NiCrAlY/MAR-M421

Figure 59. Zirconia and NiCrAlY Coated Bars After 1000-Hour Endurance Test

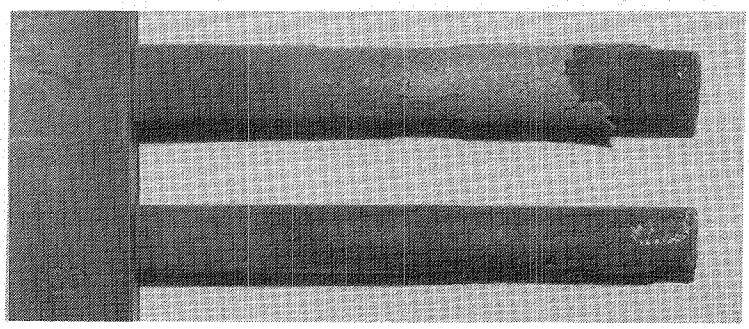

$ZrO_2 \cdot 8Y_2O_3$

MAR-M421 (Uncoated)

Figure 60. Zirconia Coated X-45M and Bare MAR-M421 Bars After 1000-Hour Endurance Test

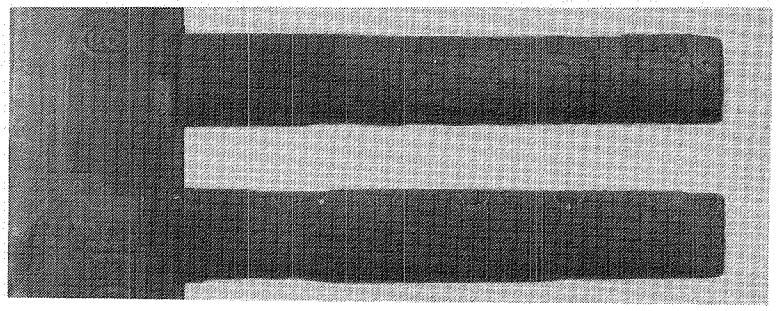

$ZrO_2 \cdot 8Y_2O_3$

$CaO \cdot TiO_2$/Hastelloy X

Figure 61. Zirconia and Calcium Titanate Coated Hastelloy X Bars After 1000-Hour Endurance Test

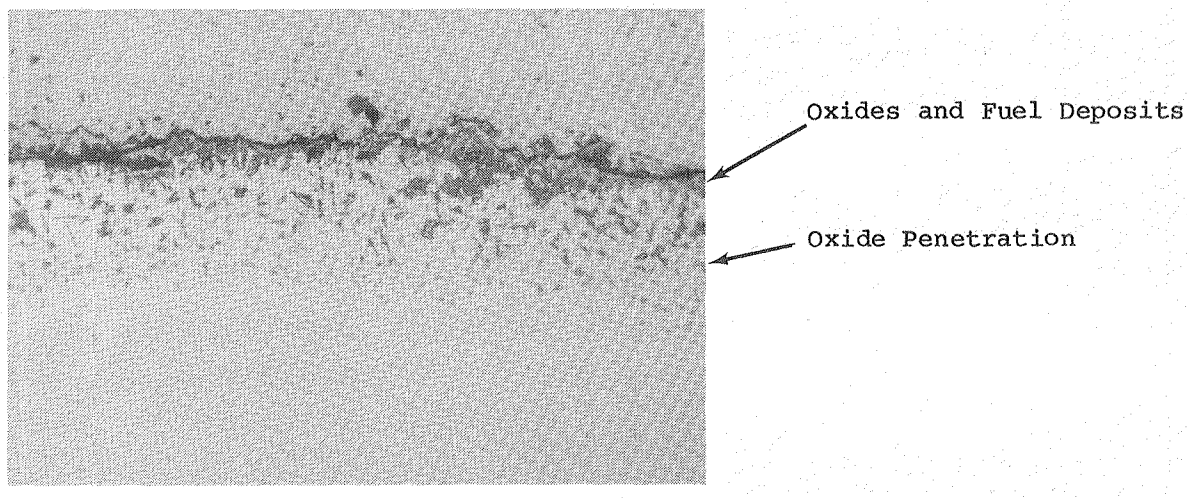

Figure 62. NiCrAlY Coated Test Bar at Completion of 1000-Hour Endurance Test. (Magnification: 100X; Mount No. 2667)

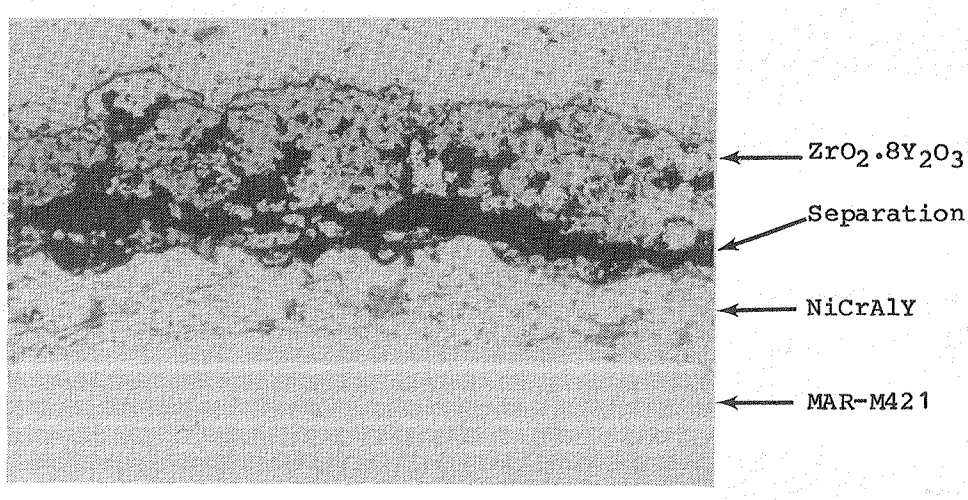

Figure 63. Baseline $ZrO_2.8Y_2O_3$ TBC After 1000-Hour Endurance Test (Magnification: 100X; Mount No. 2666)

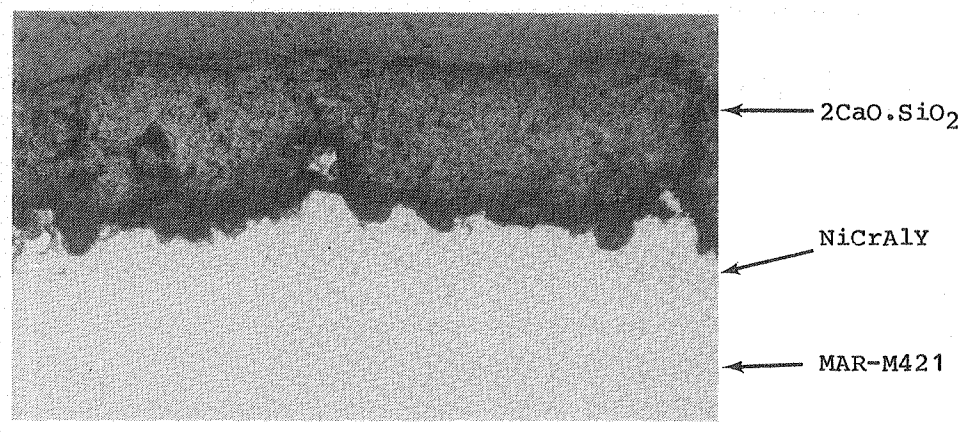

Figure 64. A $2CaO.TiO_2$ TBC After 1000-Hour Testing (Magnification: 100X; Mount No. 2565)

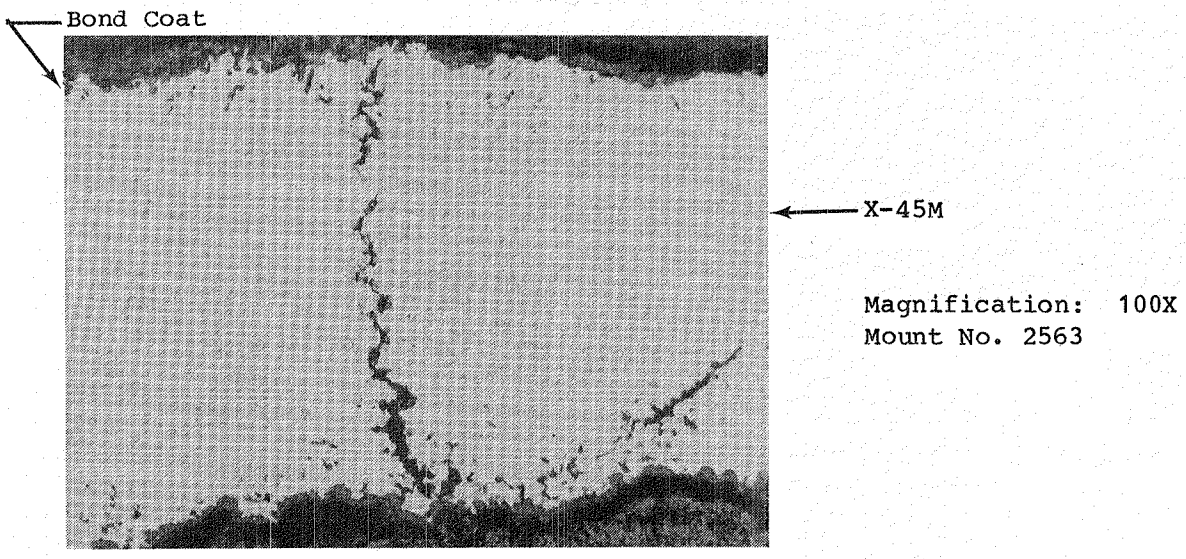

Figure 65. Cobalt-Base Alloy X-45M With $ZrO_2.8Y_2O_3$ TBC After 1000-Hour Endurance Test

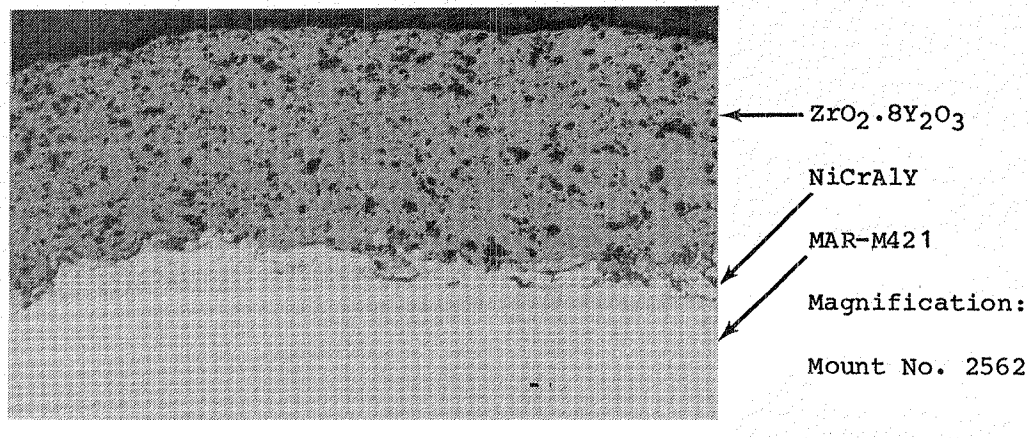

Figure 66. Nickel-Base Alloy MAR-M421 Coated With $ZrO_2.8Y_2O_3$ TBC After 1000-Hour Endurance Test

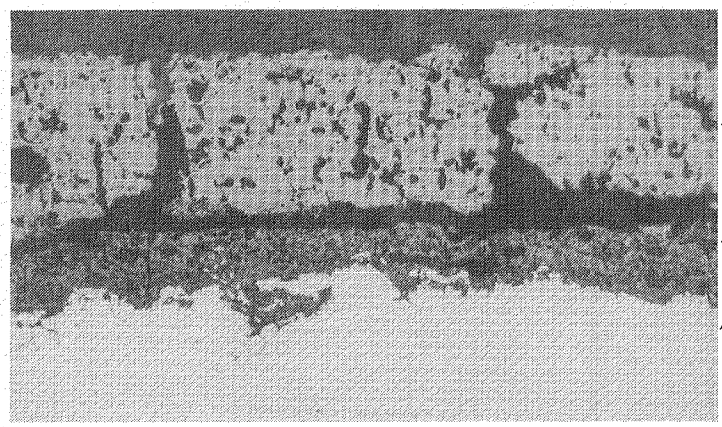

Figure 67. Calcium Titanate Coated Cobalt-Base Alloy X-45M Specimen After 1000-Hour Endurance Test

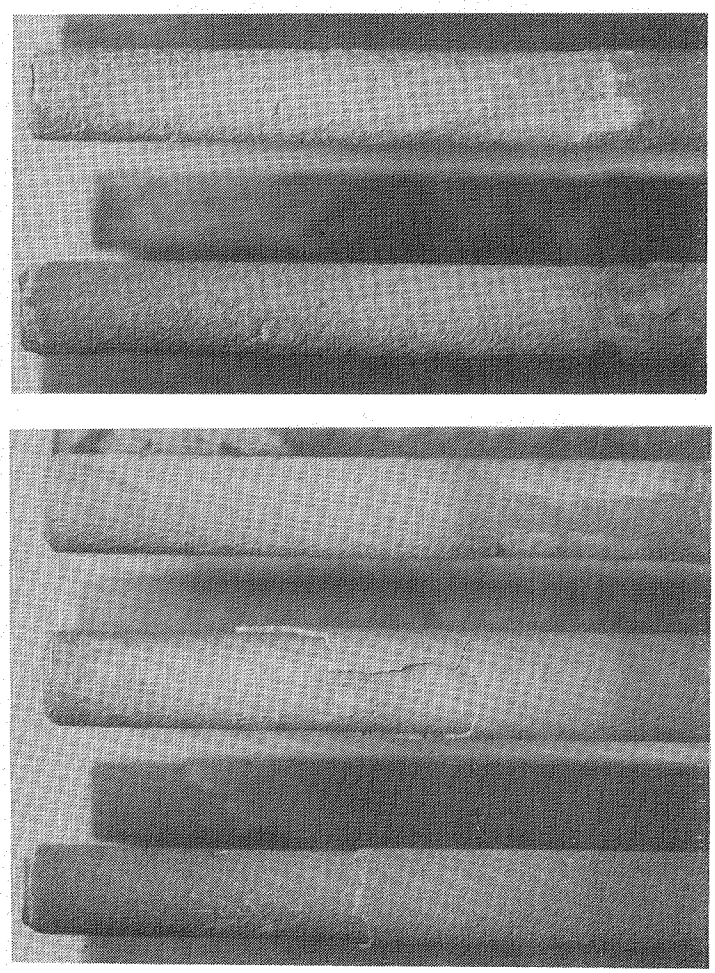

Figure 68. Endurance Specimens After 1000-Hour Hot Corrosion Test (Sheet 1 of 2)

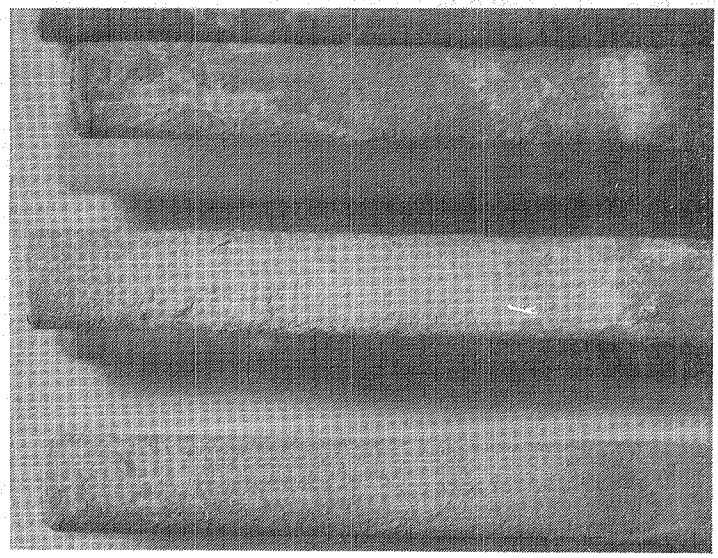

NASA $2CaO.SiO_2$/MAR-M421

NiCrAlY/MAR-M421

$ZrO_2.8Y_2O_3$/Hastelloy X

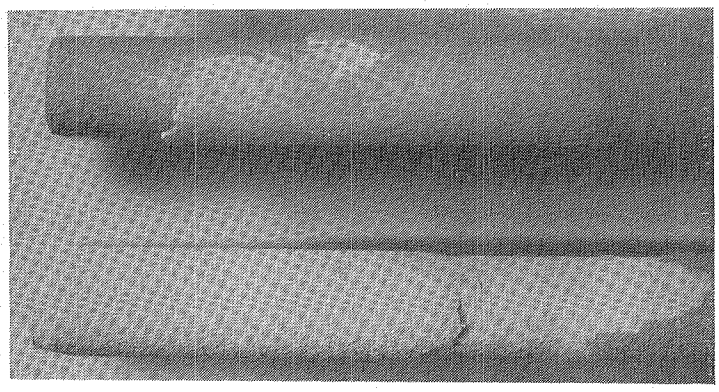

$CaO.TiO_2$/X-45M

$ZrO_2.8Y_2O_3$/X-45M

Figure 68. Endurance Specimens After 1000-Hour Hot Corrosion Test (Sheet 2 of 2)

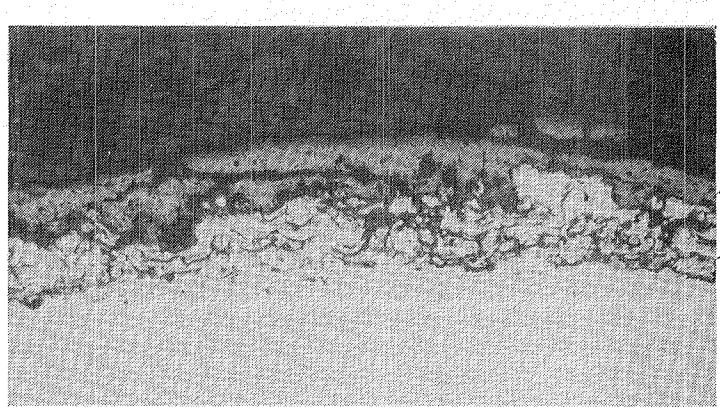

Figure 69. Calcium Titanate Coated Hastelloy X Specimen After 1000-Hour Hot Corrosion Test (Magnification: 100X; Mount No. 3141)

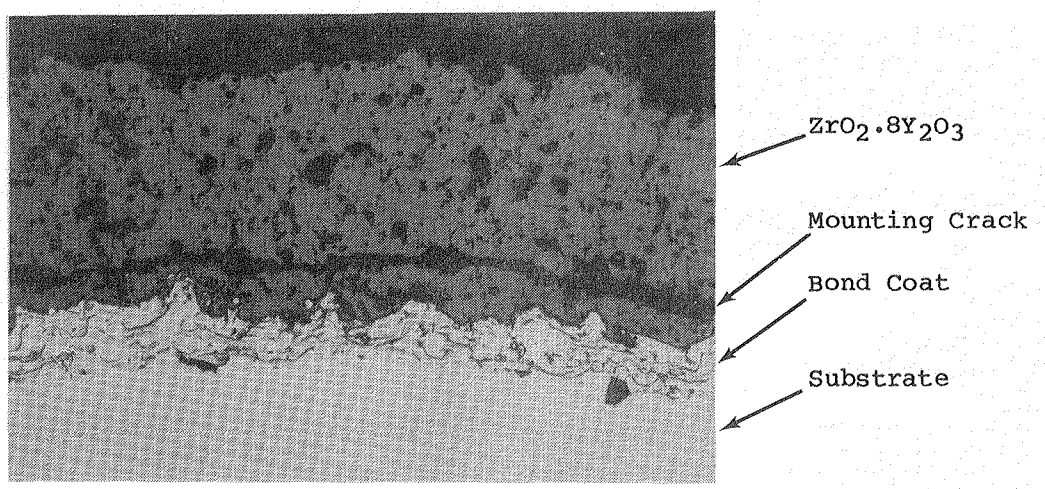

Figure 70. X-45M Specimen With $ZrO_2.8Y_2O_3$ TBC After 1000-Hour Hot Corrosion Test (Magnification: 100X; Mount No. 3150)

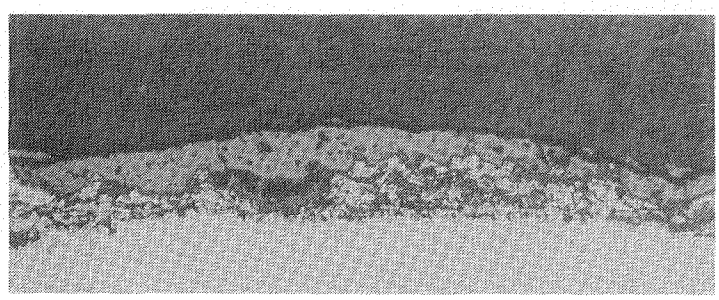

Figure 71.

Bare MAR-M421 Specimen After 1000-Hour Hot Corrosion Test

Magnification: 100X

Mount No. 3142

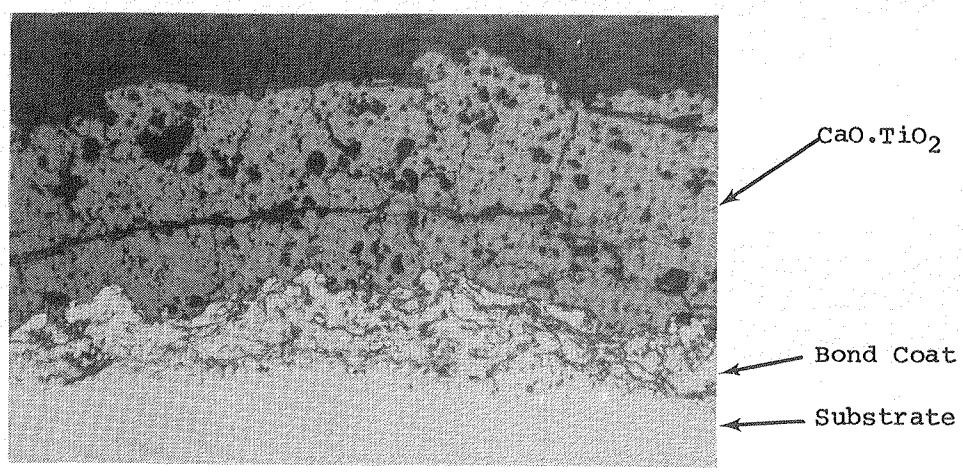

Figure 72. Calcium Titanate TBC With MAR-M421 Substrate After 1000-Hour Hot Corrosion Test (Magnification: 100X; Mount No. 3143)

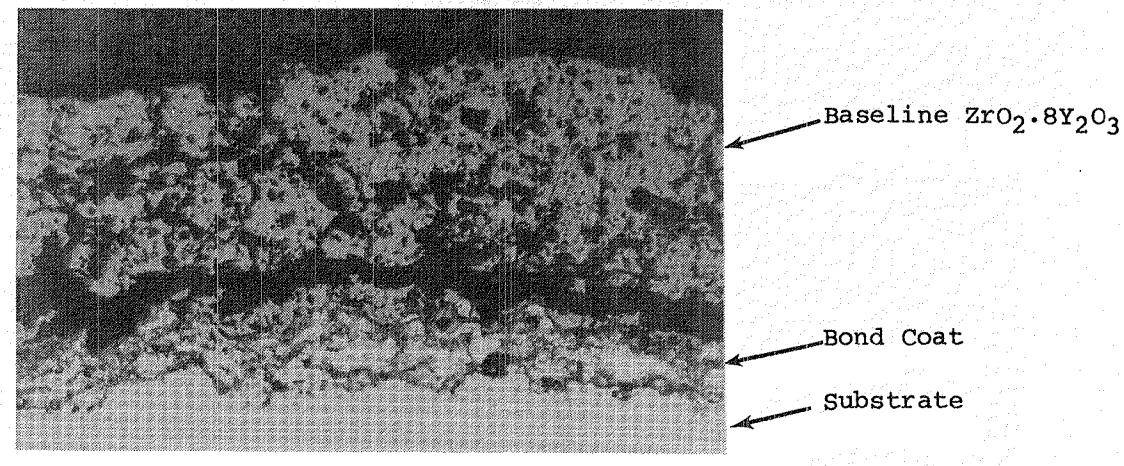

Figure 73. NASA Baseline Coating With MAR-M421 Substrate After 1000-Hour Hot Corrosion Test (Magnification: 100X; Mount No. 3145)

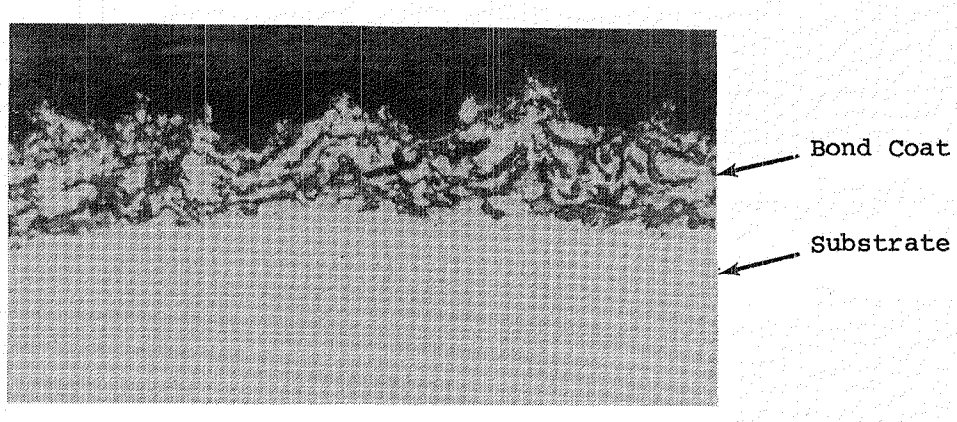

Figure 74. Baseline Calcium Silicate Coating With MAR-M421 Substrate After 1000-Hour Hot Corrosion Test (Magnification: 100X; Mount No. 3146)

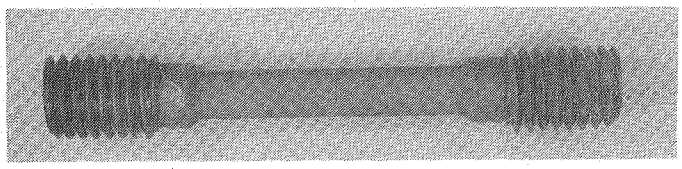

A. Magnification: 1X

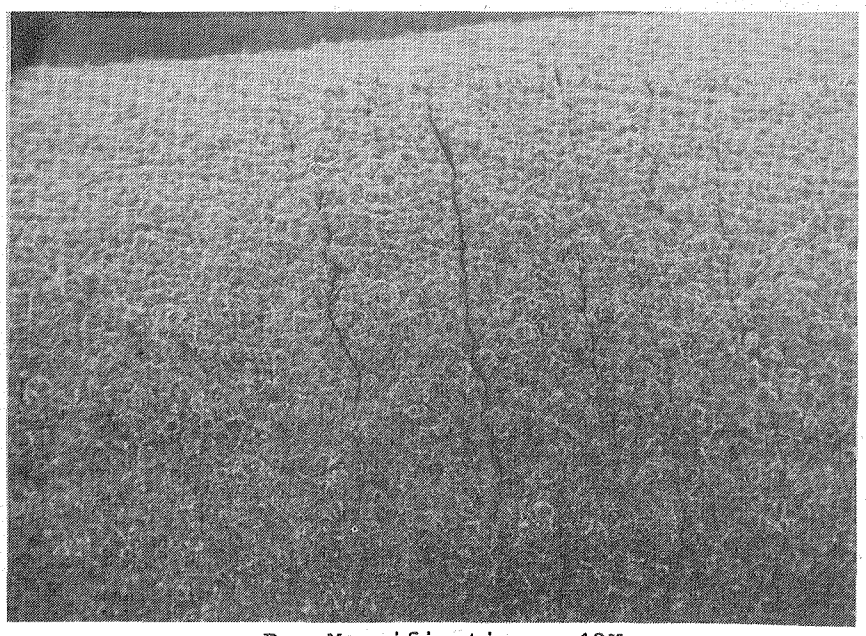

B. Magnification: 12X

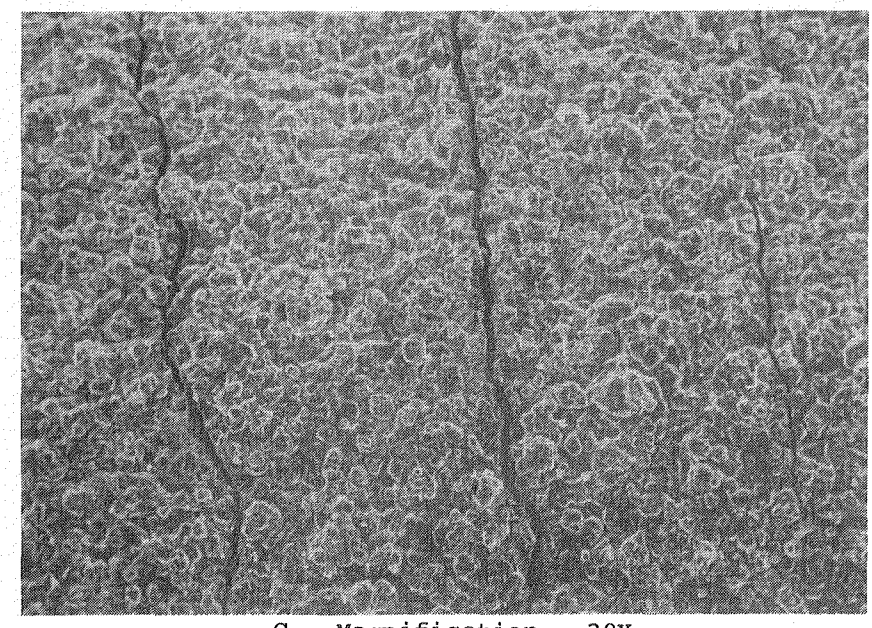

C. Magnification: 30X

Figure 75. Calcium Titanate Plasma Sprayed Hastelloy X After One Percent Total Tensile Strain (0.038 mm Elastic Plus 0.22 mm Plastic). Ceramic is 0.25 mm Thick.

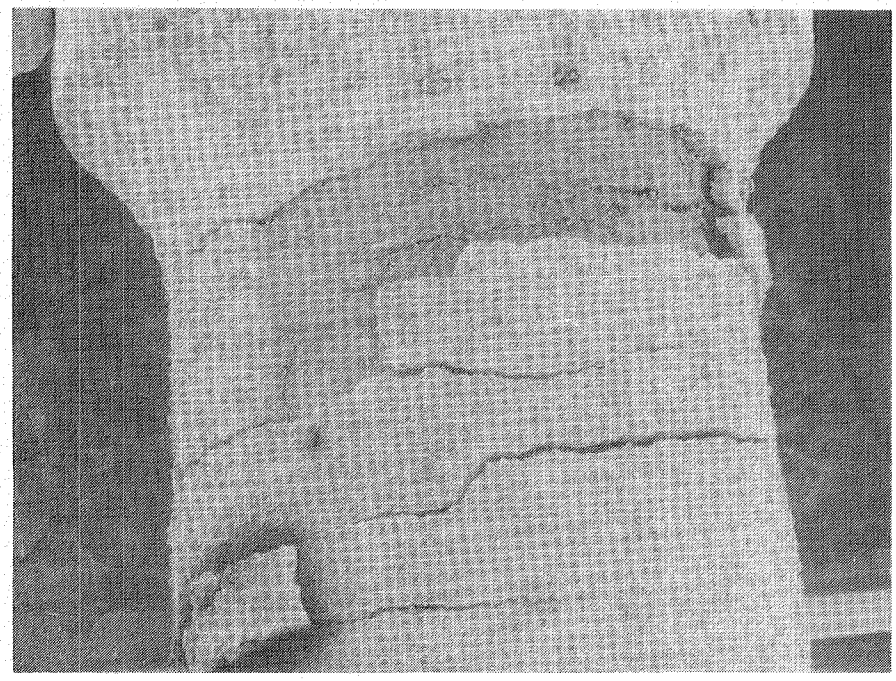

Magnification: 12X

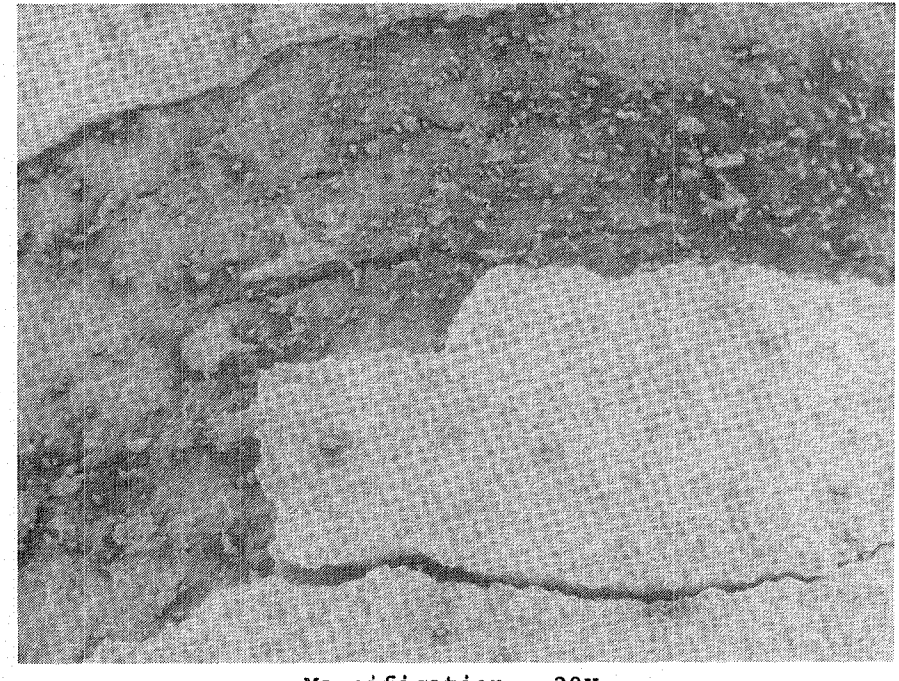

Magnification: 30X

Figure 76. Tensile Strain Tolerance Test Specimen Coated With Zirconia-8 Percent Yttria After 1.4 Percent Total Tensile Strain

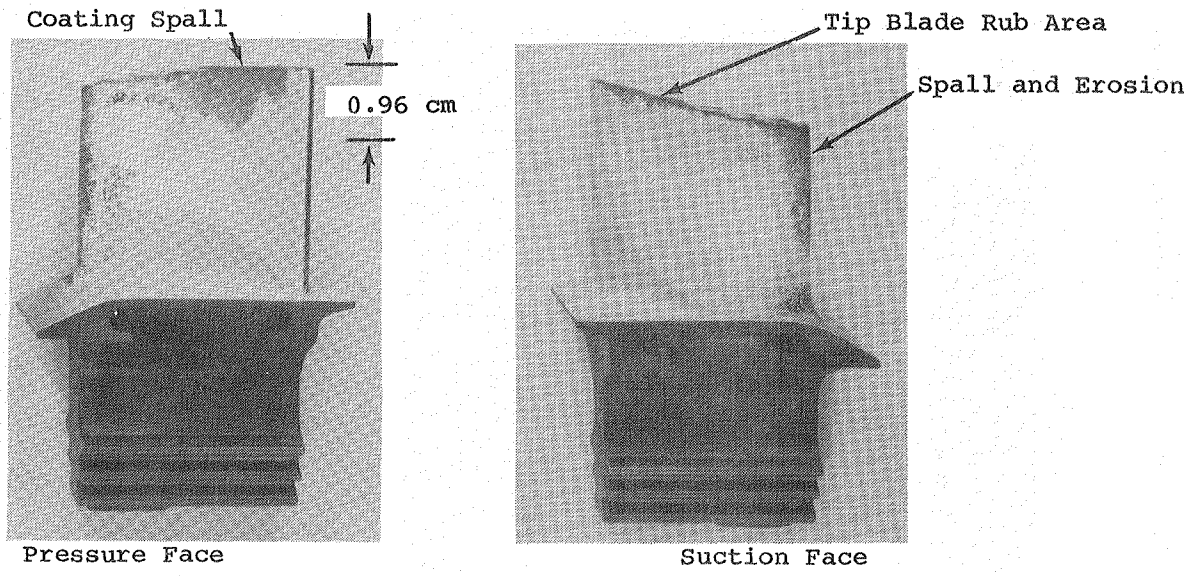

Figure 77. Calcium Silicate TBC Blade After 550-Hour Engine Endurance Test

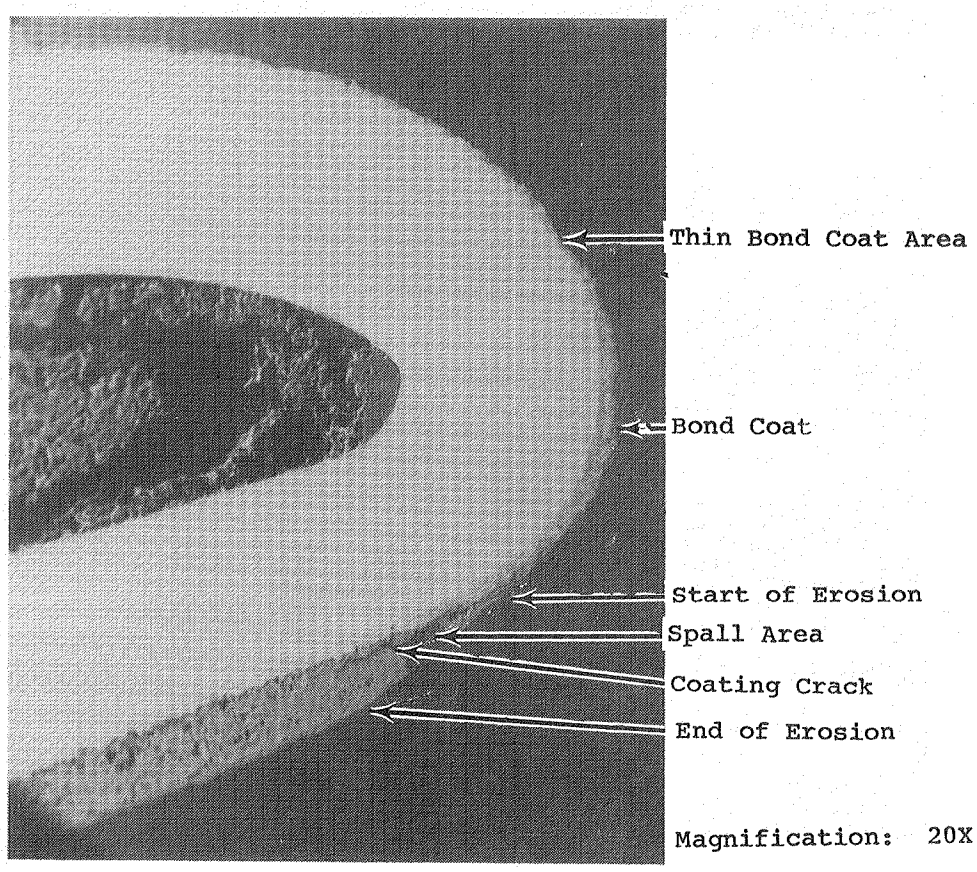

Figure 78. Leading Edge Section of Calcium Silicate TBC Blade After 550-Hour Engine Endurance Test

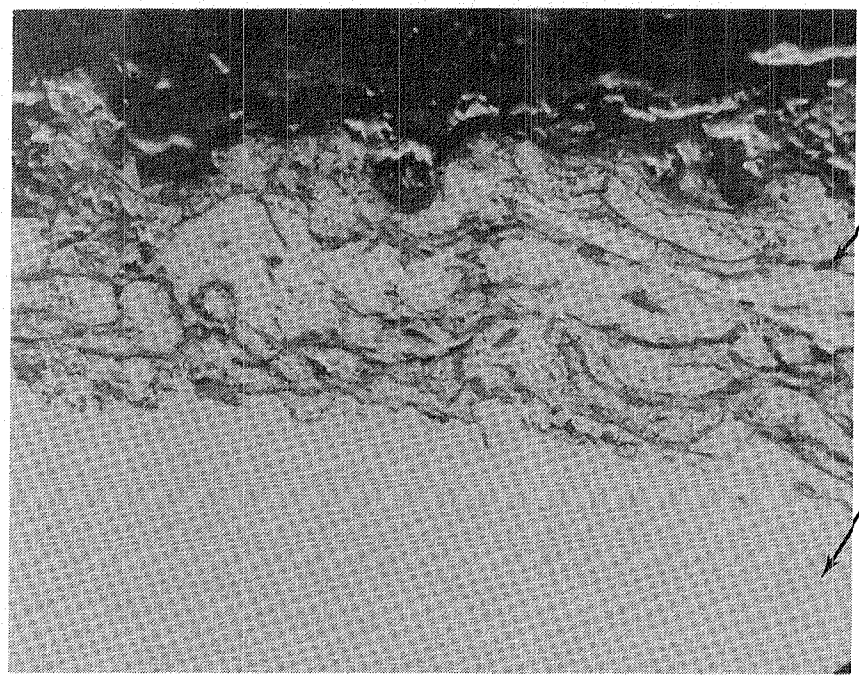

Figure 79. Bond Coat on Leading Edge of Ca_2SiO_3 TBC Blade After 550-Hour Engine Endurance Test

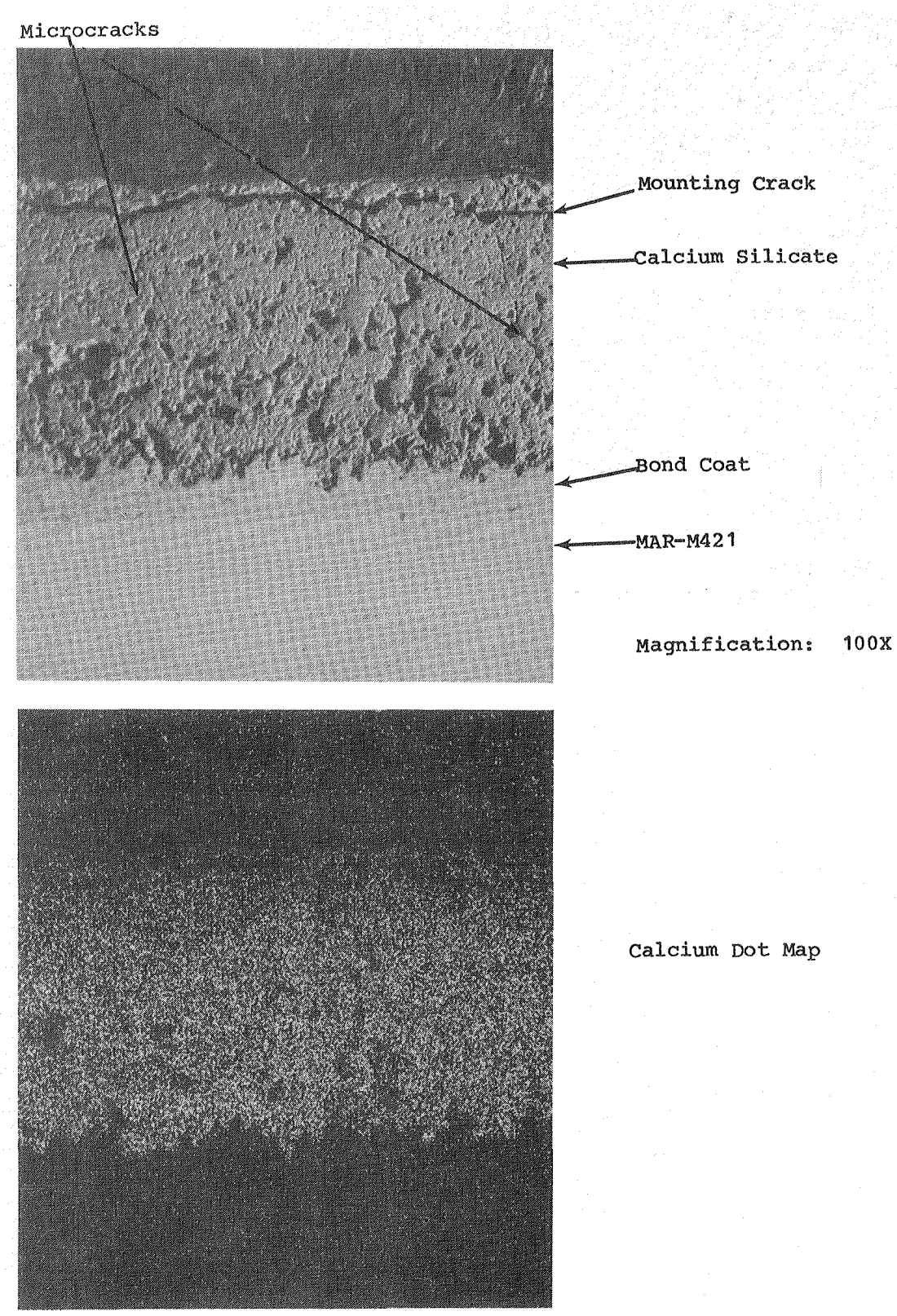

Figure 80. Calcium Silicate TBC After 550-Hour Engine Endurance Test

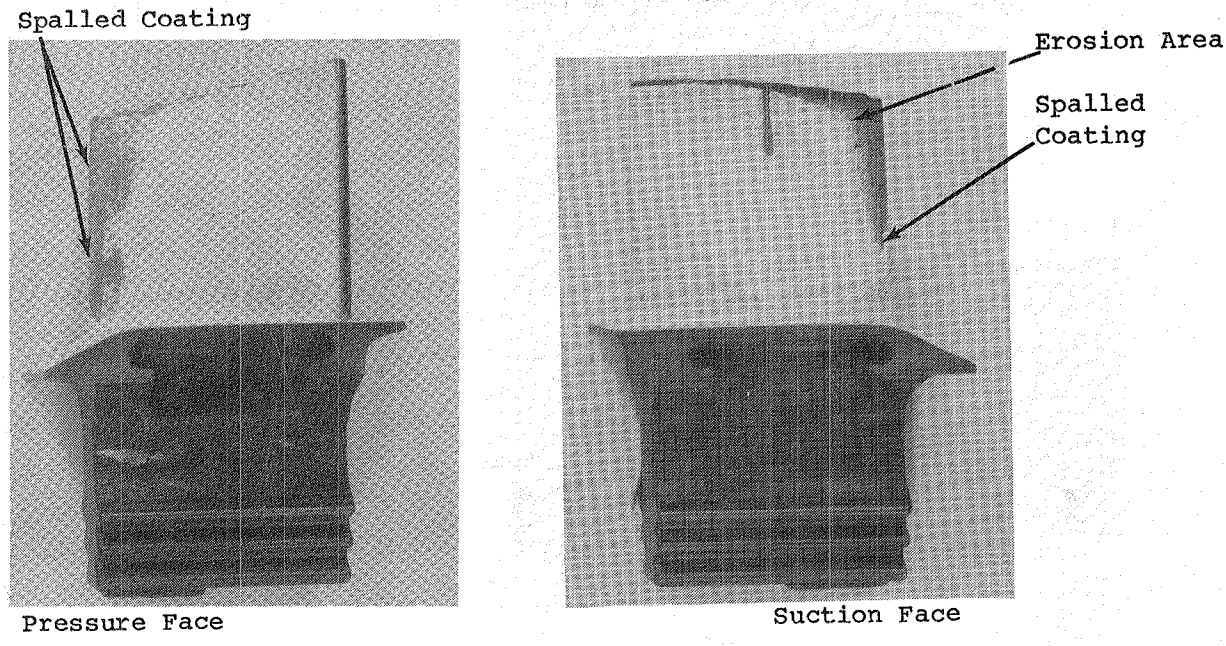

Figure 81. Sintered $ZrO_2 \cdot 8Y_2O_3$ TBC Blade After 550-Hour Engine Endurance Test

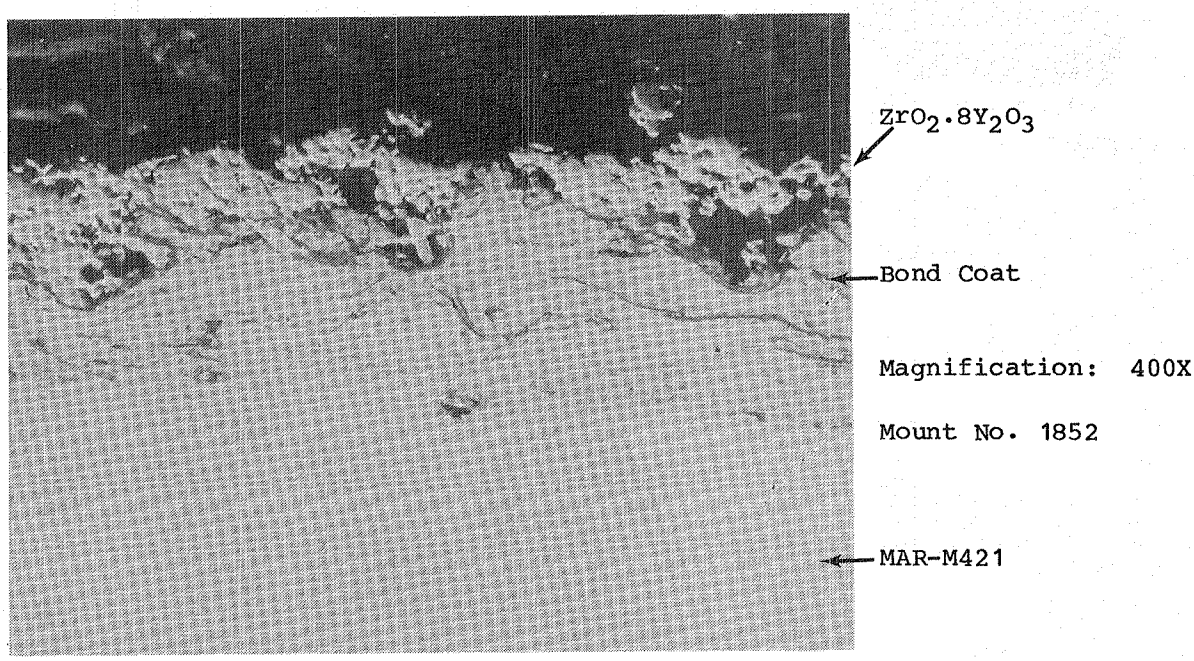

Figure 82. Leading Edge of Sintered $ZrO_2 \cdot 8Y_2O_3$ TBC Blade After 550-Hour Engine Endurance Test

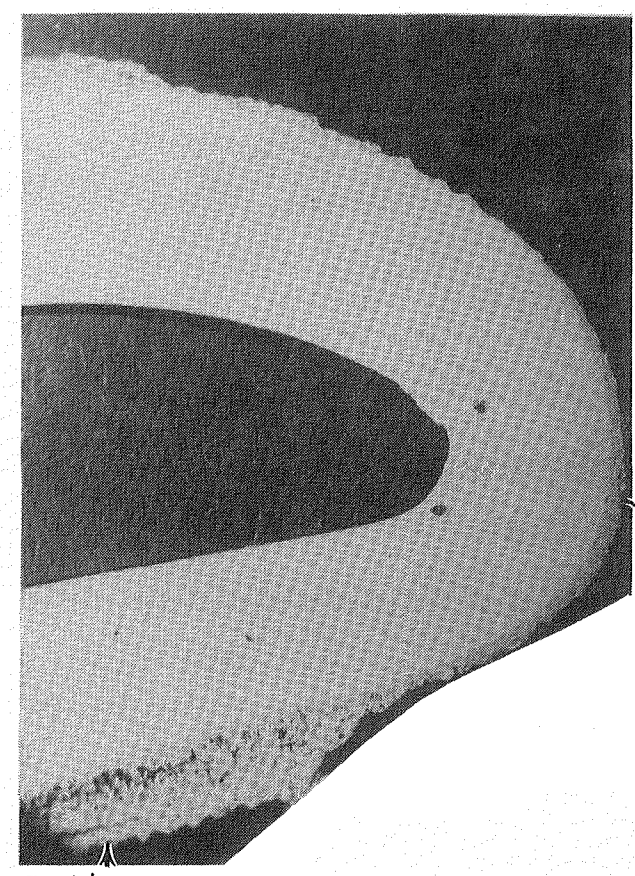

Figure 83. Section of Sintered $ZrO_2 \cdot 8Y_2O_3$ TBC Blade After 550-Hour Engine Endurance Test

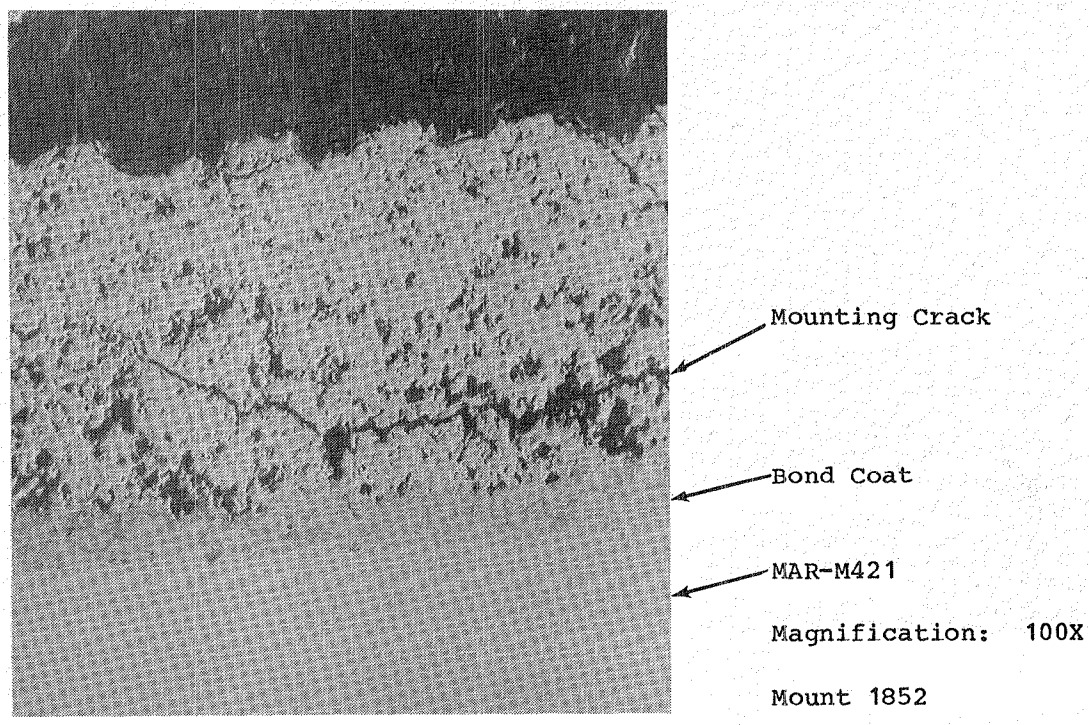

Figure 84. Sintered $ZrO_2 \cdot 8Y_2O_3$ TBC Structure After 550-Hour Engine Endurance Test

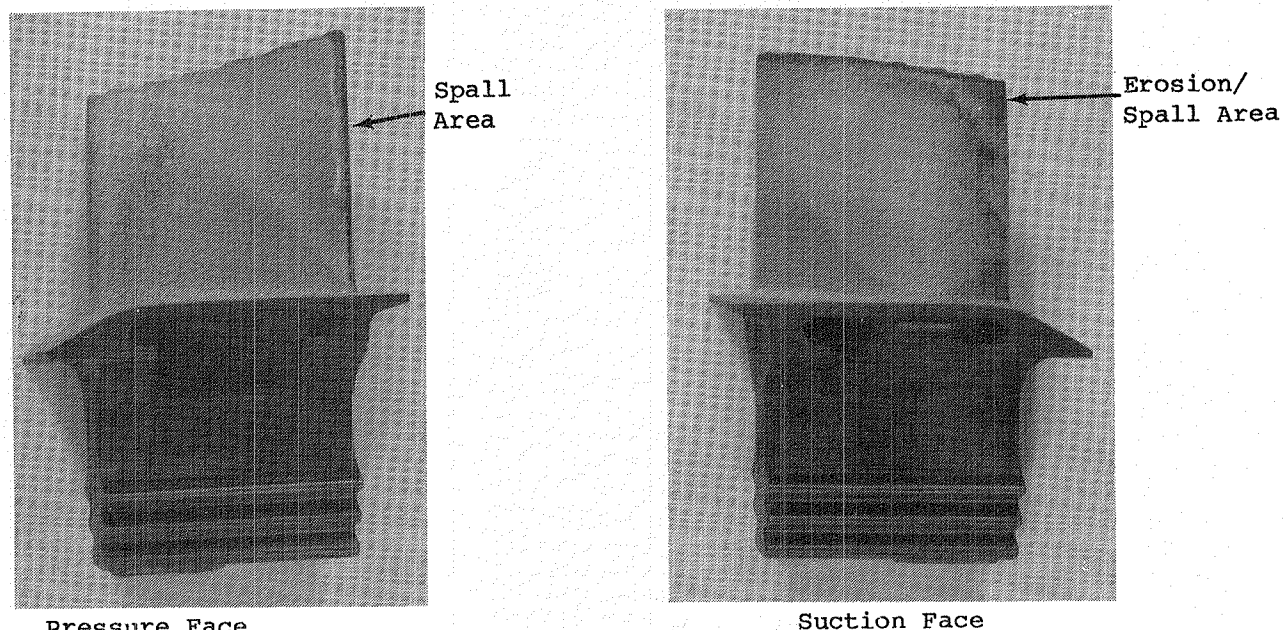

Figure 85. Calcium Titanate TBC After 550-Hour Engine Endurance Test

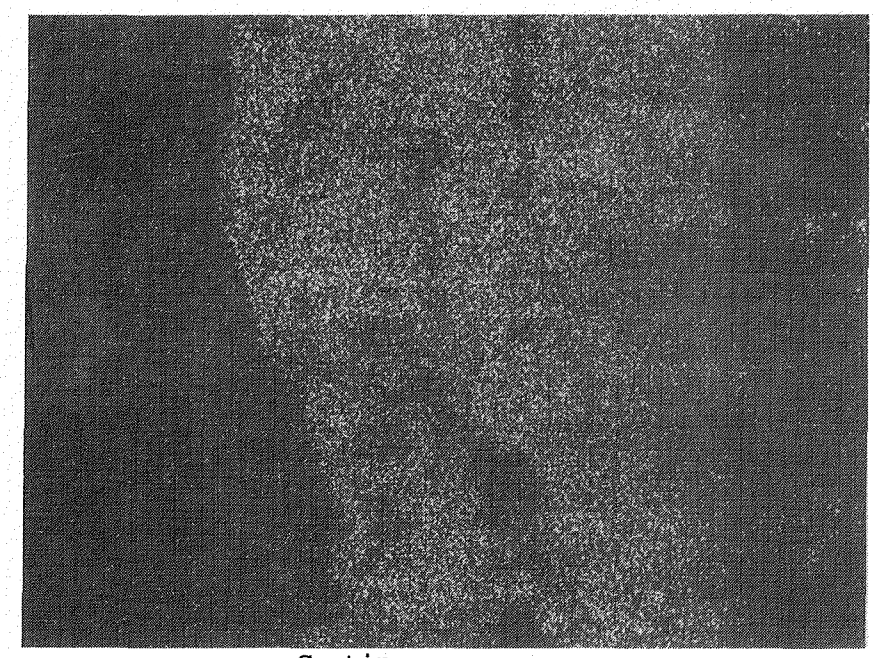

Coating

Figure 86.

Dot Map of Calcium Content in the $CaTiO_3$ Coating

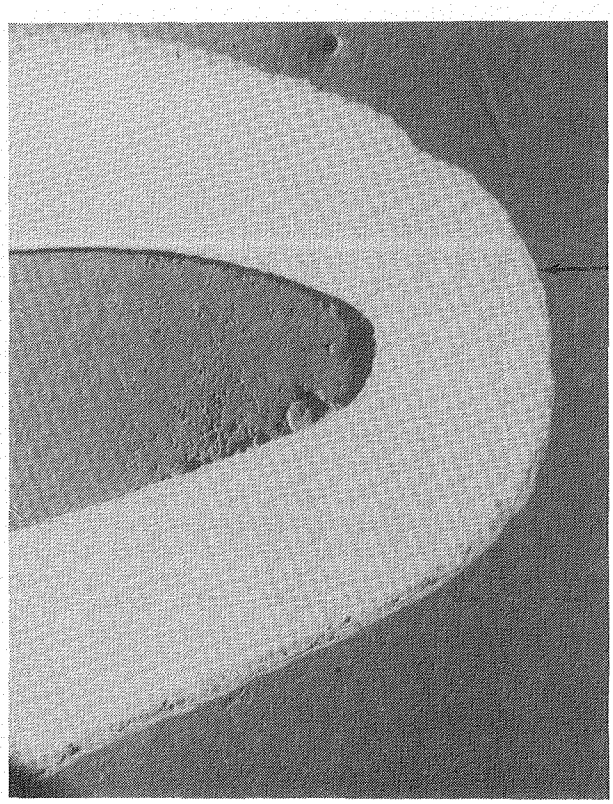

Bond Coat

Magnification: 18X

Figure 87. Leading Edge of Calcium Titanate TBC Blade After 550-Hour Engine Endurance Test

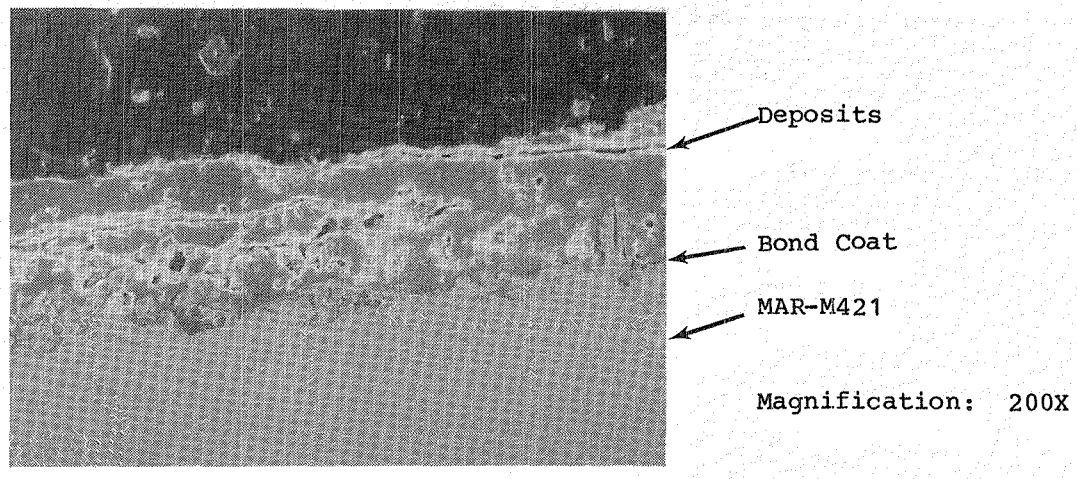

Figure 88. Calcium Titanate TBC Blade After 550-Hour Engine Endurance Test

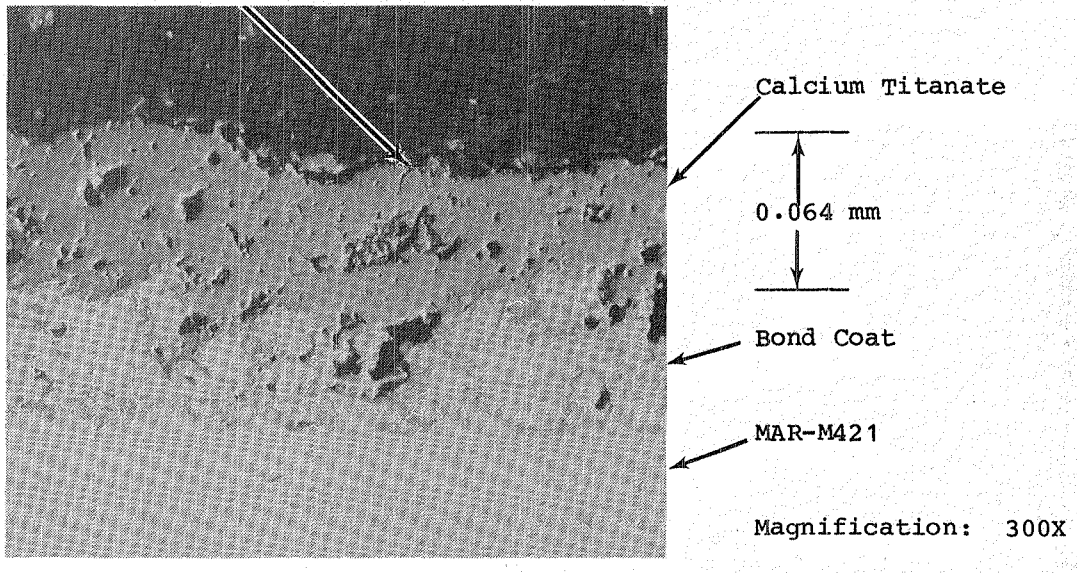

Figure 89. Calcium Titanate TBC After 550-Hour Engine Endurance Test

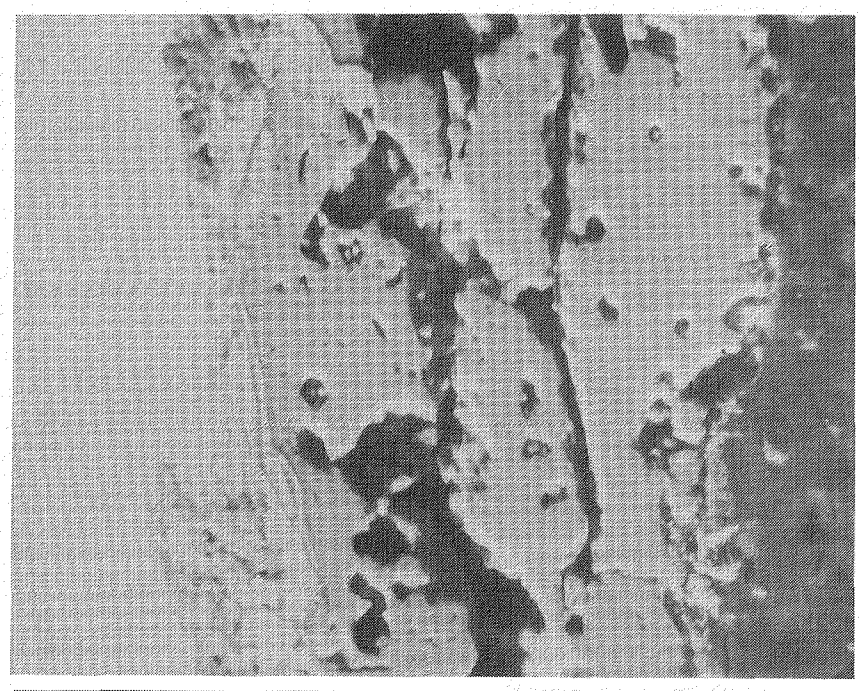

Mount No. 1853

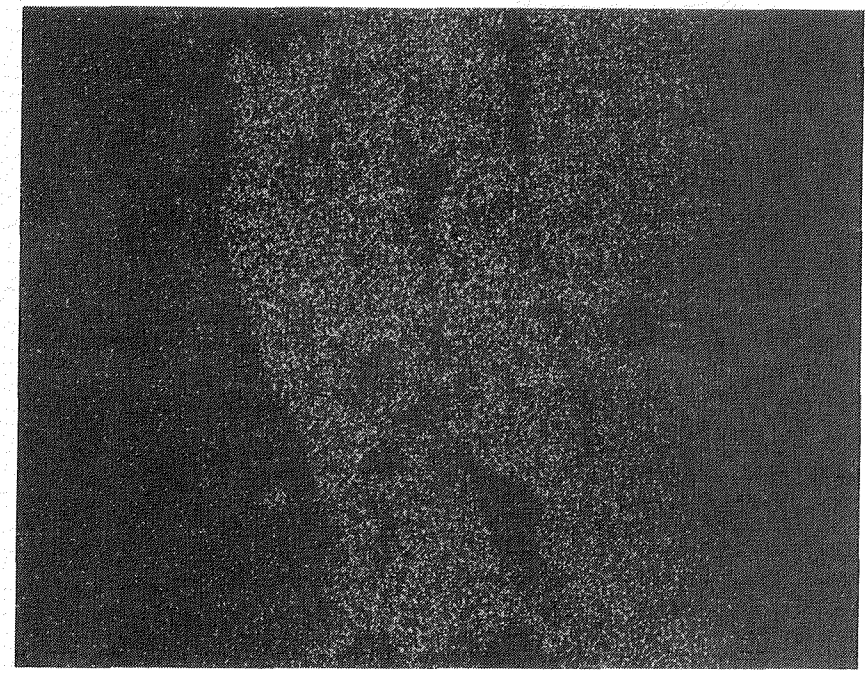

Mount No. 1853

Figure 90. SEM Photomicrograph and Dot Map of Calcium Distribution in Calcium Titanate TBC After 550-Hour Engine Endurance Test

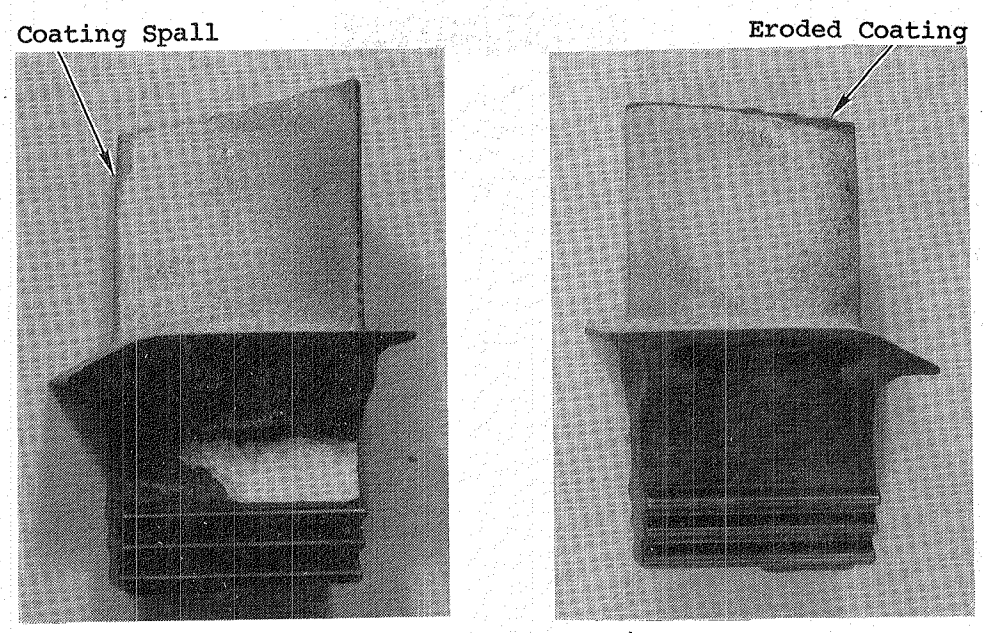

Figure 91. Fused $ZrO_2 \cdot 8Y_2O_3$ TBC Blade After 550-Hour Engine Endurance Test

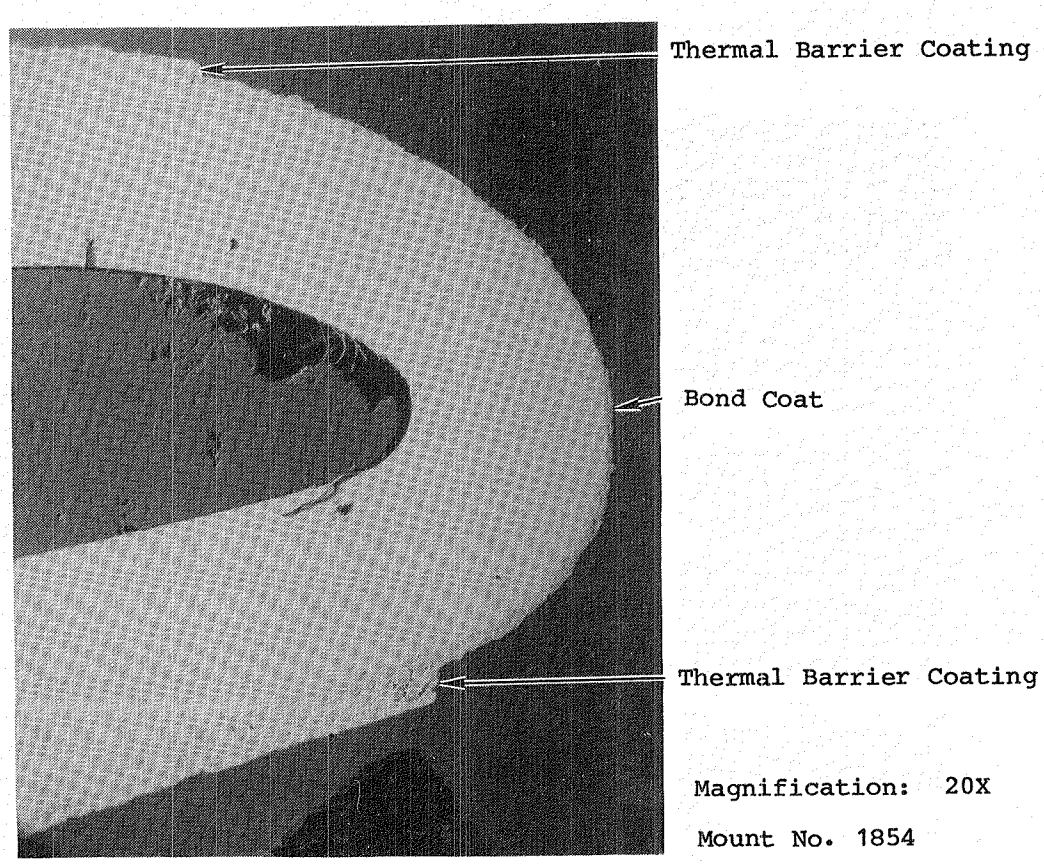

Figure 92. Fused $ZrO_2 \cdot 8Y_2O_3$ TBC Blade Leading Edge After 550-Hour Engine Endurance Test

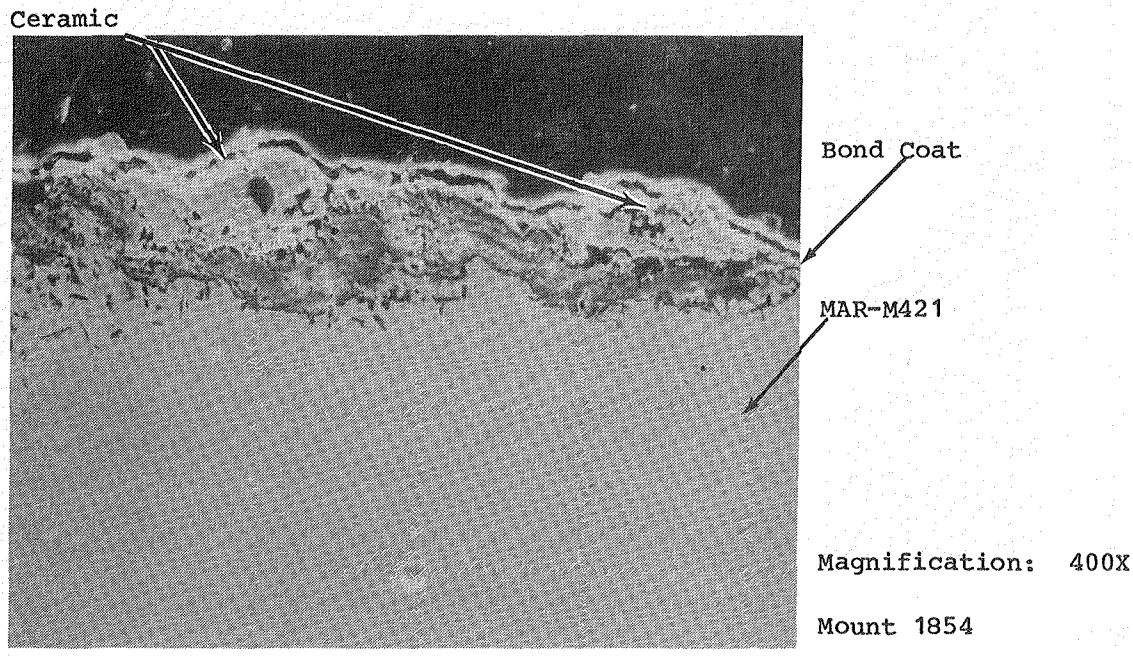

Figure 93. Bond Coat at Leading Edge of Fused $ZrO2.8Y_2O_3$ TBC Blade After 550-Hour Engine Endurance Test

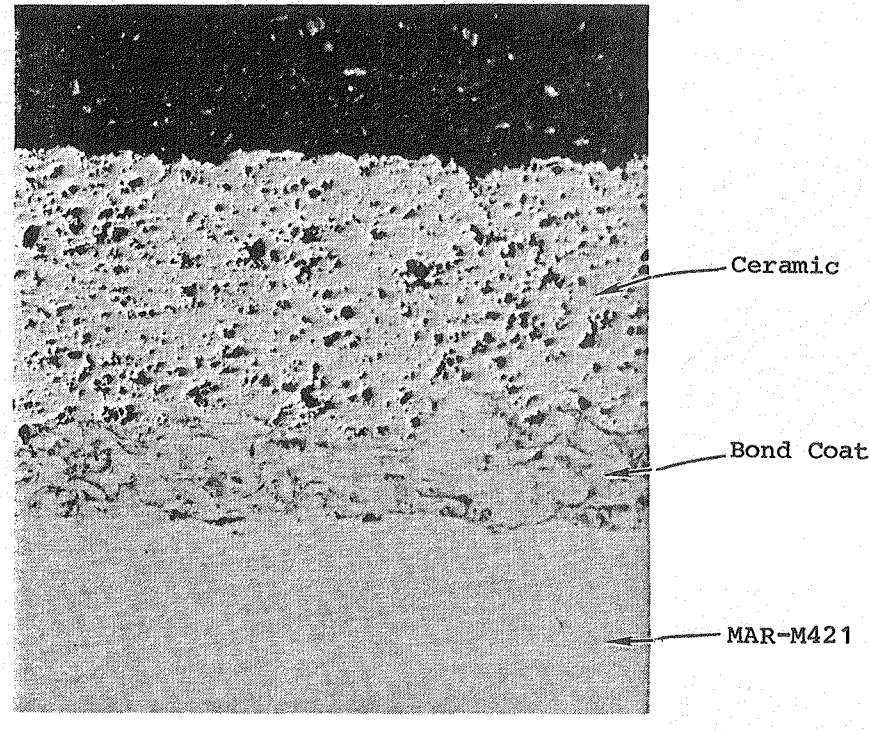

Figure 94. Fused $ZrO_2 \cdot 8Y_2O_3$ TBC After 550-Hour Engine Endurance Test

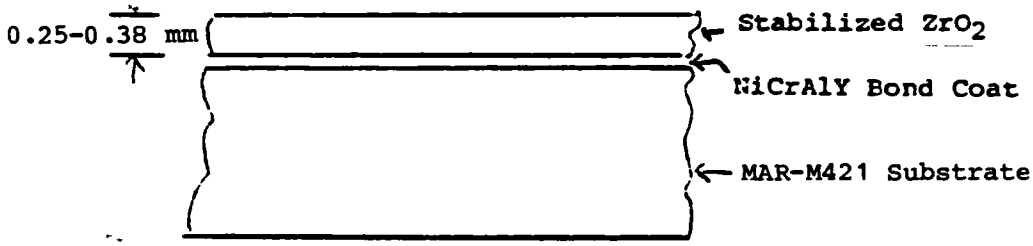

Figure 95. Approximate Physical Condition of Plasma Sprayed TBC

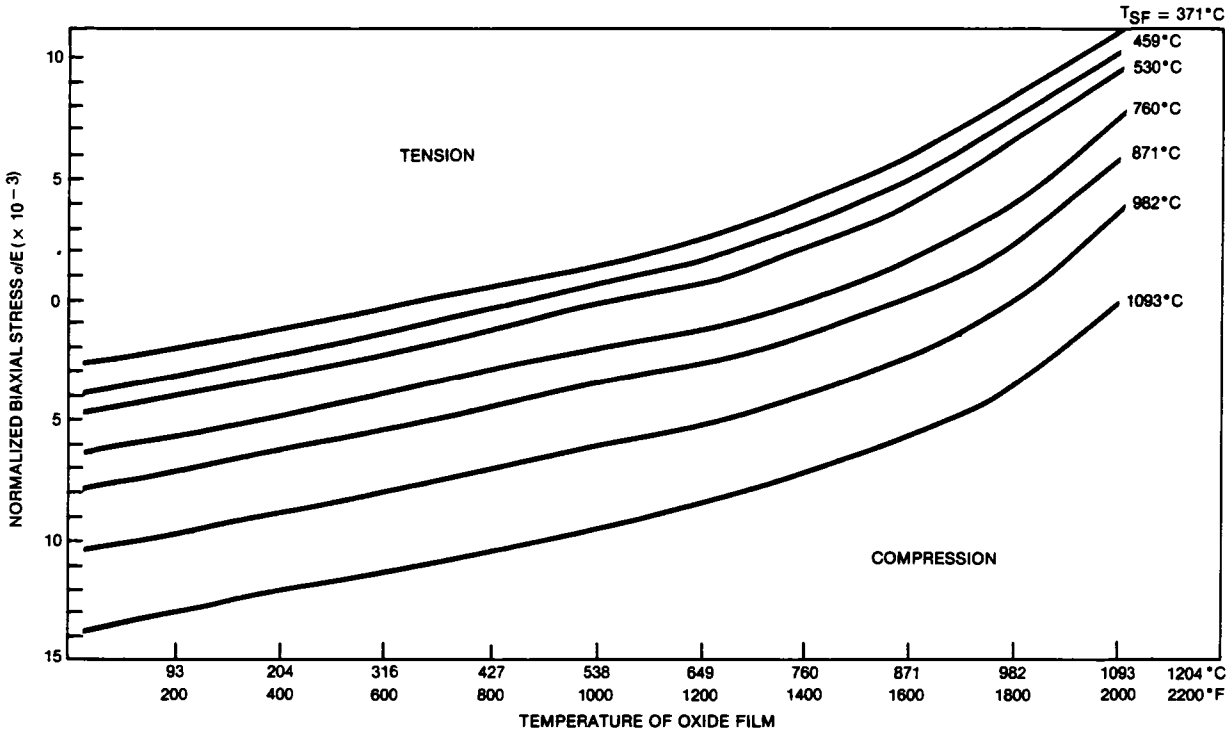

Figure 96. Stress Induced in TBC Due to Thermal Expansion at Selected Stress-Free Temperatures

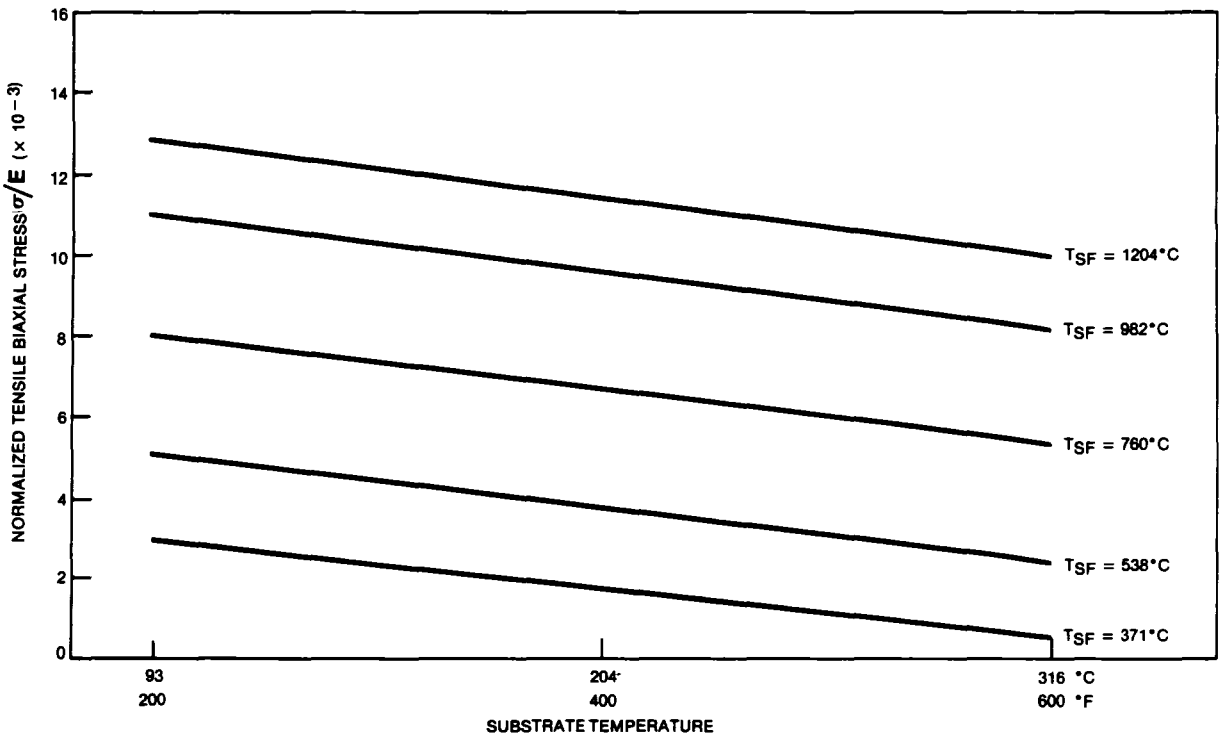

Figure 97. Stress in Oxide Coating With Initial Temperature Different Than T_{SF} After Cooling Coating to the Substrate Temperature

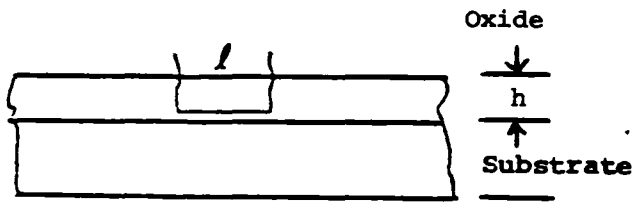

Figure 98. Idealized Condition

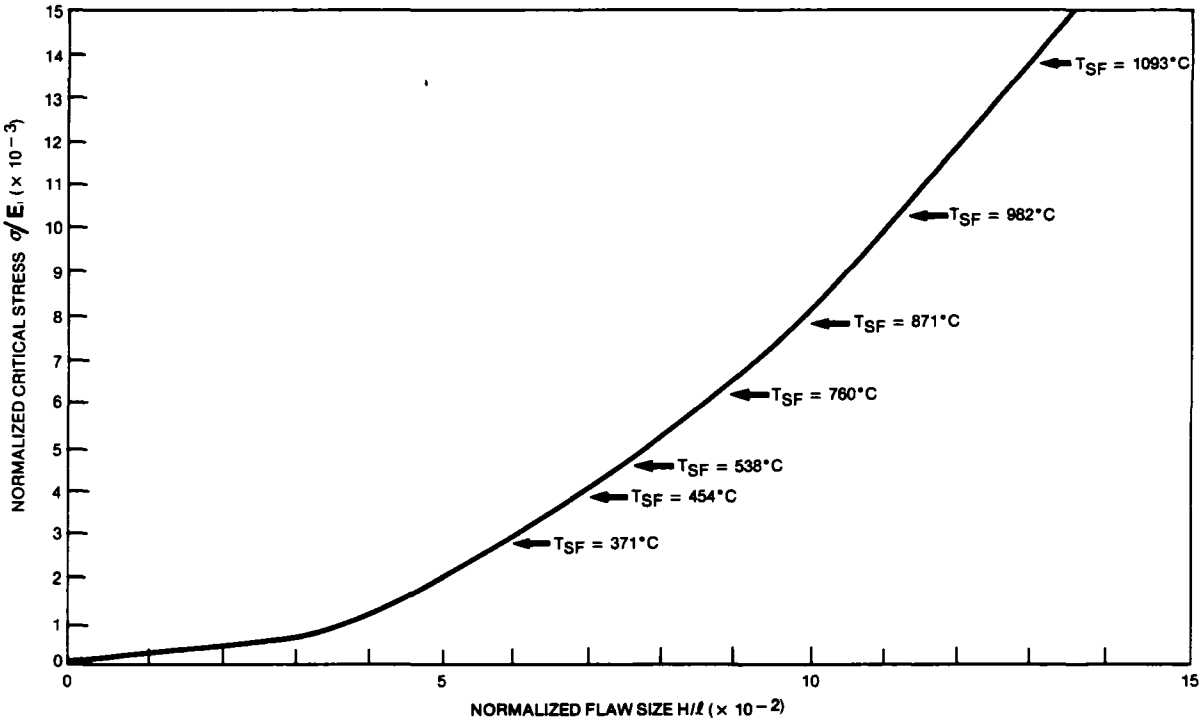

Figure 99. Use of Euler's Equation to Predict the Critical Flaw Size of a Thin Film

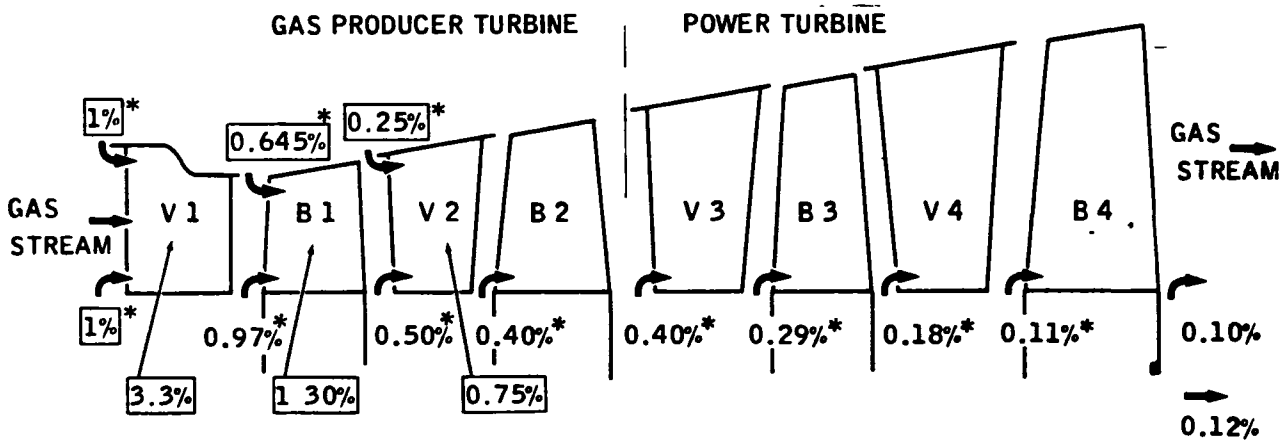

COOLANT FLOWS ARE IN % OF ENGINE INLET AIR FLOW
TOTAL: 11.315%
V = VANE
B = BLADE
* = SHROUD COOLING AIR.
OTHER % ARE VANE OR BLADE COOLING AIR

Figure 100. Mars Turbine Cooling Air Management

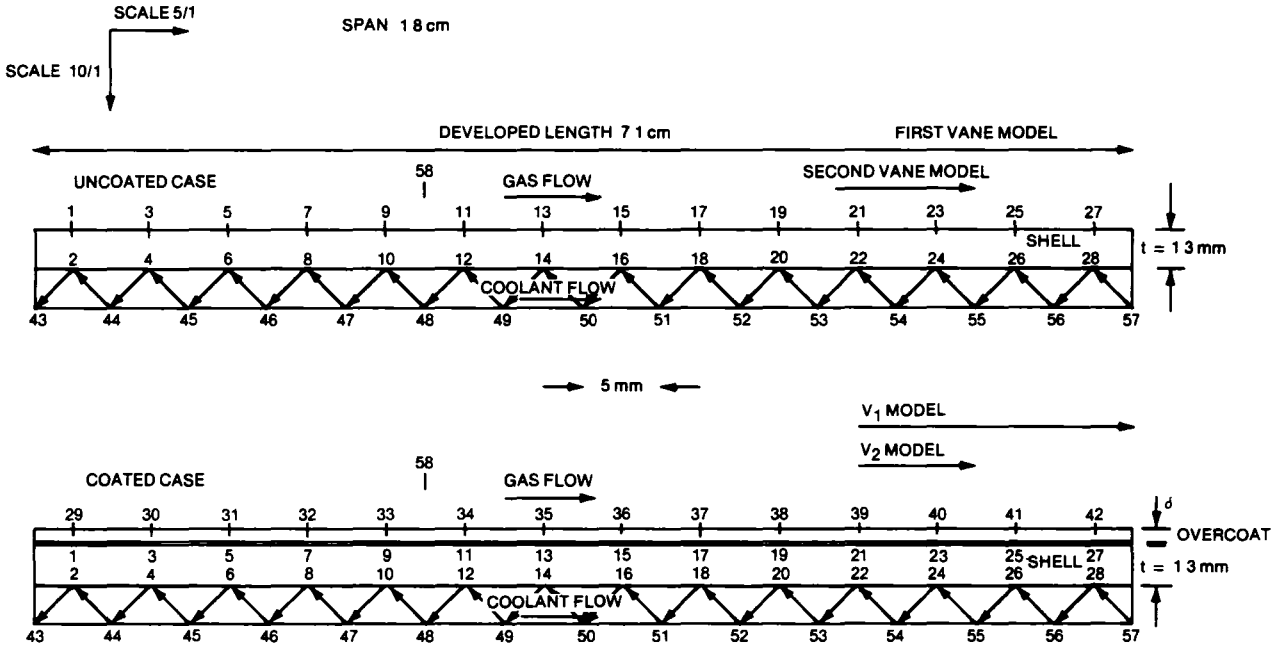

Figure 101. Thermal Models, Typical Coated or Uncoated. Airfoil Wall With Convective Cooling.

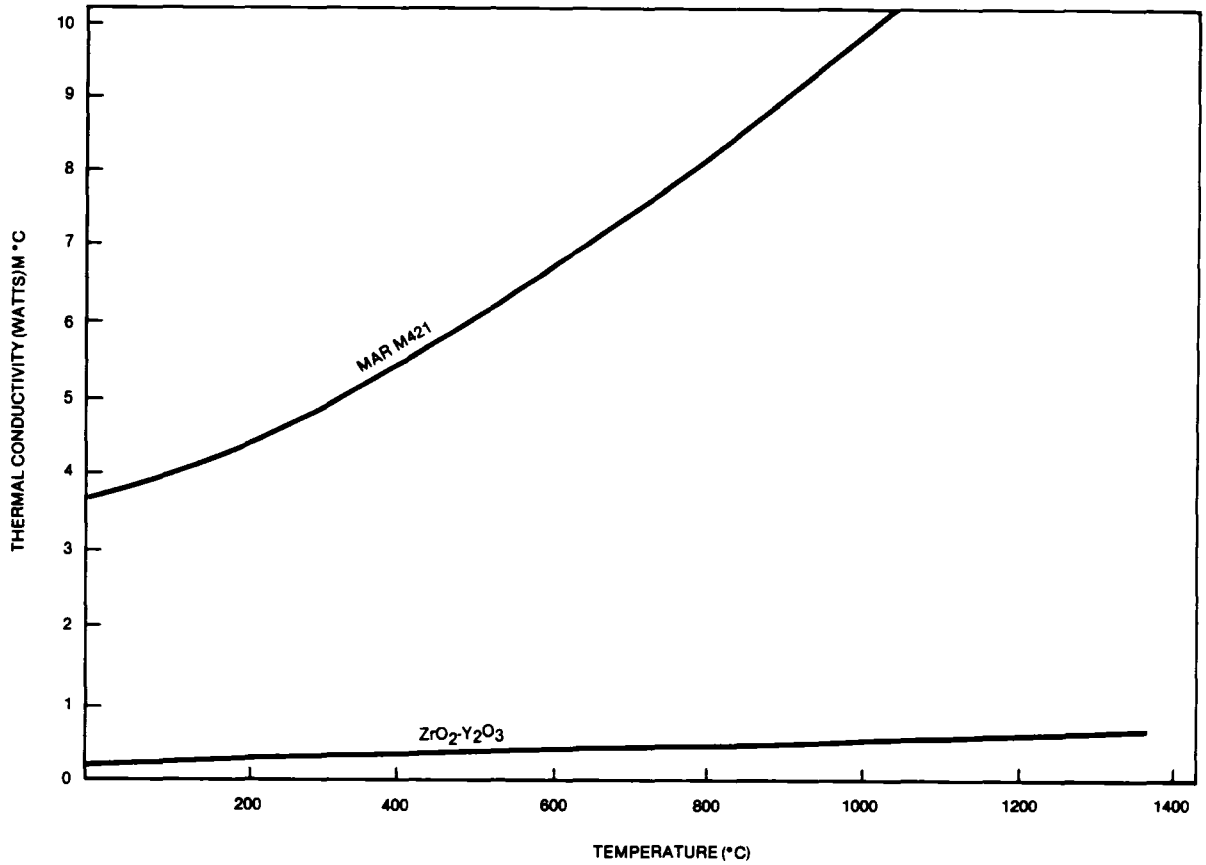

Figure 102. Thermal Conductivities

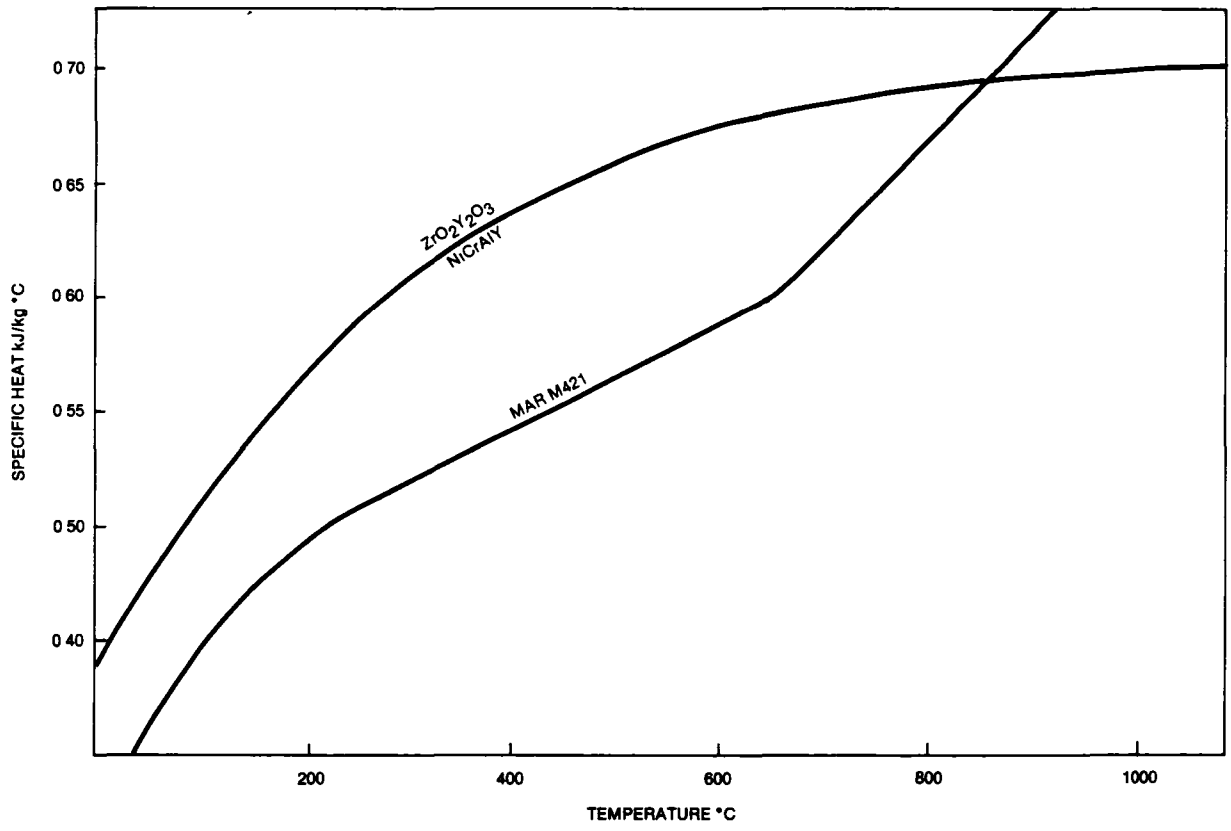

Figure 103. Specific Heats

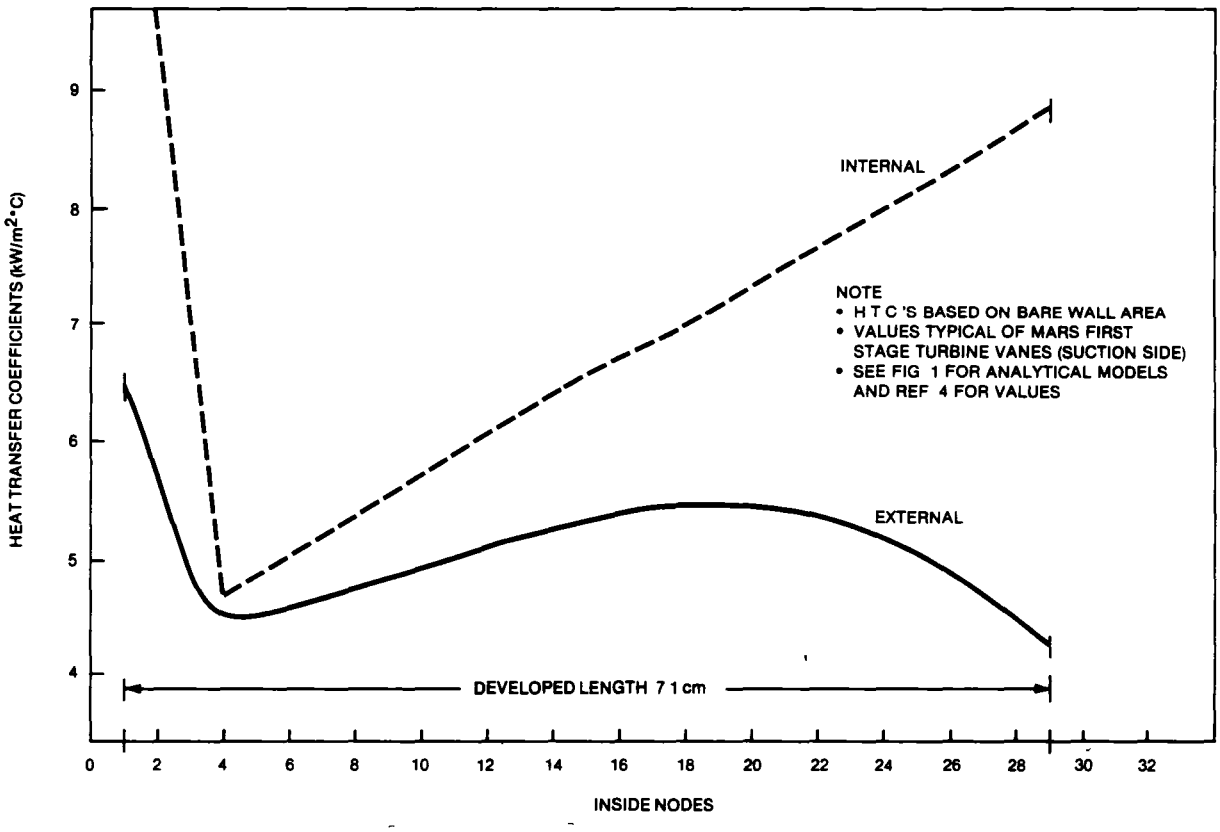

Figure 104. Model Heat Transfer Coefficients Based on Bare Wall Area

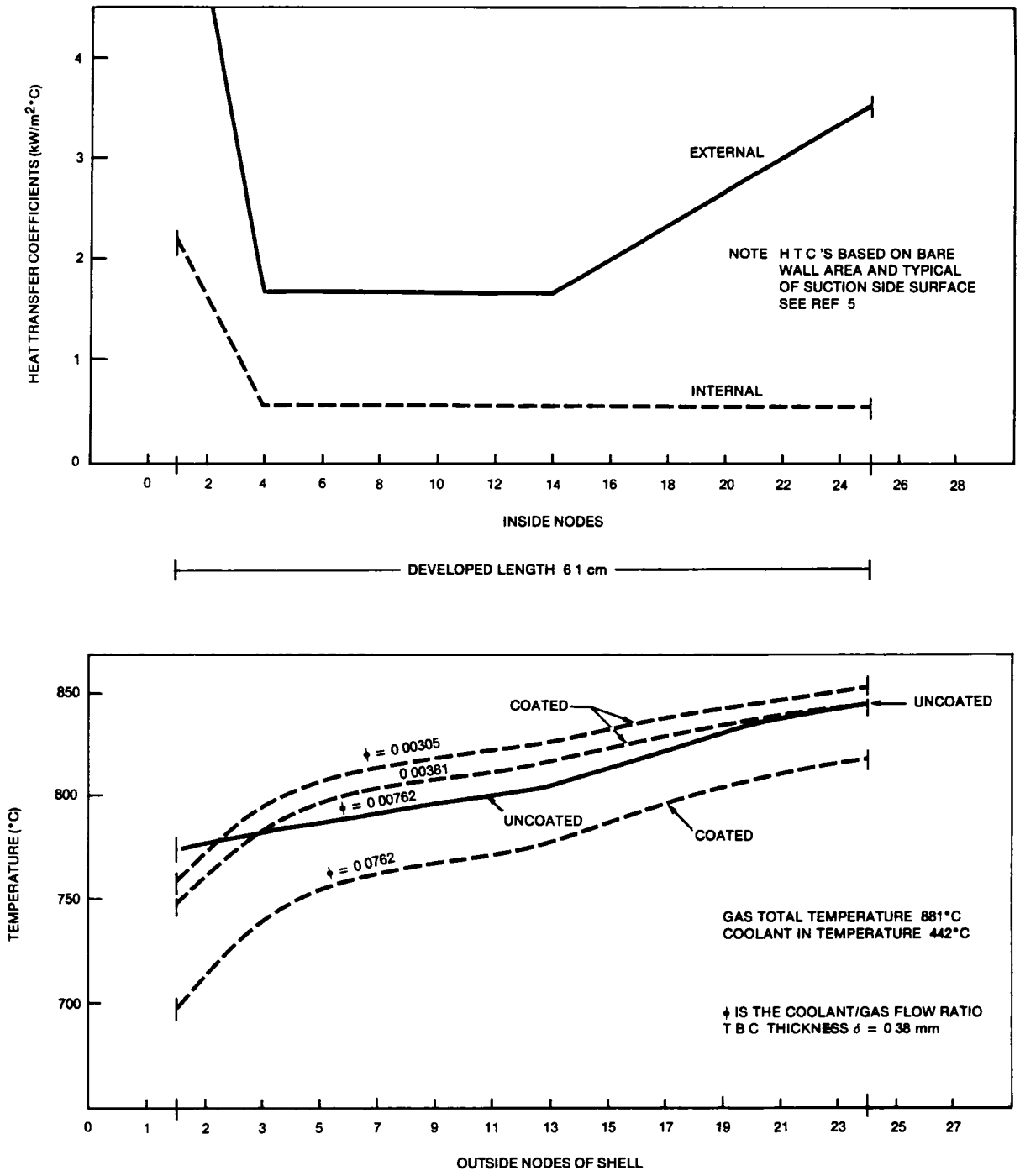

Figure 105. Effect of TBC on the Mars Second-Stage Cooled Nozzles

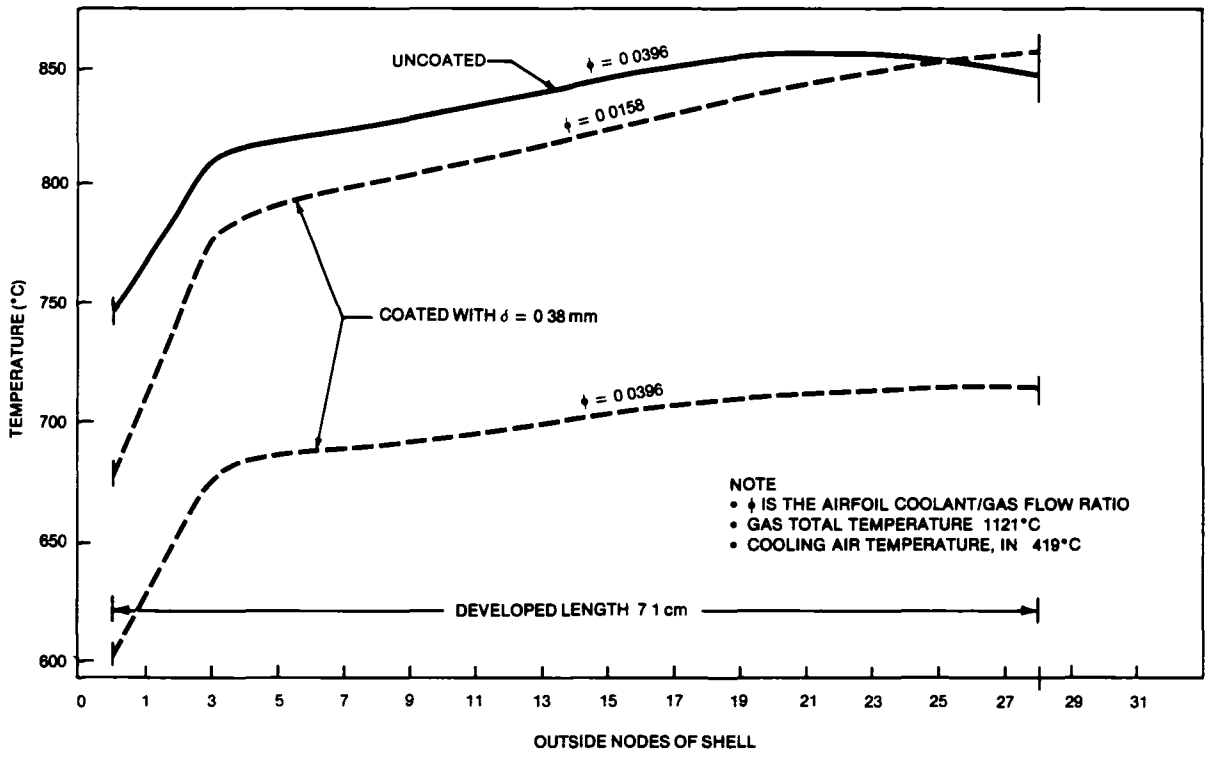

Figure 106. Mars First-Stage Vanes Outer Skin Metal Temperature

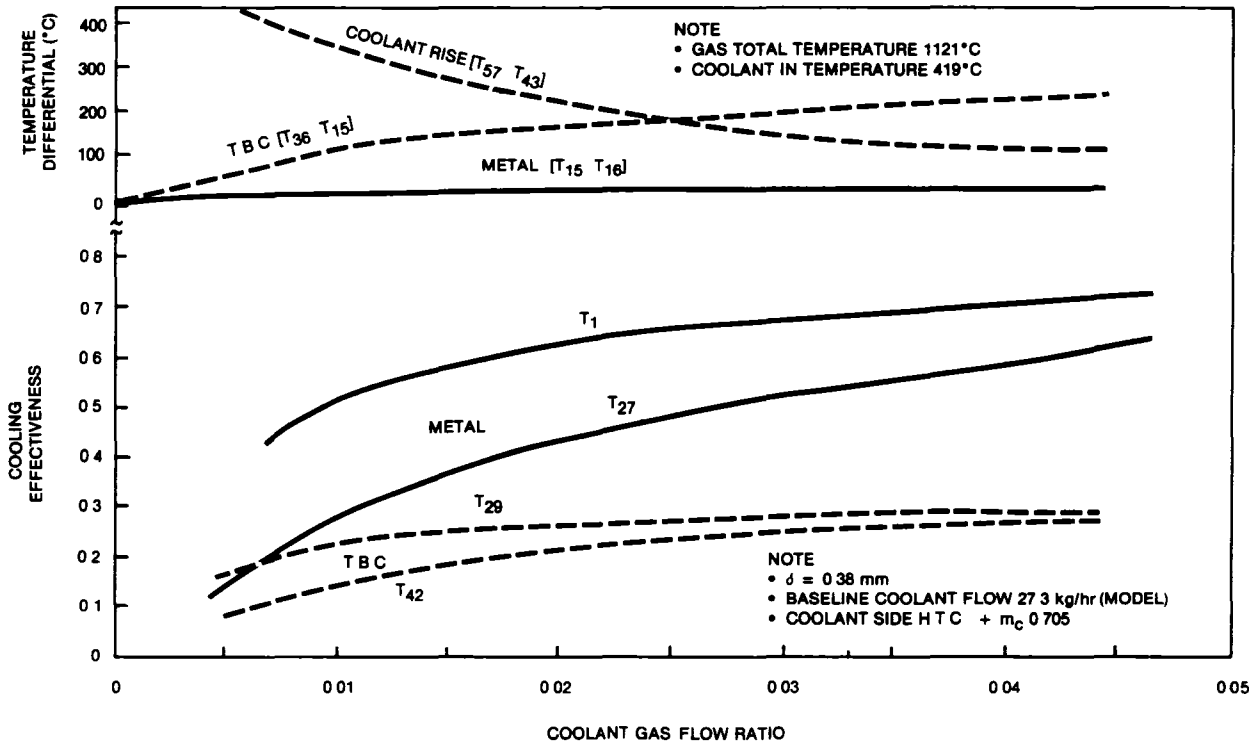

Figure 107. Mars First-Stage Coated Vanes Cooling Performance; 0.38 mm Thick Overcoat

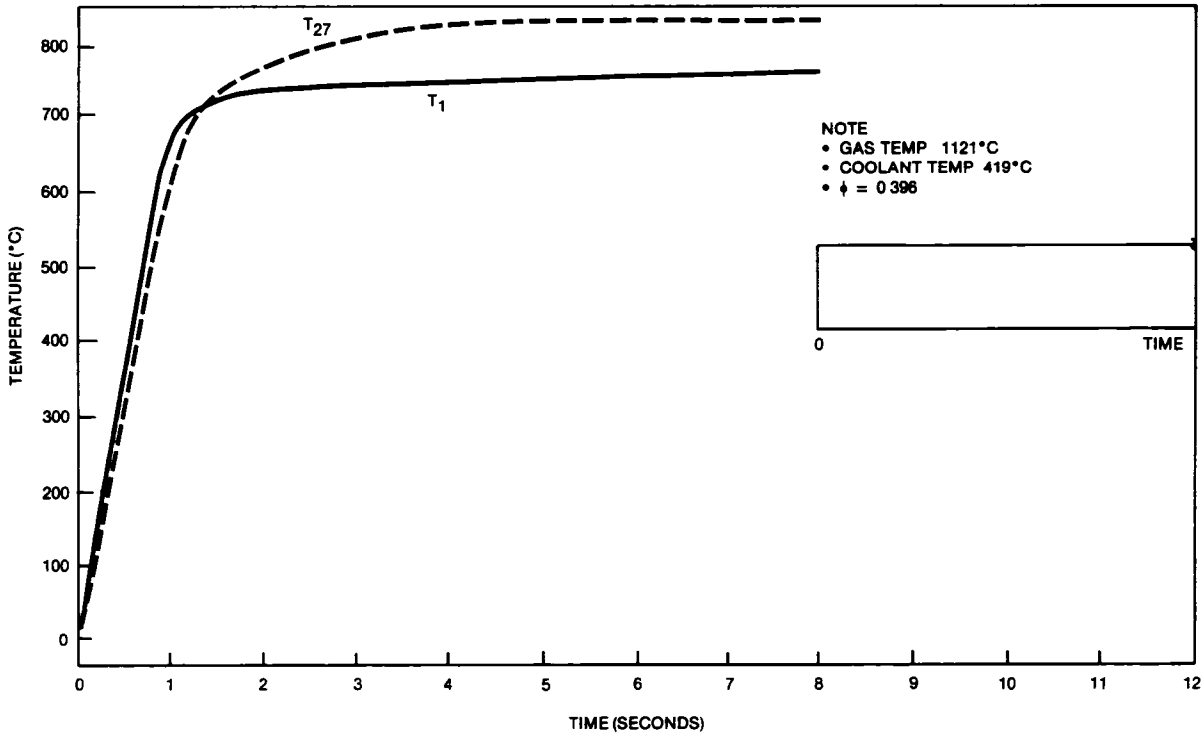

Figure 108. Uncoated First-Stage Vane Airfoil Thermal Response; Time-Step Change in Gas and Coolant Conditions

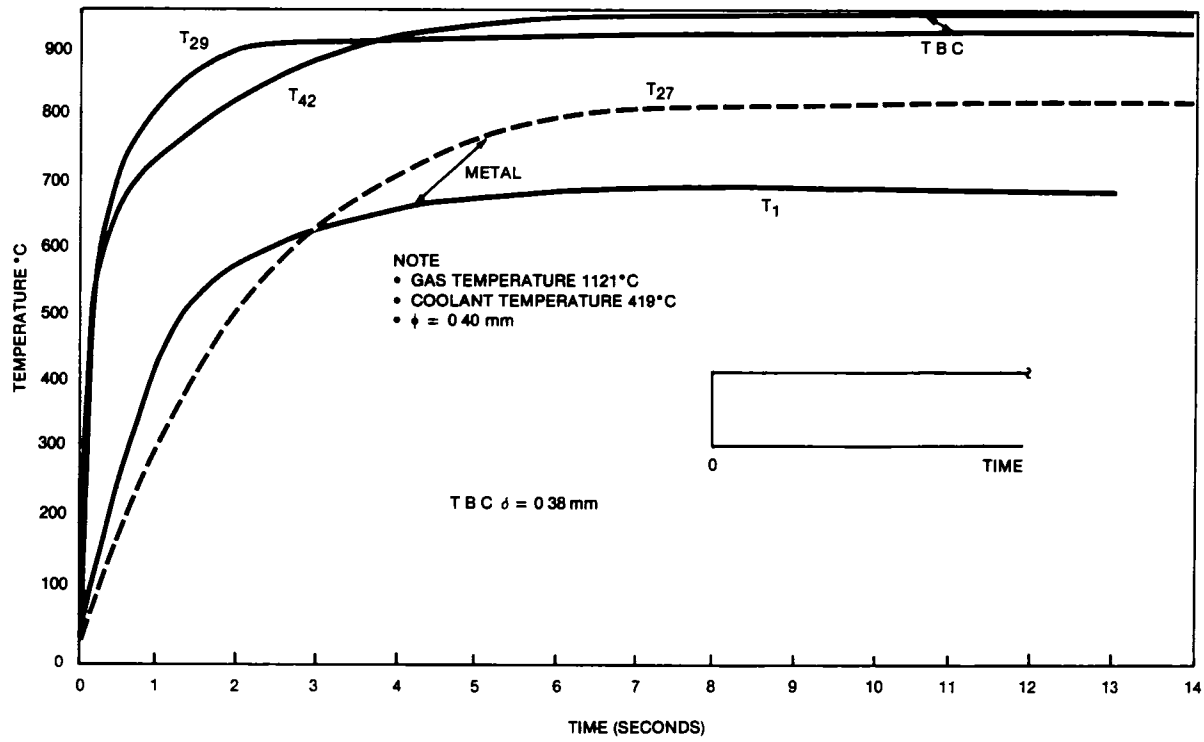

Figure 109. Coated First-Stage Vane Airfoil Thermal Response; Time-Step Change in Gas and Coolant Conditions

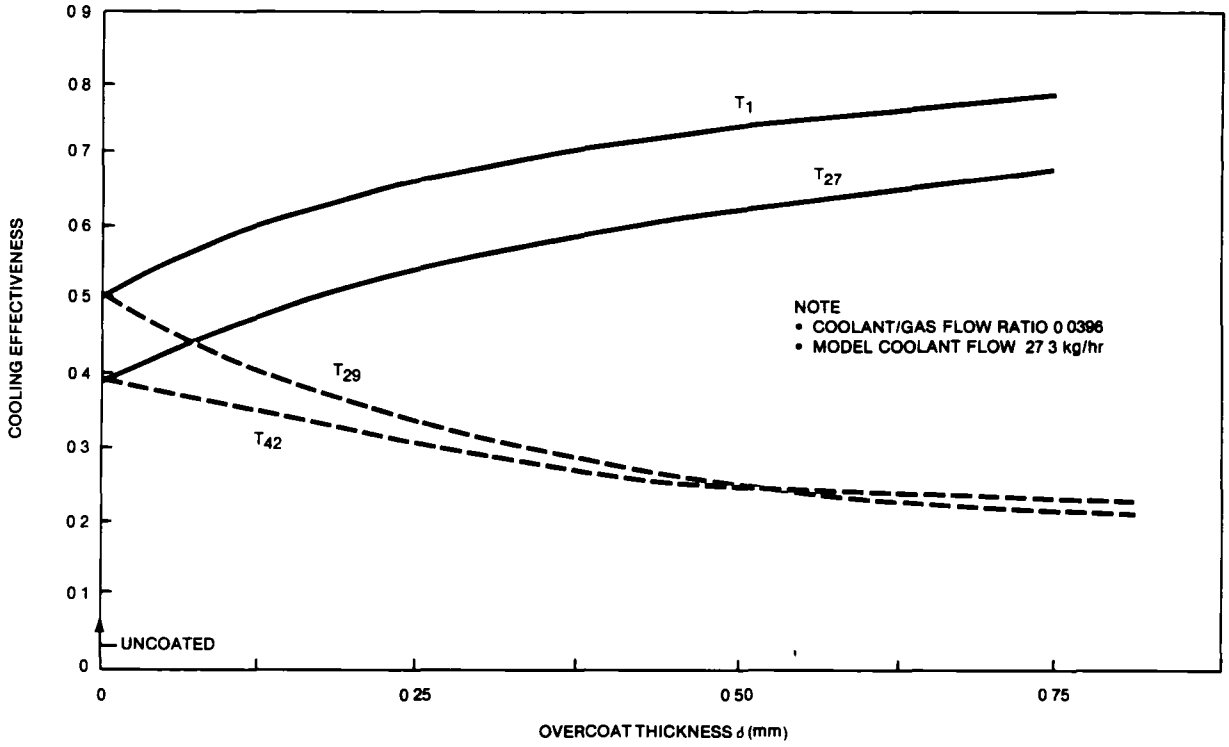

Figure 110. Mars First-Stage Coated Vanes; Effect of Overcoat Thickness on Cooling Effectiveness

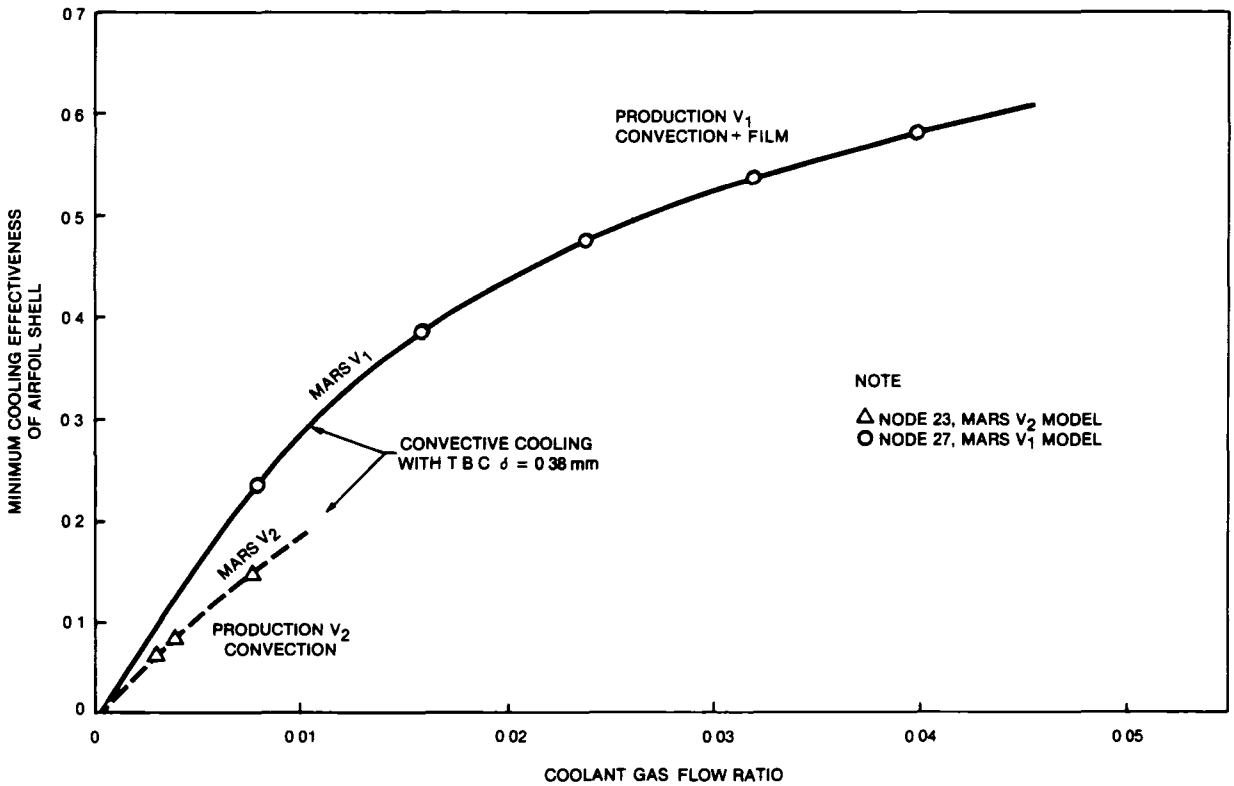

Figure 111. Minimum Cooling Effectivensss of Airfoil Shell

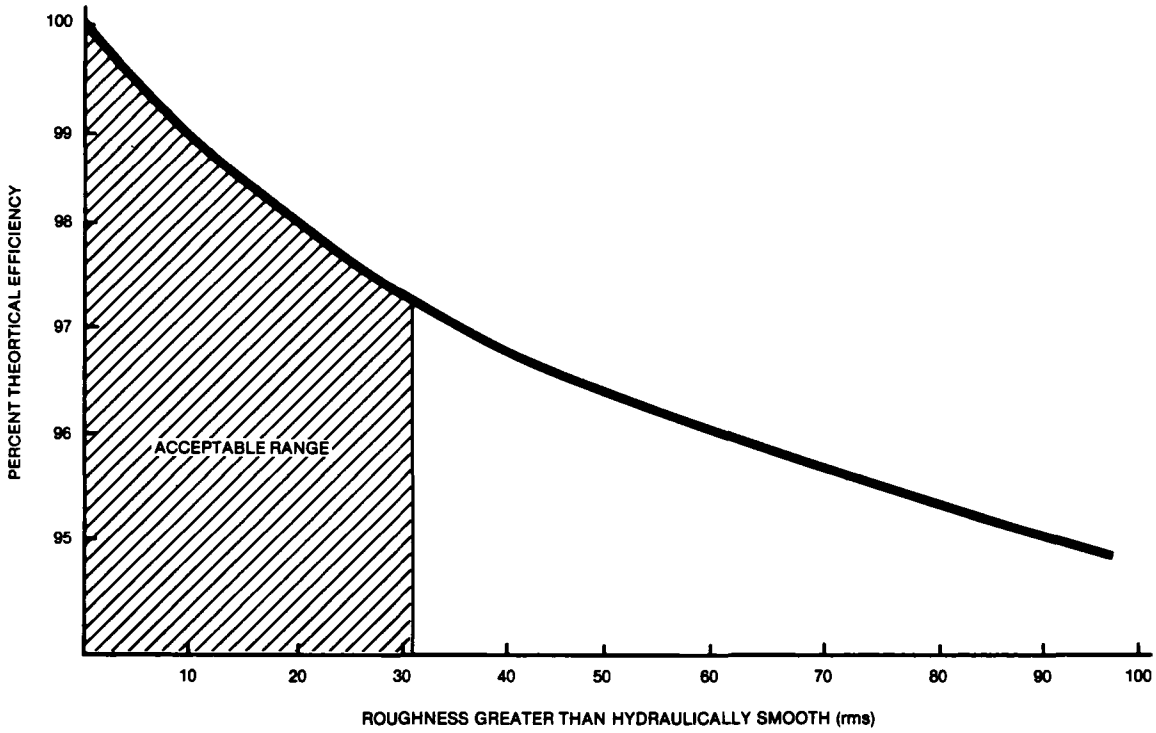

Figure 112. Efficiency Loss Due to Surface Roughness on a Turbine Blade

1 Report No	2 Government Accession No	3 Recipient's Catalog No
NASA CR-167852		

4 Title and Subtitle	5 Report Date
ADVANCED CERAMIC COATING DEVELOPMENT FOR INDUSTRIAL/UTILITY GAS TURBINES	January 1982
	6 Performing Organization Code
7 Author(s)	8 Performing Organization Report No
James W. Vogan and Alvin R. Stetson	SR82-R-4792-28
	10 Work Unit No
9 Performing Organization Name and Address	
Solar Turbines Incorporated P.O. Box 80966 San Diego, California 92138	11 Contract or Grant No DEN3-109
	13 Type of Report and Period Covered Contractor Report 3/11/79 - 9/1/81
12 Sponsoring Agency Name and Address	
U.S. Department of Energy Office of Fossil Energy Programs Washington, DC 20545	14 Sponsoring Agency Code

15 Supplementary Notes

Final Report. Prepared under Interagence Agreement DE-AI01-77 ET13111. Project Manager, John P. Merutka, Materials Division, NASA Lewis Research Center, Cleveland, Ohio 44135.

16 Abstract

A program was conducted with the objective of developing advanced thermal barrier coating (TBC) systems. Coating application was by plasma spray. Duplex, triplex and graded coatings were tested. Coating systems incorporated both NiCrAlY and CoCrAlY bond coats. Four ceramic overlays were tested: $ZrO_2 \cdot 8Y_2O_3$; $CaO \cdot TiO_2$; $2CaO \cdot SiO_2$; and $MgO \cdot Al_2O_3$. The best overall results were obtained with a $CaO \cdot TiO_2$ coating applied to a NiCrAlY bond coat. This coating was less sensitive than the $ZrO_2 \cdot 8Y_2O_3$ coating to process variables and part geometry.

Testing with fuels contaminated with compounds containing sulfur, phosphorus and alkali metals showed the zirconia coatings were destabilized. The calcium titanate coatings were not affected by these contaminants. However, when fuels were used containing 50 ppm of vanadium and 150 ppm of magnesium, heavy deposits were formed on the test specimens and combustor components that required frequent cleaning of the test rig.

During the program Mars engine first-stage turbine blades were coated and installed for an engine cyclic endurance run with the zirconia, calcium titanate, and calcium silicate coatings. Heavy spalling developed with the calcium silicate system. The zirconia and calcium titanate systems survived the full test duration.

It was concluded that these two TBC's showed potential for application in gas turbines.

Process variables and substrate composition were found to be critical and further work is required to relate them to coating performance.

17 Key Words (Suggested by Author(s))		18 Distribution Statement
Thermal Barriers	Ceramics	Unclassified - unlimited
Turbine Efficiency	Fuel Economy	STAR Category 26
Plasma Spray	Coatings	DOE Category UC25

19 Security Classif (of this report)	20 Security Classif (of this page)	21 No of Pages	22 Price*
UNCLASSIFIED	UNCLASSIFIED	121	

* For sale by the National Technical Information Service, Springfield Virginia 22161

End of Document